Magnetic field effects in organic semiconductors : theory and simulations

Magnetic Field Effects in Organic Semiconductors: Theory and Simulations

PROEFSCHRIFT

ter verkrijging van de graad van doctor aan de Technische Universiteit Eindhoven, op gezag van de rector magnificus, prof.dr.ir. C.J. van Duijn, voor een commissie aangewezen door het College voor Promoties in het openbaar te verdedigen op donderdag 28 maart 2013 om 16.00 uur

door

Sander Paul Kersten

geboren te Schelluinen

Dit proefschrift is goedgekeurd door de promotoren:

prof.dr. M.A.J. Michels
en
prof.dr. B. Koopmans

Copromotor:
dr. P.A. Bobbert

A catalogue record is available from the Eindhoven University of Technology Library

ISBN: 978-90-386-3342-8

Printed by Universiteitsdrukkerij Technische Universiteit Eindhoven.

This work is part of the research programme of the Foundation for Fundamental Research on Matter (FOM), which is part of the Netherlands Organisation for Scientific Research (NWO).

Contents

1

Introduction

In this chapter, magnetic field effects in organic semiconductors are introduced. First, an overview is given of organic semiconductors. The way these materials conduct current by hopping of charges is very important for the occurrence of magnetic field effects. One of the most important applications of organic semiconductors is the organic light-emitting diode. How light is produced by those diodes is briefly discussed. In the second part of this chapter, the phenomenology of magnetoconductance and magneto-electroluminescence is discussed. It is made clear that spin mixing by hyperfine interactions lies at their origin. Besides hyperfine interaction, other sources of spin mixing that are relevant for this thesis are described as well. Next, several mechanisms that can give rise to magnetic field effect are discussed in detail. The chapter concludes with an outline of this thesis.

1.1 Organic Semiconductors

An organic semiconductor consists of molecules or polymers that are made up primarily from carbon and hydrogen atoms, but that could also contain nitrogen or sulfur and sometimes even metal atoms. While the first conducting organic materials were discovered earlier, the discovery of highly conducting polymers after doping with halides in 1977 accelerated the field.[25] Heeger, MacDiarmid and Shirakawa were awarded a Nobel prize for this discovery. The first time electroluminescence was observed in an organic material was in 1953 by Bernanose and coworkers.[10] A technological breakthrough was made in 1987 when Tang and VanSlyke, working for Kodak, made the first organic light emitting diode (OLED).[113] Since then, much progress has been made and other electronic devices have been made, like Organic Field-Effect Transistors (OFETs),[108] Organic Photovoltaic Cells (OPCs),[19] and Polymer OLEDs (PLEDs).[20]

Organic semiconductors have several advantages over inorganic semiconductors. The materials are generally cheap and easy to process. Also, the properties of molecules are relatively easy to tune chemically. Being organic, devices made

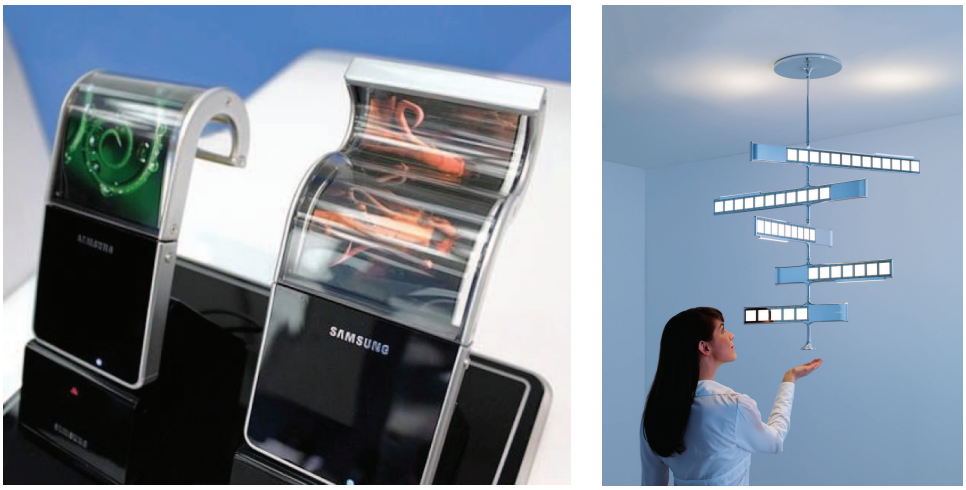

Figure 1.1 Two applications of organic semiconductors: (left) A flexible, very thin OLED display demonstrated by Samsung (© Samsung) and (right) decorative lighting from Philips[91].

from them could be disposed of in an environmentally friendly way or even be biodegradable. Moreover, organic devices can be flexible. In addition, while most other light sources are point sources (or line sources), OLEDs emit light from a large surface. Those properties open up a lot of new possibilities, like flexible displays [see Figure 1.1 at the left], decorative lighting [see Figure 1.1 at the right], or complete ceilings that function as a light source. Displays made of OLEDs are potentially more energy efficient than liquid crystal displays (LCDs), because only active pixels emit light and consume energy, while in an LCD already produced light is blocked in case of a black pixel. When used for lighting applications, OLEDs have as an advantage over other efficient light sources that their color temperature—how well the color resembles that of sun light—is nicer and their color rendering index—how well the light reproduces the color of an object it shines on—is higher. Currently, OLED displays are used in some smartphones and a few (very expensive) televisions. For lighting, OLEDs are commercially available, for example the Philips Lumiblade, see Figure 1.1 at the right.

1.1.1 Conduction

What makes an organic semiconductor conducting is the presence of π-conjugation, that is, alternating single and double bonds between carbon atoms. The result is that the s and two of the p orbitals hybridize to form three σ-bonds with other atoms. That leaves a half-filled (singly occupied) p_z orbital per carbon atom free. Those p_z orbitals hybridize to form molecular orbitals that are delocalized over the whole molecule.* Every carbon atom provides one orbital and one electron. Since every orbital could be doubly occupied, that would make the molecule or

*In the case of a polymer, bends and twists in the polymer chain limit the delocalization to unbent stretches of the polymer.

polymer metallic, if not for the Peierls instability.[90] The configuration where all bonds between carbon atoms have equal length turns out not to have the lowest energy. By alternatingly moving atoms closer or further apart, the energy of the highest occupied molecular orbital (HOMO) is lowered, while that of the lowest unoccupied molecular orbital (LUMO) is raised. In this way a bandgap is created that is typically a few electronvolt, making a material consisting of those molecules a semiconductor.

Although crystalline organic semiconductors exist, the organic semiconductors that are relevant for the work presented in this thesis are positionally and energetically disordered. Their HOMO and LUMO energy levels are usually assumed to be distributed according to a Gaussian distribution with a standard deviation σ of $\sim$0.1 eV.[6,49] This energetic disorder together with strong electron-phonon coupling leads to electrons and holes that are localized to single molecules or parts of polymers.[109] An electron (or hole) together with its phonons—which are, in effect, a deformation of the molecule—is called an electron (hole) polaron. When speaking specifically about an electron polaron or a hole polaron, the word "polaron" is omitted in the rest of this thesis. A molecule or part of a polymer to which a polaron is localized is called a "site".

Hopping

Charge transport happens by phonon-assisted tunneling of electrons or holes from site to site. This process is called hopping. In the literature, two types of hopping rates are commonly used. The first are Miller-Abrahams rates, which come from the field of inorganic electronics.[77] For a hop from site i to j, they are given by

$$k_{i\to j}^{\mathrm{MA}} = \begin{cases} \nu_0 e^{-2\alpha R_{ij}} e^{-\Delta E_{ij}/k_{\mathrm{B}}T} & \text{if } \Delta E_{ij} > 0, \\ \nu_0 e^{-2\alpha R_{ij}} & \text{if } \Delta E_{ij} \leq 0, \end{cases} \tag{1.1}$$

where R_{ij} is the distance between sites i and j, α is the inverse of the wave-function decay length, ΔE_{ij} is the energy of the state after the hop minus the energy of the state before the hop, $k_{\mathrm{B}}T$ is the thermal energy, and ν_0 is the attempt-to-jump frequency.

The second type are Marcus rates,[66] which have their background in chemistry. The Marcus rate for a hop from site i to site j is given by,

$$k_{i\to j}^{\mathrm{M}} = \nu_0 \sqrt{\frac{\pi}{4\lambda k_{\mathrm{B}}T}} e^{-2\alpha R_{ij}} e^{-\frac{(\Delta E_{ij}+\lambda)^2}{4\lambda k_{\mathrm{B}}T}}, \tag{1.2}$$

where λ is the reorganization energy. The reorganization energy is the energy needed to move the charge from the source to the target site, while keeping the phonons that are associated with the charge on the source site. It is typically between 0.1 eV and 0.8 eV and it is material specific.[109]

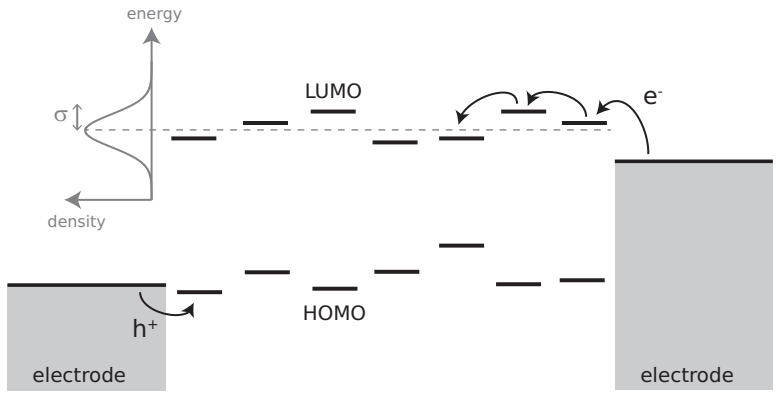

Figure 1.2 A typical organic device, consisting of two electrodes with an organic semiconductor in between. The organic semiconductor consists of sites of which the energies are distributed according to a Guassian with standard deviation σ. Electrons and holes are injected into the LUMO and HOMO, respectively, of the organic semiconductor from the electrodes. The charges then continue their transport through the device by hopping from site to site.

Both types of rates are used in the literature. Marcus rates are more appropriate for hopping in organic materials but Miller-Abrahams rates have as an advantage that there is one parameter fewer.

It is clear from Equations 1.1 and 1.2 that hops to sites with a higher energy are more difficult (happen with a lower rate) than hops to sites with a lower energy. Also hops to sites further away are more difficult than hops to sites close by. As a consequence, the current through a layer of organic semiconductor will follow a meandering path of least resistance through the energy landscape—just like water finding its way through coffee powder in a percolator. This process is, therefore, aptly named *percolation*. The result is that current will flow along preferential paths through the semiconductor.[46]

For simplicity, we will ignore positional disorder in our modelling and assume that all sites are on a square lattice—or on a line in case of a one-dimensional system—with lattice spacing a. Furthermore, we assume that only nearest-neighbor hopping takes place. With this assumption, the tunnelling factor $e^{-2\alpha a}$ and ν_0 can be absorbed into a prefactor $k_0 = \nu_0 e^{-2\alpha a}$.

Space charge

The band gaps of organic semiconductors are much larger than the thermal energy at room temperature, which is 25 meV. The intrinsic conductivity will therefore be very low and electrons and holes need to be introduced into the semiconductor in order to obtain a sizeable conductivity. This is commonly done by injection from electrodes. Figure 1.2 shows a simple device consisting of an organic semiconductor sandwiched between two electrodes. It is easy to understand that with every charge that is injected into the organic semiconductor it becomes more difficult to inject the next charge, because of the build-up *space charge*. If injection is suffi-

ciently easy, the current through the device will be limited by the amount of space charge. In the case of unipolar devices, the *space-charge-limited current* is given by

$$J = \frac{9}{8}\mu\epsilon\frac{V^2}{d^3}, \tag{1.3}$$

where μ is the charge mobility, ϵ is the permittivity of the organic semiconductor, V is the voltage applied over the device, and d is the thickness of the device.[88]

When both holes and electrons are injected, in the case of a bipolar device, the positive space charge of the holes and the negative space charge of the electrons will (partially) cancel each other, provided the recombination is weak. Recombination is weak when most electrons and holes reach the collecting electrode instead of recombine. That results in more charge being injected and consequently in a higher current. In this case the current is given by

$$J = \frac{9}{8}\epsilon\sqrt{\frac{2\pi\mu_e\mu_h(\mu_e+\mu_h)}{\mu_r}}\frac{V^2}{d^3}. \tag{1.4}$$

Here, μ_e and μ_h are the electron and hole charge mobility, respectively, and μ_r is the recombination mobility.[88] The recombination mobility is a measure of how easily electrons and holes recombine and is defined as $\mu_r = \epsilon B/2e$, where e is the elementary charge and B is *total recombination rate*.[9] The previous equation for the space charge limited current is only valid when recombination is weak, that is, when $\mu_r \ll \mu_e, \mu_h$. If, on the other hand, the recombination is strong, that is, $\mu_r \gg \mu_e, \mu_h$, an electron and a hole that meet each other will immediately recombine. That results in a narrow recombination zone somewhere in the organic layer with only electrons on one side of it and only holes on the other site. In this case, the recombination rate does not affect the current.

Photocurrent

Another way of introducing carriers is by photo-excitation. When a molecule or polymer absorbs a photon, an exciton is generated that can dissociate into an electron-hole pair. Under influence of an electric field, this electron-hole pair can be pulled apart. The resulting current is called a *photocurrent*. The dissociation can be more efficient at the interface of two organic semiconductors with different energy levels, because in that case the state where the electron is in one semiconductor and the hole is in the other could be lower in energy than the excitonic state. This is the basic principle of how an organic solar cell works.

Doping

A third way of introducing charges into an organic semiconductor is by doping.[122] By putting molecules into the material that have their HOMO and LUMO energies suitably shifted with respect to the host semiconductor, those dopant molecules can donate an electron or hole to a host site, see Figure 1.3. In the case of electron doping, the HOMO of the dopant site should be energetically aligned with the LUMO of the host to get the largest amount of doping. In that case, one of the

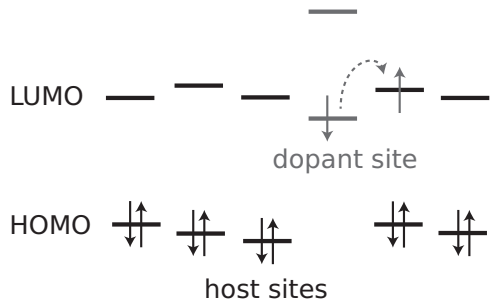

Figure 1.3 A few host sites with one of them replaced by a dopant site with shifted energy levels. In general, the dopant's HOMO will not be exactly aligned with the host's LUMO, but ionisation of the dopant site is easier when the dopant's HOMO is aligned (or has a higher energy) than the host's LUMO. One electron of the dopant's HOMO has hopped to a neighboring host site's LUMO.

electrons from the dopant's HOMO can hop without an energy penalty to a nearby host site.

A hole-doped layer is often used in devices to facilitate hole injection from an electrode. Electron doping is considerably more difficult, because the required high HOMO energy makes such dopant molecules chemically instable.[122]

1.1.2 Light production

At present, the most prominent application of organic semiconductors is in displays. OLEDs also have the promise to become more efficient than other light sources. Light can be produced when both electrons and holes are injected into an organic semiconductor. When an electron and hole meet, they can form an exciton, which can then decay to the ground state by emitting a photon if the exciton is a singlet.

Efficacy

An important measure of a light source is its efficacy. That is, how much of the energy used by the OLED is converted into light, measured in lumen? The efficacy of an OLED depends on several factors:

1. How well does the voltage over the OLED match the energy of the emitted photons? The energy difference will be lost as heat.

2. How many injected electrons and holes recombine and form excitons, instead of hopping through the organic semiconductor and being collected at the other electrode?

3. How many of the excitons that are formed are singlets? Since triplets have a total spin equal to one, they cannot decay by emitting a photon, so only singlets emit light.

4. How many of the singlet excitons will decay by emitting a photon? A singlet exciton can, for example, be quenched by interaction with a charge or a triplet. A singlet can also decay non-radiatively.

5. And finally, how many of those photons can leave the OLED? Organic materials have a high refractive index of 1.7–1.9, which leads to total internal reflection, making light out-coupling one of the main challenges in creating an efficient OLED.[115]

Of those five factors, the third is relevant for the study of magneto-electroluminescence as will become clear in the next section. When an electron and hole that are injected from the electrodes meet to form an exciton, their spins will be random. That means that there is a 25% probability that their spins are in a singlet configuration and a 75% probability that they are in a triplet configuration. There has been much debate in the literature about whether or not this statistical ratio of 1:3 singlet to triplet excitons can be violated during exciton formation. There are several reports claiming the formation of either more[22,33,98,126,127] or less[23,106,129] than 25% singlets.

It should be noted that on molecules with a large spin-orbit interaction—for example, due to the presence of a heavy metal atom—the energy eigenstates are no longer pure singlets and triplets. Instead, the "triplet" state will also have some singlet character and the "singlet" state will also have some triplet character. On those phosphorescent molecules, "triplet" excitons can decay radiatively as well. This is used to increase the efficacy of OLEDs:[55] Triplet excitons can also contribute to the efficacy by triplet-triplet annihilation.[59,134] When the total spin configuration of a triplet pair is a singlet, a radiative decay to the ground state is possible when they encounter each other. Recently, Uoyama and coworkers[116] have shown that triplets can also be made to contribute to the luminescence by designing an organic semiconductor such that it has only a small (compared to the thermal energy) energy difference between the singlet and triplet states. If that energy difference is small, the intersystem crossing from the triplet states to the singlet state is relatively fast, resulting in effective thermally activated delayed fluorescence.

Spin-OLED

In the previous section, it was assumed that the spins of an electron and a hole that meet each other are random, as is the case when charges are injected from non-magnetic electrodes. However, when charges are injected from magnetic electrodes, these charges will be spin-polarized. Let us imagine the ideal situation where the electrodes inject fully spin-polarized charges and let us ignore spin relaxation for the moment. If now the two electrodes inject electrons and holes that are oppositely polarized, 50% of the excitons that are formed will be singlets instead of 25%. Oppositely, when the two electrodes inject charges with the same polarization, only triplet excitons will be formed. So, not only can this be used to increase the OLED's efficiency, it also leads to a very large magneto-electroluminescence when the electrodes are such that their magnetization direction can be switched individually by an applied magnetic field.[31] However, in reality, the injected spins will lose some

of their polarization when moving through the organic semiconductor before they meet, due to hyperfine interactions[17] or spin-orbit interactions.[131] Also, charges are not injected in a fully spin-polarized way. That seems to be a problem especially at the higher voltages needed to make OLEDs emit light.[128] Nguyen and coworkers were the first to report a working spin-OLED, although they found an magneto-electroluminescence due to the effects described above of only $\sim 1\%$.[80,81]

1.2 Magnetic Field Effects

We will define a magnetic-field effect as the relative change in some property X as a function of an applied magnetic field, B:

$$\mathrm{MFE}(B) = \frac{X(B) - X(0)}{X(0)}, \tag{1.5}$$

where X could be the current, in which case we speak of *magnetoconduction* (MC), the electroluminescence, in which case we speak of *magneto-electroluminescence* (MEL), or it could be the diffusion constant, in which case we speak of *magnetodiffusion*. Instead of magnetoconduction, sometimes the term *magnetoresistance* (MR) is used for a change in the resistance.

In 1992, Frankevich and coworkers observed a magnetic-field dependence of the photocurrent of a polymer film (PPV[†]) of little over 3% at only several tens of millitesla and at room temperature.[37] Later, a magnetic field effect of similar size was also measured in the electroluminescence and conduction of OLEDs made from the small molecule Alq_3[‡] by Kalinowski *et al.*[53] Soon thereafter effects of over 10% were measured by Francis *et al.*, sparking a lot of interest.[36] In the meantime, a magnetoconductance of over 25% and a magneto-electroluminescence of over 50% have been reported.[85] A magnetic field effect in the photocurrent of $\sim$300% was found, but only at very small currents.[32]

All these measurements were done on bulk semiconducting small molecules or polymers, at room temperature, and without magnetic electrodes. The magnetoconductance was found not to depend on the device thickness,[74] so interface effects are not dominant.[§] The temperature dependence was found to be weak.[74]

1.2.1 Lineshapes

Measurements of the magnetoconductance have been done on devices of many different organic semiconductors, all yielding very similar results, see Figure 1.4(a). This indicates that the effects are relatively independent of the material choice. A second thing to note from Figure 1.4(a) is that all curves can be fitted with either of two lineshapes: a Lorentzian and a "non-Lorentzian" lineshape. These lineshapes

[†] PPV: poly(*p*-phenylene vinylene)
[‡] Alq_3: aluminium tris(8-hydroxyquinoline)
[§] Increasing the device thickness decreases the effect the interface has on the current, so it would decrease the magnetoconductance if the magnetoconductance were an interface effect.

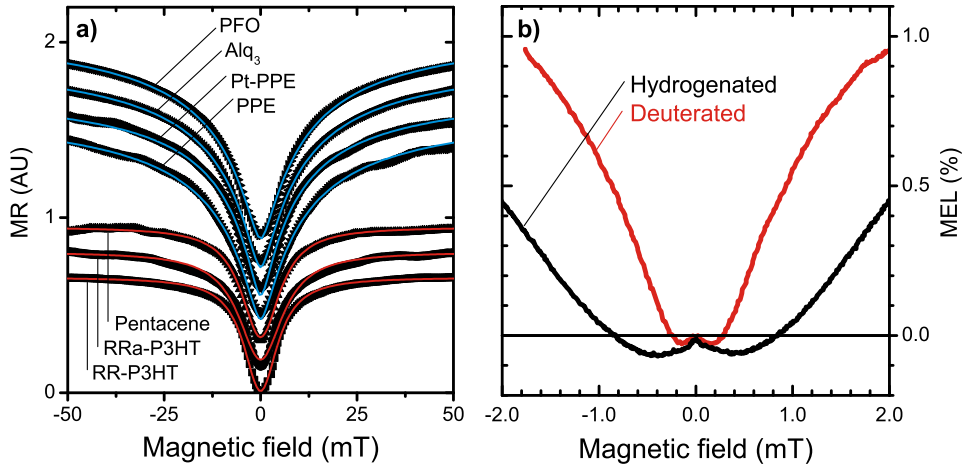

Figure 1.4 (a) Magnetoconductance as a function of the applied magnetic field for devices of several different organic semiconductors. The lineshape can either be fitted by a Lorentzian (red curves) or by a non-Lorentzian (blue curves). Figure adapted from Reference 74. (b) Magneto-electroluminescence as a function of the applied magnetic field for DOO-PPV (black) and its deuterated variant (red). Figure adapted from Reference 82.

are defined as

$$\mathrm{MFE}(B) = \frac{B^2}{B^2 + B_0^2} \qquad \text{(Lorentzian)}, \tag{1.6}$$

$$\mathrm{MFE}(B) = \frac{B^2}{(|B| + B_0)^2} \qquad \text{(non-Lorentzian)}, \tag{1.7}$$

where B is the applied magnetic field and B_0 is a material-dependent constant that is typically a few mT. (When comparing B_0 of different fits, it should be noted that fitting the same curve with both lineshapes results in different B_0.)

Often additional features are observed in the measured lineshape. So called *high-field effects* are observed: The saturation at high magnetic fields can be slower than that of the Lorentzian or non-Lorentzian lineshapes. The magnetic field effect could also saturate to a value that is lower than it was for intermediate fields. In addition, Nguyen and coworkers have observed a feature at small magnetic field (< 1 mT), which they have called *Ultra-Small-Magnetic-Field Effect* (USMFE), see Figure 1.4(b).[82] While Nguyen and coworkers explain the USMFE as arising from additional spin mixing due to level crossings at zero applied magnetic field, we have found that it can be explained by the competition between spin mixing and exciton formation, see Chapter 3.

1.2.2 Hyperfine interaction

It is known from the field of spin chemistry that reactions between spin-carrying molecules, or radicals, can have a magnetic-field dependence on a field scale of a few millitesla.[111] Because organic molecules consist of light atoms—like carbon,

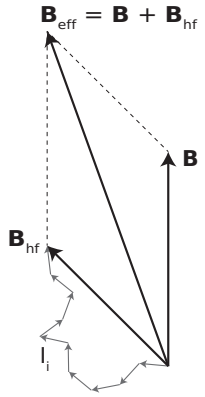

Figure 1.5 The hyperfine interactions of a polaron spin with the nuclear magnetic moments, I_i, of the atoms that make up the molecule can be approximated by a hyperfine field, $\mathbf{B}_{\mathrm{hf}}$, which is an effective static magnetic field, see the main text. The total magnetic field felt by the polaron, $\mathbf{B}_{\mathrm{eff}}$, is the sum of this hyperfine field and the applied magnetic field, $\mathbf{B}$.

oxygen, hydrogen and nitrogen—the spin-orbit interaction is generally weak (see the discussion later on in this section on page 12). The dominant interaction of electron or hole spins is the hyperfine interaction with the nuclear magnetic moments of hydrogen and nitrogen. (99% of the naturally occurring isotopes of carbon and oxygen have no nuclear magnetic moment.) In the so-called *radical-pair mechanism*, the reaction between two radicals in a pair depends on the pair's spin configuration. The hyperfine interaction mixes the singlet and triplet states and, therefore, affects the reaction rate between the radicals. Applying a magnetic field suppresses the spin mixing and leads to a different reaction rate.

Already in the paper by Frankevich[37] it was proposed that the same spin mixing by hyperfine fields is at the origin of the magnetic field effects. Most of the mechanisms that were later introduced to explain the magnetoconductance and magneto-electroluminescence—see the next section—rely on this spin mixing. The importance of hyperfine interactions was finally confirmed by deuteration experiments done by Nguyen *et al.*[82,83] They replaced the hydrogen atoms of DOO-PPV[¶] with deuterium atoms. Deuterium has a smaller magnetic moment, resulting in a smaller hyperfine interaction. The experiments showed that the linewidth scaled accordingly, see Figure 1.4. Similar experiments were done where naturally abundant carbon-12 atoms (which don't have a nuclear magnetic moment) were replaced by carbon-13 (which do have a nuclear magnetic moment). Again, the lineshape broadened as expected. A similar effect of deuteration was observed in experiments on Alq_3 by Rolfe *et al.*[97] An effect of deuteration was also found in magnetic resonance experiments performed on MEH-PPV[‖] by Lee *et al.*[62]

Semiclassical approximation

A typical organic molecule consists of many atoms—usually of the order of 10—that have a non-zero nuclear magnetic moment, $\mathbf{I}_i$. Taking hyperfine interactions between a polaron spin and all those nuclear magnetic moments into account individually is mathematically cumbersome and would not provide much insight into the problem. Instead, the effect of those nuclear magnetic moments on the polaron spin can be approximated by an effective static magnetic field, called the *hyperfine field*, as was shown by Schulten and Wolynes.[105] In this approximation, the nuclear magnetic moments are assumed to be randomly oriented and stationary on the time scales that the polaron resides on a molecule. The hyperfine field is then proportional to the sum of those randomly oriented magnetic moments times the hyperfine coupling constants, see Figure 1.5 on the preceding page. The resulting hyperfine fields are distributed according to a three-dimensional Gaussian distribution with standard deviation B_{hf}, given by[105]:

$$B_{\mathrm{hf}} = \sqrt{\frac{1}{3}\sum_i a_i^2 I_i(I_i+1)}, \tag{1.8}$$

where a_i is the hyperfine coupling constant with nucleus i. The hyperfine field is of the order of 1 mT and varies slightly depending on the specific molecule. Since the nuclear magnetic moments are now treated as a classical magnetic field while the polaron spin is still treated quantummechanically, this is called the *semiclassical approximation*.

McConnell rule

There are two contributions to the hyperfine interaction of a nuclear spin with an electron spin: the Fermi contact interaction, which is proportional to the electron density at the nucleus, and the magnetic dipolar interaction. Since the π-orbitals have no overlap with the hydrogen nuclei, one would expect the Fermi contact interaction to be zero, leaving only the dipolar interactions. This led to a paradox in the spin-chemistry field, where hyperfine interactions were observed for molecules in solution, whereas the tumbling of the molecules should have averaged out the dipolar interactions.[125] McConnell solved this paradox when he derived that the Fermi contact interaction on σ-electrons is transmitted to a π-electron via exchange coupling.[70] This has led to the *McConnell rule*[71] for the hyperfine coupling constant of a hydrogen nucleus:

$$a_i = Q\rho_i, \tag{1.9}$$

where ρ_i is the spin density on the carbon atom bonded to the hydrogen atom, and Q is a constant between 2.2 and 3 mT.

Consider now a (hypothetical) symmetric organic molecule with N hydrogen atoms. In that case, the spin density is homogeneously distributed ($\rho_i \sim 1/N$) and the hyperfine coupling constants are all identical ($a_i = a$). Combining Equations 1.8

¶ DOO-PPV: poly[2,5-dioctyloxy-1,4-*p*-phenylene vinylene]
‖ MEH-PPV: poly[2-methoxy-5-(2′-ethylhexyloxy)-*p*-phenylene vinylene]

and 1.9 yields $B_{\mathrm{hf}} \sim 1/\sqrt{N}$. Larger delocalization of an electron or hole leads therefore to a smaller hyperfine field. This has been experimentally confirmed for phenylene-vinylene oligomers.[133]

1.2.3 Spin-orbit coupling

Spin-orbit interaction in organic semiconductors is usually assumed to be negligible due to the absence of heavy atoms in those materials—the spin-orbit interaction scales with the number of protons Z as Z^4.** The assumption that spin-orbit interaction is negligible, obviously, does not hold for molecules that do contain heavy atoms, like CuPc†† and Ir(ppy)$_3$‡‡. In addition, Yu[131,132] has pointed out that also the non-planar geometry of molecules can give rise to a larger spin-orbit coupling than expected. He found that, especially, Alq$_3$ has a relatively strong spin-orbit coupling due to the orthogonal arrangement of its ligands.

With spin-orbit coupling, the energy eigenstates are no longer pure spin-up or spin-down states, but a mixture of both. This leads to a loss in spin polarization with every hop, independent of the hopping rate. This is in contrast to spin relaxation due to hyperfine interactions, where spin polarization is lost between hops, so that the amount of loss of spin polarization is proportional to the time between hops.[17] That time is inversely proportional to the hopping rate.

The loss in spin polarization due to spin-orbit coupling does not have a magnetic-field dependence.[132] The presence of spin-orbit coupling therefore reduces the magnetic-field dependence of spin mixing relative to the total amount of spin-mixing. That is, magnetic-field effects will become smaller. The observation of magnetic field effect, therefore, indicates that, in general, the effect on a polaron spin of spin-orbit coupling seems to be much weaker than the effect of hyperfine interactions.

1.2.4 Mechanisms

Since the discovery of magnetic field effects in organic semiconductors, several mechanisms have been proposed to explain those effects. These mechanisms can be divided in four groups, which are discussed below.

Bipolaron mechanism

The easiest understandable mechanism is the bipolaron mechanism.[16] This mechanism explains a magnetic-field-dependent current. A bipolaron is a (quasi)particle consisting of two equally charged polarons—either two electrons or two holes—on the same site. A polaron that has been trapped, either at a trap site or a site that happens to lie low in the Gaussian energy distribution, will block other polarons,

**Spin-orbit coupling is proportional to the nuclear charge Z and inversely proportional to the Bohr radius cubed. The Bohr radius is inversely proportional to the Z, making the spin-orbit coupling proportional to Z^4. See for example Reference 42.

††CuPc: copper phthalocyanine

‡‡Ir(ppy)$_3$: *fac*-tris(2-phenylpyridine) iridium

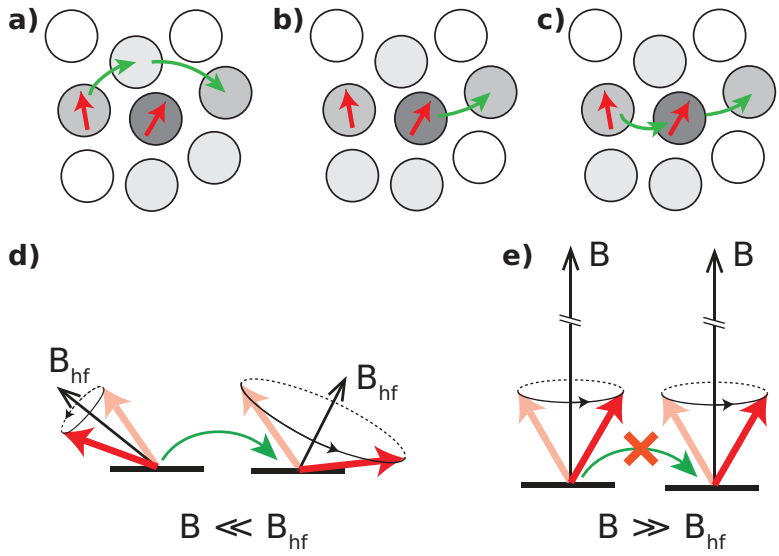

Figure 1.6 A trapped polaron (at the dark gray site) can block other polarons. For the current to flow, (a) the block polaron (at the left) has to hop around the trapped polaron, or (b) the trapped polaron has to detrap, or (c) the blocked polaron has to form a bipolaron with the trapped polaron. Bipolaron formation is only possible to the singlet state. (d) Spin precession about hyperfine fields, B_{hf}, leads to spin mixing and makes it possible for triplet polaron pairs to form (singlet) bipolarons as well. (e) When the external magnetic field, B, is much larger than the hyperfine fields, the spins will precess in sync and the spin mixing is suppressed. Now, a polaron pair that started as a T_+ (or T_-) triplet cannot form a bipolaron.

see Figure 1.6. For the current to flow, one of the following processes has to happen: a) The blocked polaron can hop around the trapped one. b) The trapped polaron can detrap. c) The blocked polaron can form a bipolaron on the trapped polaron's site, which in turn can dissociate, allowing effectively the passage of a polaron. The first two processes do not depend on the applied magnetic field, but the third does.

A bipolaron can only be formed in the singlet (ground) state, because the triplet state is much higher in energy[21,24] and has, therefore, a very small formation rate. Since spin is preserved during bipolaron formation (because of total spin conservation), whether or not a bipolaron can be formed depends on the spin configuration of the two polarons. The spins of two polarons that meet each other are random, so their spin configuration can be either a singlet or a triplet. In the latter case, bipolaron formation is not possible. However, the polarons' spins will precess about their different hyperfine fields and this will mix their spin configuration, allowing even those polarons that are initially triplets to form a bipolaron, see Figure 1.6(d). This is called *spin mixing*. If now an external magnetic field is applied, the spins will no longer precess about the hyperfine fields, but about the *effective magnetic fields* which are the sum of the hyperfine fields and the external magnetic field. When the external magnetic field is larger than the hyperfine fields, the effective magnetic fields that both spins experience will be

aligned, see Figure 1.6(e). As a result, the two spins will now only dephase. That is, the T_- and T_+ triplets no longer mix with the singlet and T_0 triplet. Two polarons that are initially in one of those triplet states cannot form a bipolaron. This, in turn, leads to a lower current.

In this way, the bipolaron mechanism leads to a negative magnetoconductance, that is, a current that decreases as a function of the applied magnetic field. The bipolaron mechanism could also lead to positive magnetoconductance in two ways. Using Monte Carlo simulations, Bobbert *et al.* have shown that a positive magnetoconductance could results from this mechanism due to an increase in the number of polarons when bipolaron formation is decreased when an magnetic field is applied.[16] Because polarons are mobile and bipolarons are not, an increase in polarons leads to an increase in current. The second way in which the bipolaron mechanism can lead to positive magnetoconductance is via the sign-change mechanism introduced by Bloom *et al.* in the case of a space-charge-limited current.[12] A decrease in the mobility of, say, the electrons could lead to an increase in the total space charge and thereby to an increase in the current.

The other mechanisms described below all rely on the presence of both holes and electrons. When magnetoconduction is observed in a unipolar device (hole only or electron only) it is likely due to the bipolaron mechanism. Indeed a small negative magnetoconduction of about 1% and less has been observed in unipolar devices and has been attributed to bipolaron formation.[5,82,124] Recently, a magnetoconduction of up to 0.6% has been measured in an organic field-effect transistor, which could be due to the bipolaron mechanism.[94] A possible reason for the relatively small size of this effect is the large formation energy of a bipolaron. The Coulomb repulsion of two equally charged polarons on the same site is partially offset because of the shared relaxation of the atomic configuration. Although the resulting bipolaron formation energy U can be as small as 0.1 to 0.3 eV for PPV or perylene,[45,67,117] this is still several times larger than the thermal energy of 25 meV at room temperature. The rates for the processes circumventing bipolaron formation [Figure 1.6(a) and (b)] are not much smaller (if at all) than the rate for bipolaron formation.

The energetically disordered nature of organic semiconductors probably plays an important role, as it leads both to filamentary charge transport as well as trapping of polarons, thereby reducing the rates of the processes shown in Figure 1.6(a) and (b). Indeed, taking filamentary transport to its extreme—to completely one-dimensional transport—will lead to very large magnetic field effects, as will be shown in Chapters 5 and 6.

Electron-hole mechanisms

It turns out to be quite difficult to make a completely unipolar device and often a device is bipolar by its very nature, like in the case of an OLED where one wants electrons and holes to form excitons. Moreover, the largest magnetic field effects have been measured in bipolar devices.

As explained earlier in the context of OLEDs, electron-hole pairs that meet randomly can be either in a singlet or in a triplet configuration. Like for bipolaron formation, hyperfine fields can mix the spin configuration between singlet and triplet states and an externally applied magnetic field can suppress this mixing. If the formation rates for singlets and triplets are different, this will lead to a magnetic-field-dependent fraction of singlet excitons and subsequently to a magnetic-field-dependent light output—magneto-electroluminescence. This is discussed in more detail in Chapter 3.

How the current reacts to a change in the exciton formation rate, and thus to what magnetoconduction it leads, depends on the device physics. Several mechanisms have been proposed:

1. In a space-charge-limited device, the magnetic field dependence of the exciton formation rate affects the current through the recombination mobility in Equation 1.4.[9,48,92]

2. In a recombination-limited device, like a liquid electro-chemical cell with two sharply separated regions of n-doping and p-doping,[93] the device is separated into two regions with either only electrons or only holes, which meet in a narrow recombination zone. In such a device, the current is proportional to the recombination rate. A magnetic field effect in the exciton formation rate will, in this case, directly affect the current through the device.

3. In a device that is neither space-charge-limited nor recombination-limited, the formation of a Coulombically bound polaron pair takes away two charges that would otherwise contribute to the current. The recombination rate of that polaron pair affects the probability of its dissociation.[48] If the pair dissociates, the electron and hole can again contribute to the current.

4. Finally, the amount of triplet excitons that are formed can affect the current. As explained earlier, singlets can decay radiatively, while triplets cannot. As a result, triplets have a much longer life time. The amount of triplets present can have an effect on the current in several ways. The triplets can simply hinder the movement of electrons and holes, thereby reducing the current. A triplet exciton can also detrap a charge while decaying to the ground state, thereby creating a free charge that can contribute to the current.[48] Since triplets have a non-zero spin, their interaction with polarons has a magnetic field dependence as well. This will be discussed next.

Charge-triplet mechanisms

A triplet exciton can diffuse to a trapped charge and detrap the charge while decaying to the ground state. In this way, trapped charges can be freed and the resulting increase in free charges will lead to a larger current.[48] The final result of this process is a single free charge, which is a spin doublet. This process can, therefore, only happen when the initial charge–triplet exciton pair is a doublet as

well. The other possible initial spin configuration, a quartet, cannot lead to detrapping in this way. As for the mechanisms described before, hyperfine fields will mix the quartet and doublet states of the charge-triplet pair. Again, a magnetic field dependence arises because the spin mixing can be suppressed by an external magnetic field. Unlike the previous mechanisms, though, the width of the lineshape is now determined by the zero-field splitting of the triplet exciton: The effect of the hyperfine interactions on the linewidth is cancelled out when an average is taken over all possible hyperfine field.[103] The zero-field splitting is the splitting of the triplet energy levels even in absence of an applied magnetic field and is typically about 100 mT.[38,87]

Triplet-triplet annihilation

One of the first magnetic field effects observed in organic semiconductors was in the delayed fluorescence due to triplet-triplet annihilation.[52] When two triplets annihilate each other, light is emitted. This effect is found to increase the efficacy of an OLED in some cases.[59,134] Two triplets can only annihilate when their combined spin configuration is a singlet. Just as for charge-triplet interactions, hyperfine fields and the zero-field splitting lead to spin mixing that can be suppressed by an applied magnetic field. This results in a magneto-electroluminescence with a linewidth determined by the zero-field splitting.[103,134,135]

1.2.5 Δg-effect

Besides hyperfine interactions, there is a second mechanism that gives rise to spin mixing, which is related to the difference in g-factors between an electron and a hole. But unlike hyperfine interactions, this so-called Δg-effect leads to spin mixing at large—instead of small—applied magnetic fields.

To understand how the Δg-effect leads to spin mixing, consider an electron in a magnetic field B. The spin of that electron will precess about the magnetic field with a frequency given by

$$f_B = g\mu_B B/h, \tag{1.10}$$

where g is the g-factor, μ_B is the Bohr magneton, and h is Planck's constant. The g-factor for an electron spin in vacuum has been measured to great accuracy and its first eight digits are 2.0023193. Due to the (weak) spin-orbit interactions in organic semiconductors, the g-factor of a polaron will be slightly different from that of a free electron and will be different for hole and electron polarons. In addition, it will vary slightly throughout the organic semiconductor. In Reference 132, g-factors for several commonly used molecules and polymers are listed.

The difference in g-factors, Δg, of two polarons will lead to a difference in precession frequency, $\Delta f_B = \Delta g \mu_B B/h$, proportional to the applied magnetic field. The resulting dephasing of the polaron pair's spin configuration leads to an increase in spin mixing between the singlet and T_0 triplet, partially compensating for the loss in spin mixing due to the alignment of the effective magnetic fields.

In the literature, the Δg-effect has been proposed to explain a $\sqrt{B}$ dependence of the magneto-electroluminescence at high applied magnetic fields.[124] However, a Lorentzian lineshape was found from calculations by Schellekens and coworkers.[103] Moreover, the difference in g-factors of $\sim$1% needed to explain the measurements on organic semiconductors is unrealistically large.[132] It is, therefore, not completely clear whether the Δg-effect is indeed the cause of the measured $\sqrt{B}$ dependence.

1.2.6 Traps

In 2008, Niedermeier and coworkers[86] discovered that in a polymer OLED, the magnetoresistance could be increased from $\sim$1% to more than 15% by operating it for an hour at a current density (125 mA/cm^2) much higher than under normal operating conditions (< 1 mA/cm^2). They called this procedure *conditioning*. In a follow-up paper,[3] they showed that the effect was reversed after keeping the device a few days at room temperature or after a few hours at $\sim$420 K. Conditioning could increase the magnetic field effect again and this cycle was repeatable several times. This suggests that not chemical changes but morphological changes lie at the origin of the enhanced magnetic field effects. In the same paper, the creation of traps by conditioning is put forth as the source of the enhancement. They showed that the enhancement could be (partially) countered by illumination with infrared light, which detraps charges.

More recently, a similar increase in the magnetoconduction was reported by Rybicki and coworkers.[99] They created traps by irradiating the device with x-rays, which create traps with a depth of $\sim$0.5 eV. By varying the duration of the irradiation, the number of traps created could be tuned. A stronger increase in the magnetoconductance was observed for longer durations.

There are also indications that traps created by exposure of the organic material to air can lead to an increased magnetic field effect. Kanemoto *et al.*[54] reported that an air-treated MEH-PPV diode showed a much larger transient Electrically Detected Magnetic Resonance (EDMR) (see the next section) response than the untreated device. They also observed an increase in EDMR linewidth after air-treatment, indicating that indeed polarons on different kinds of sites—intrinsic sites and trap sites that have been created by the air-treatment—are responsible for the increase in magnetic field effect.

Why the presence of traps increases the magnetoconduction and magneto-electroluminescence is not entirely clear. All the mechanisms that are described in the previous section rely on reactions between two (quasi)particles—polarons, triplets, etc. One possible explanation is that it is easier for two particles to meet when one is fixed (trapped) than when both can move around. In addition, the bipolaron mechanism relies on polarons being blocked by a trapped polaron. It is expected that more traps will lead to more spin-blocked polaron pairs. Furthermore, the trap depth could partially offset the bipolaron formation energy, making the mag-

netic-field-dependent bipolaron formation more favourable than the alternative processes (see Section 1.2.4).

1.2.7 Electrically detected magnetic resonance

In what has been discussed up to now, hyperfine fields lead to spin mixing that can be suppressed by applying an external magnetic field. It is, however, also possible to introduce other ways of spin mixing. A powerful way of doing this is by means of spin resonance. Depending on whether the effect of the additional spin mixing is detected in the light output or in the current, this technique is called *Optically Detected Magnetic Resonance* (ODMR) or *Electrically Detected Magnetic Resonance* (EDMR).[§§]

When a magnetic field B is applied to a device, the energy levels of spin-up and spin-down polarons in this field will split with an energy difference $\Delta E = g\mu_B B$. In the presence of electromagnetic radiation, the polaron spin can oscillate between the spin-up and spin-down states. These so-called Rabi oscillations happen only when the frequency of the electromagnetic radiation exactly matches the energy splitting of the spin-up and spin-down states, that is, when the resonance condition is fulfilled. Since two polarons that are about to form a bipolaron or an exciton experience different hyperfine fields and can have different g-factors, their resonance conditions differ. Therefore, it is possible to make only one of the two polarons resonate, leading to mixing of their spin configuration. In a typical EDMR experiment, the change in current is measured when the applied magnetic field is swept while the frequency of the electromagnetic radiation is kept constant. A peak in the current will occur when the applied magnetic field matches the resonance condition. The g-factor can then be derived from the peak position and the peak width is a measure for the strength of the hyperfine fields. McCamey *et al.* used this technique to establish that, in their MEH-PPV OLED, a reaction takes place between two polarons that experience hyperfine fields of different magnitude.[68]

Even more information can be obtained by using Pulsed EDMR (PEDMR). Instead of continuous electromagnetic radiation, a pulse of a definite length is used. When the resonance condition is fulfilled, the oscillating magnetic field of the pulse acts as a static field in the reference frame that rotates with a spin that precesses about the applied magnetic field. The spin will rotate away from the direction of the applied magnetic field over an angle that is proportional to the pulse length and its power—the power is proportional to the magnitude of the pulse's oscillating magnetic field. A rotation over π will results in the maximal change in current, while a rotation of 2π yields no change at all. From the decay of the Rabi oscillations with increasing pulse lengths, it has been established that the spin lifetime in MEH-PPV OLEDs is larger than 0.5 μs.[68,69]

[§§] As a side note: Similar experiments on the behaviour of European Robins—a migratory bird that possibly has a compass based on the radical-pair mechanism—subject to resonant radio waves have been dubbed *Animal-Detected Magnetic Resonance*, see for example Reference 95.

1.2.8 Fringe fields

Another way of controlling the amount of spin mixing is with the fringe fields of a magnetic layer. Near a magnetic layer, a fluctuating magnetic field (a fringe field) is present with a strength and correlation length that depend on the domain structure and thickness of the magnetic layer and the distance from the layer. These fringe field lead to spin mixing in a similar way as the random hyperfine fields do. Cohen has proposed to use the fringe fields of magnetic nanoparticles to influence the reaction rate of molecules around them via the radical-pair mechanism.[27] The same idea was applied to organic semiconductors by Wang and coworkers.[123] They used a magnetic layer that generates fringe fields when its magnetisation is switched by an applied magnetic field. A magnetoconductivity of about 10% was observed.

1.2.9 Spin valves

The subject of this thesis is magnetic field effects that originate in the bulk of a device without magnetic electrodes. However, there is a second class of organic magnetic field effects, caused by some mechanism at the interfaces between the organic semiconductor and magnetic electrodes. The spin-OLED that was already mentioned before is an example of this kind of devices, but the most prominent one is the spin valve. A spin valve consists of two magnetic electrodes with a non-magnetic layer between them. Spin-polarized charges are injected from one electrode, pass through the non-magnetic layer, and are collected at the other electrode. The collection efficiency depends on the charge's spin direction with respect to the polarization of the collecting electrode. The current through the device depends, therefore, on the relative orientation of the polarizations of the electrodes.

The demonstration of an organic spin valve would prove that spin injection from magnetic electrodes is possible. Spin injection is one of the requirements for making organic spintronics devices—devices that use the electronic spin to process information.[31,78,101,102] Several claims have been made in the literature about working organic spin valves, see Reference 31 and references therein. Typically, magnetic field effects of 30–40% are found at 10 K while less than 1% remains at room temperature.

However, several other effects look very much like the spin valve effect. An example is the fringe-field effect mentioned above.[100,123] Also, the tunnelling anisotropic magnetoresistance, which arises from magnetic-field-dependent injection from a magnetic electrode due to strong spin-orbit interaction, has similar features as the spin valve effect.[41] The definite proof of a working spin valve would be the observation of the Hanle effect.[50,63] The Hanle effect is the periodic dependence of the current through a spin valve on an applied magnetic field perpendicular to the magnetisation direction of the electrodes. The applied magnetic field causes the polarisation of the injected electrons to rotate a certain angle proportional to the magnitude of the magnetic field and the time it takes the electrons to reach

the collecting electrode. Since the current through a spin valve depends on the angle between the polarisation of the electrons that reach the collecting electrode and that electrode's magnetisation direction, the current will depend periodically on the applied magnetic field. Calculations by Wagemans (pages 86 and 87 of Reference 120) show that even in a disordered organic semiconductor—where the time it takes electrons to reach the collecting electrode is not shapely defined—the Hanle effect should be observable. However, no Hanle effect has been observed in organic spin valves to date. On the order hand, two-photon photo-emission experiments by Cinchetti *et al.*[26] and muon spin rotation experiments by Drew *et al.*[34] indicate that spin injection into an organic semiconductor is indeed possible. The absence of spin detection at the collector (or the independence of the current on the spin detection at the collector) might therefore be the reason for the failure to observe the Hanle effect.

1.3 Outline of this thesis

The goals of this thesis are to both explain experimentally observed magnetic field effects as well as to make predictions for even larger effects in organic semiconductors. The theoretical frameworks with which these effects are described are Stochastic Liouville equations and Monte Carlo simulations. Both are described in **Chapter 2**. The question whether the statistical singlet–versus–triplet exciton ratio can be violated and the connection of this issue with magneto-electroluminescence will be investigated in **Chapter 3** using a two-site model for which we solve the stochastic Liouville equation. In addition, it will be shown that the recently measured ultra-small-magnetic-field effect can be explained with our model. It is argued that the largest magnetic-field effects are expected when hopping is slower than the hyperfine frequency. However, modelling of the charge mobility in polymers has shown that the hopping rate might not be that slow. This paradox is solved in **Chapter 4** when the role played by energetic disorder is discussed using a multi-site model. In that chapter we get to the limitations of the Stochastic Liouville equation, with which only a relatively small number of sites and charges can be described. To investigate larger systems and, more importantly, systems containing more than two charges, Monte Carlo simulations can be used. In **Chapter 5**, we do such simulations, to show that huge magnetoconductance and magnetodiffusion in doped polymers can occur for vanishingly small applied electric fields. The huge effects are found to be the result of interactions between the charges and of the one-dimensionality of the system. In **Chapter 6**, similar simulations are used to explain the huge magnetoconduction that was measured in wires of molecules embedded in a zeolite crystal. The spin blocking resulting from bipolaron formation is found to be very effective in this one-dimensional system. It is shown that the magnetoconductance is further enhanced by the presence of traps. The magnetic field effects described in Chapters 3 to 6 results from spin mixing by hyperfine fields. In **Chapter 7**, we investigate a magnetic field effect that is caused by a difference in magnitude of the local magnetic fields experienced by two polarons. This mechanism could explain the magnetoconductance that

was recently observed in organic devices where the fringe fields of a magnetic layer give rise to a magnetic field that varies from site to site. In **Chapter 8**, the main conclusions of of this thesis are summarised and an outlook on the future of modelling of magnetic field effects in organic semiconductors is given.

2

Analytical and numerical methods

The analytical and numerical methods used in this thesis will be described in this chapter. The spin state of two polarons that encounter each other is unknown. This uncertainty can be described by the density operator formalism, of which a short introduction will be given. While spin precession is a coherent process, hopping of a polaron is an incoherent process. To describe the spin-dependent hopping processes that lie at the origin of magnetic field effects in organic materials, coherent and incoherent processes need to be treated at the same time. For that, a stochastic Liouville equation, an extension of the Liouville equation in the density matrix formalism, is introduced next. Special attention is given to the slow-hopping limit. In this limit, spin-dependent hopping can be described with simple rate equations. This allows us to perform Monte Carlo simulations, which are discussed next. Finally, it is shown how the rate equations for a hopping polaron can be mapped onto a resistor network. The current through the latter can easily be calculated.

2.1 Density operator formalism

The Schrödinger equation can be used to describe the evolution of a system that is in a single, known quantum state. When it is only known with a certain probability in which state the system is—or when describing an ensemble of systems, each possibly in a different state—the density operator formalism, developed by von Neumann, can be used.[14,35,118] Consider a quantum system with a Hamiltonian H and a basis of states $|\psi_j\rangle$ that span the Hilbert space—for example, the eigenstates of H. The *density operator* for this system is

$$\rho = \sum_j p_j |\psi_j\rangle\langle\psi_j|, \tag{2.1}$$

where p_j is the probability that the system is in $|\psi_j\rangle$. Because the sum of all the probabilities is unity, the following equation should hold: $\mathrm{Tr}[\rho] = \sum_j p_j = 1$. The

probability that the system is in an arbitrary state $|\chi\rangle$ is given by $\mathrm{Tr}[|\chi\rangle\langle\chi|\rho]$. The density operator contains all information that can be known about the system.

When a basis has been chosen, a *density matrix* can be constructed that has the elements $\rho_{ij} = \langle\psi_i|\rho|\psi_j\rangle$. It is often more convenient to work with the elements of the density matrix than with the density operator, especially when doing numerical calculations. The probability of finding the system in state i is given by the diagonal element ρ_{ii} of the density matrix.

If there is a basis $|\phi_i\rangle$ for which $p_1 = 1$ and all other $p_i = 0$, the density operator is a *pure* state. If no such basis exists, the operator is in a *mixed* state. The latter could be the case if there is uncertainty about the state of the system. Also, the entangled subsystems of a pure state are mixed states. An example of two entangled subsystems that is relevant for this thesis are the position and spin of a polaron and its phonons. The phonon systems absorbs (gives) the energy that is released (needed) for a hop of the polaron downwards (upwards) in energy.

If there is complete uncertainty about the state of the system, the density matrix is proportional to the identity operator. The density matrix is then diagonal with all diagonal elements equal to $1/n$, where n is the dimension of the matrix.

The expectation value of an observable O can be found from the density operator:

$$\langle O\rangle = \sum_j p_j \langle\psi_j|O|\psi_j\rangle = \mathrm{Tr}[\rho O]\,. \tag{2.2}$$

Using the Schrödinger equation it is easy to derive that the time evolution of the density operator is given by the Liouville-von Neumann equation:

$$\frac{\partial\rho}{\partial t} = -\frac{i}{\hbar}[H,\rho], \tag{2.3}$$

where $\hbar$ is the reduced Planck constant and $[\,\cdot\,,\cdot\,]$ is the commutator.

If the density operator can be written in the form of Equation 2.1 on the preceding page for a basis $|\chi_i\rangle$, it means that there is just uncertainty about in which of those basis states the system is—the system is not in a superposition of several basis states. If, in addition, the basis $|\chi_i\rangle$ is the basis of the energy eigenstates, then the density operator will not evolve in time. That can be found easily from Equation 2.3, as the $|\chi_i\rangle\langle\chi_i|$ operators commute with each other and both ρ and H are linear combinations of them.

2.2 Stochastic Liouville equation

While taking into account the uncertainty in the initial state, the Liouville-von Neumann equation only describes the coherent evolution of the density operator. In many cases, it is not desirable of even possible to treat the whole system quantum mechanically when one is only interested in the behavior of a subsystem.

For example, hopping of polarons in an organic semiconductor takes place by interactions with the phonons of the material, which provide or absorb the energy difference between the initial and final states of the polaron. However, we are only interested in the behavior of the polaron and not in the detailed evolution of the phonon system. Moreover, the phonon system is material dependent, while hopping and magnetic field effects are much less so. Therefore, we want to have a description in which the phonon system is not explicitly considered.

When the subsystem that one is not interested in consists of a large number of small interactions with the subsystem of interest, the former can be treated in a stochastic way.[114] This idea was used by Anderson[2] and Kubo[60] to explain the observed lineshapes of magnetic resonance absorption. This led to *stochastic Liouville equations*, which extend the Liouville-von Neumann equation to include stochastic or incoherent interactions.

Stochastic Liouville equations in the form as used in this thesis were introduced in 1970 by Johnson and Merrifield[51] for studying the magnetic field dependence of triplet-triplet annihilation in anthracene crystals. They used a stochastic Liouville equation that models the annihilation of two reacting triplet excitons, taking into account an external magnetic field and dipolar interactions. Later, hyperfine fields were taken into account as well.[43] Stochastic Liouville equations describing hopping between more than two sites were first introduced by Suna *et al.*[112] for their study of triplet-triplet annihilation.

2.2.1 General model

In this thesis we use stochastic Liouville equations to describe one or two spin-carrying (quasi)particles on a lattice of sites N. Every site i, with $1 \leq i \leq N$, has a random energy E_i taken from a Gaussian distribution with standard deviation σ, see Section 1.1.1 on page 2. Furthermore, at every site i there is an effective magnetic field $\mathbf{B}_{\mathrm{eff},i}$ that is the sum of an externally applied magnetic field $\mathbf{B}$ and the site's hyperfine field $\mathbf{B}_{\mathrm{hf},i}$, taken from a three-dimensional Gaussian distribution, see Section 1.2.2 on page 11. Below, we will consider the case of two particles, as the case for one particle easily follows from it.

For every *positional configuration*, denoted by (i,j), with the first particle on site i and the second particle on site j, there is a density operator $\rho_{(i,j)}$, describing the spin state of the two particles when they are on those two sites.* Since every density operator $\rho_{(i,j)}$ describes only a single possible configuration, its trace is equal to the probability of the system being in that configuration. The sum of all those traces is equal to unity: $\sum_{i,j} \mathrm{Tr}\left[\rho_{(i,j)}\right] = 1$. For every configuration, there is a Hamiltonian $H_{(i,j)}$ that describes the evolution of the particles' spins:

$$H_{(i,j)} = g\mu_{\mathrm{B}}\mathbf{B}_{\mathrm{eff},i} \cdot \mathbf{S}_1/\hbar + g\mu_{\mathrm{B}}\mathbf{B}_{\mathrm{eff},j} \cdot \mathbf{S}_2/\hbar, \tag{2.4}$$

*Although it is possible to use a single, large density operator to describe the whole system, it is more intuitive to consider several coupled density operators.

where g is the g-factor, μ_B is the Bohr magneton, $\mathbf{S}_m$ is the spin operator for particle $m = 1, 2$, and $\hbar$ is the reduced Planck constant. The time evolution of the density operators is then given by the following stochastic Liouville equation:

$$\frac{\partial \rho_{(i,j)}}{\partial t} = -\frac{i}{\hbar}\left[H_{(i,j)}, \rho_{(i,j)}\right] - \frac{1}{2}\left\{\Lambda_{(i,j)}, \rho_{(i,j)}\right\} + \Gamma_{(i,j)}, \tag{2.5}$$

where $\{\cdot, \cdot\}$ is the anticommutator. The first term on the right hand side is the same as in the Liouville-von Neumann equation and accounts for the (coherent) evolution of the spins of the particles involved.

The second term accounts for the decrease of the population of the density operator, for example due to hopping to another site or exciton formation. The operator $\Lambda_{(i,j)}$ contains one term for every process by which the population of density operator $\rho_{(i,j)}$ can decrease. For example, the part of $\Lambda_{(i,j)}$ accounting for hopping of particle 2 from site j to sites k is simply given by:[†]

$$\sum_k r_{j\to k}, \tag{2.6}$$

where the summation is over all sites k to which particle 2 can hop from site j. The hopping rate $r_{j\to k}$ depends on the energy difference between the two sites and could be the Miller-Abrahams or the Marcus hopping rate, see Section 1.1.1 on page 3. In the case of a spin-dependent process, like bipolaron formation or exciton formation, the operator $\Lambda_{(i,j)}$ contains projections onto the spin subspaces multiplied by the rates with which the process happens. For bipolaron formation, which can occur only to the singlet state, on either site i or site j, $\Lambda_{(i,j)}$ contains the terms:

$$r^{\text{bip}}_{i\to j}|\mathrm{S}\rangle\langle\mathrm{S}| + r^{\text{bip}}_{j\to i}|\mathrm{S}\rangle\langle\mathrm{S}|, \tag{2.7}$$

where $r^{\text{bip}}_{i\to j}$ is rate for forming a bipolaron on site j and $|\mathrm{S}\rangle$ is the singlet state.

In the last term of the Stochastic Liouville equation, the source operator $\Gamma_{(i,j)}$ accounts for the increase of population of density operator $\rho_{(i,j)}$. For every process that increases the population of $\rho_{(i,j)}$, $\Gamma_{(i,j)}$ contains a source term. For example, for hops of particle 2 from sites k to site j with a rate $r_{k\to j}$, the source operator $\Gamma_{(i,j)}$ contains the following term:[‡]

$$\sum_k r_{k\to j}\,\rho_{(i,k)}, \tag{2.8}$$

where the summation is over all sites k from which particle 2 can hop to site j.

[†]This expression is valid in the limit of vanishing particle densities. For a higher density, an additional factor $(1 - \mathrm{Tr}[\rho_{(i,k)}])$ should be included, because the hop is only possible to an empty site. In this thesis, stochastic Liouville equations are only used in the low density limit.

[‡]This expression is valid in the limit of vanishing particle densities. For higher densities a factor $(1 - \mathrm{Tr}[\rho_{(i,j)}])$ should be included. See the footnote for Equation 2.6.

2.2.2 Solving Stochastic Liouville equations

The system of stochastic Liouville equations just described is a complicated system of coupled differential equations. We solve it by transforming it into a single matrix equation as follows. Consider, for every density operator $\rho_{(i,j)}$, the density matrix with respect to the energy eigenstates of $H_{(i,j)}$. The elements of these matrices, $\rho_{(i,j)\sigma\tau}$, where i and j run over all sites and σ and τ run over the basis states of $H_{(i,j)}$, can be written as a single vector $\tilde{\rho}$. The time evolution of this vector is given by:

$$\frac{\partial\tilde{\rho}}{\partial t} = M\tilde{\rho}. \tag{2.9}$$

Here, M is a time-independent matrix that follows directly form Equation 2.5 on the facing page. The solution to Equation 2.9 is $\tilde{\rho}(t) = \exp(Mt)\tilde{\rho}_0$, where $\tilde{\rho}_0$ is the initial condition. There is a transformation T, such that $D = TMT^{-1}$ is a diagonal matrix with the eigenvalues m_i of M. With this transformation, it is easy to get an expression for $\tilde{\rho}(t)$:

$$\tilde{\rho}(t) = \exp(T^{-1}DT)\rho_0 = T^{-1}\exp(Dt)T\rho_0 = T^{-1}\mathrm{diag}\left(e^{m_i t}\right)T\tilde{\rho}_0, \tag{2.10}$$

where $\mathrm{diag}(a_i)$ is a diagonal matrix with elements a_i.

If $\det M = 0$, there is a non-trivial steady-state solution that can be found from solving $M\tilde{\rho} = 0$.

2.2.3 Slow hopping

An interesting and important limit to consider is the *slow-hopping* limit. In this limit, hopping takes place much slower than the spin precession about the hyperfine fields: $k_{\mathrm{hop}} \ll \omega_{\mathrm{hf}}$, where $\omega_{\mathrm{hf}} = g\mu_{\mathrm{B}}B_{\mathrm{hf}}/\hbar$ is the *hyperfine frequency*, which is $2.8 \cdot 10^7$ Hz for a typical hyperfine field of 1 mT and $g = 2$. The maximum possible amount of spin mixing takes place in the slow-hopping limit. Therefore, the largest magnetic field effects are expected in this limit. Taking this limit also drastically simplifies the way calculations can be done, as will be shown for hopping between two sites.

Consider two sites, 1 and 2, and a single polaron, hopping from site 1 to site 2. The spin Hamiltonian for the polaron on site 1 (site 2) is given by

$$H_{1(2)} = g\mu_{\mathrm{B}}\mathbf{B}_{\mathrm{eff},1(2)} \cdot \mathbf{S}/\hbar, \tag{2.11}$$

where $\mathbf{B}_{\mathrm{eff},1(2)}$ is the effective magnetic field on site 1 (site 2) and $\mathbf{S}$ is the spin operator for the polaron. The eigenstates of this Hamiltonian for site 1 are denoted by $|\uparrow\rangle$ and $|\downarrow\rangle$ and those for site 2 by $|\Uparrow\rangle$ and $|\Downarrow\rangle$, see Figure 2.1 on page 29. Initially, site 2 is empty and site 1 is occupied by the polaron. Let us assume that the polaron is in one of the energy eigenstates of site 1: To be specific, assume it is in $|\uparrow\rangle$ with a probability $P_\uparrow$ and in $|\downarrow\rangle$ with probability $P_\downarrow = 1 - P_\uparrow$. Therefore, for the density operators at $t = 0$, we have $\rho_2(0) = 0$ for the configuration where the

polaron is on site 2 and $\rho_1(0) = P_\downarrow|\downarrow\rangle\langle\downarrow| + P_\uparrow|\uparrow\rangle\langle\uparrow|$ for the configuration where the polaron is on site 1.[§]

As the polaron hops to site 2, the evolution of ρ_1 is given by the following stochastic Liouville equation:

$$\frac{\partial\rho_1}{\partial t} = -\frac{i}{\hbar}\big[H_1, \rho_1\big] - k_{\text{hop}}\rho_1 \tag{2.12}$$

$$= -k_{\text{hop}}\rho_1, \tag{2.13}$$

where k_{hop} is the hopping rate. The solution to this equation is:

$$\rho_1(t) = \rho_1(0)\exp(-k_{\text{hop}}t). \tag{2.14}$$

For the density operator of site 2, it is convenient to work with the matrix elements of the density matrix with respect to the local eigenstates. Their time evolution is given by:

$$\frac{\partial\langle\sigma|\rho_2|\tau\rangle}{\partial t} = -i\omega_{\sigma\tau}\langle\sigma|\rho_2|\tau\rangle + \Big(\langle\sigma|\uparrow\rangle\langle\uparrow|\tau\rangle P_\uparrow + \langle\sigma|\downarrow\rangle\langle\downarrow|\tau\rangle P_\downarrow\Big)k_{\text{hop}}e^{-k_{\text{hop}}t}, \tag{2.15}$$

where $\sigma, \tau = \Uparrow, \Downarrow$ and $\omega_{\sigma\tau} = (E_\sigma - E_\tau)/\hbar$ with $H_2|\sigma\rangle = E_\sigma|\sigma\rangle$. The solution for $t \gg 1/k_{\text{hop}}$ when the hop has happened is:

$$\langle\sigma|\rho_2|\tau\rangle = \begin{cases} \frac{k_{\text{hop}}}{i2\omega_{\sigma\tau}+k_{\text{hop}}}e^{-2i\omega_{\sigma\tau}t}\Big(\langle\sigma|\uparrow\rangle\langle\uparrow|\tau\rangle P_\uparrow + \langle\sigma|\downarrow\rangle\langle\downarrow|\tau\rangle P_\downarrow\Big), & \text{if } \sigma \neq \tau, \\ |\langle\sigma|\uparrow\rangle|^2 P_\uparrow + |\langle\sigma|\downarrow\rangle|^2 P_\downarrow, & \text{if } \sigma = \tau. \end{cases} \tag{2.16}$$

In the case of slow hopping we have $\omega_{\sigma\tau} \approx \omega_{\text{hf}} \gg k_{\text{hop}}$ and therefore the elements with $\sigma \neq \tau$ are all zero. That is, after the hop the spin will again be in one of the local eigenstates $|\Uparrow\rangle$ or $|\Downarrow\rangle$ with probabilities $|\langle\Uparrow|\uparrow\rangle|^2 P_\uparrow + |\langle\Uparrow|\downarrow\rangle|^2 P_\downarrow$ and $|\langle\Downarrow|\uparrow\rangle|^2 P_\uparrow + |\langle\Downarrow|\downarrow\rangle|^2 P_\downarrow$, respectively.

Rates

In the slow-hopping limit, *hopping can thus be considered as taking place between energy eigenstates of the spin Hamiltonians of the source and target sites*. For example, the spin-dependent hopping rate from $|\uparrow\rangle$ on site 1 to $|\Uparrow\rangle$ on site 2 equals:

$$\tilde{k}_{1\uparrow\to 2\Uparrow} = k_{1\to 2}|\langle\uparrow|\Uparrow\rangle|^2, \tag{2.17}$$

where $k_{1\to 2}$ is the spin-independent hopping rate. The *spin projection factors* $|\langle\sigma|\tau\rangle|^2$ depend only on the angle θ between the hyperfine fields of the two sites and are given in Table 2.1 on the facing page. Hopping of a polaron is illustrated in Figure 2.1.

[§]Including also $|\downarrow\rangle\langle\uparrow|$ and $|\uparrow\rangle\langle\downarrow|$ in $\rho_1(0)$ has no effect on the final result. Furthermore, as we will see, the end result of a hop in the slow-hopping limit is exactly a density matrix like $\rho_1(0)$ with only contributions from $|\uparrow\rangle\langle\uparrow|$ and $|\downarrow\rangle\langle\downarrow|$. The assumption that the spin is either in $|\uparrow\rangle$ or $|\downarrow\rangle$ is therefore justified.

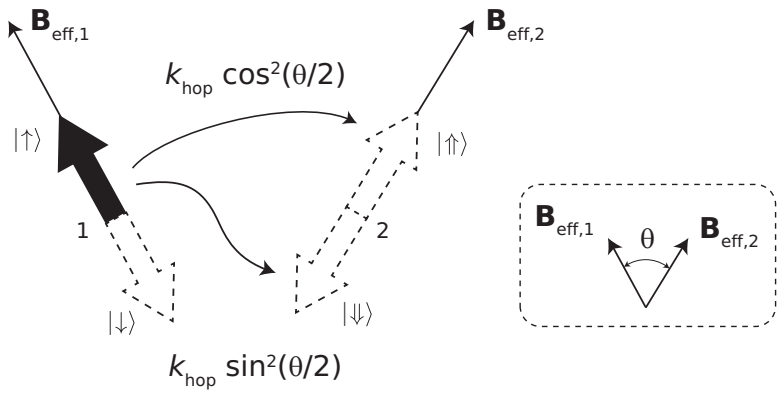

Figure 2.1 The energy eigenstates of two sites with effective magnetic fields $\mathbf{B}_{\mathrm{eff},i}$. The a polaron is in the $|\uparrow\rangle$ state of site 1. In the slow-hopping limit, hopping can be considered to take place between energy eigenstates. The hopping rates are proportional to the spin projection factors between the eigenstates of the source site and the target site: $k_{\mathrm{hop}}\cos^2(\theta/2)$ and $k_{\mathrm{hop}}\sin^2(\theta/2)$, which only depend on the angle θ between the two effective magnetic fields.

The same result can be derived for a reaction between two polarons. Because there is a large exchange interaction between two polarons on the same site (a bipolaron or an exciton), the spin eigenstates for two polarons on a single site (for site 2, see Figure 2.1) are the singlet, $|\mathrm{S}\rangle = \frac{1}{\sqrt{2}}(|\Uparrow\Downarrow\rangle - |\Downarrow\Uparrow\rangle)$, and triplet, $|\mathrm{T}_0\rangle = \frac{1}{\sqrt{2}}(|\Uparrow\Downarrow\rangle + |\Downarrow\Uparrow\rangle)$, $|\mathrm{T}_-\rangle = |\Downarrow\Downarrow\rangle$, and $|\mathrm{T}_+\rangle = |\Uparrow\Uparrow\rangle$, states. Note that the singlet and T_0 states do not depend on the direction of the effective magnetic field, while T_- and T_+ do. For example, when there is a polaron in $|\uparrow\rangle$ on site 1 and a polaron in $|\Uparrow\rangle$ on site 2, the spin-dependent rate for forming a singlet on site 2 is,

$$\tilde{k}_{1\uparrow,2\Uparrow\to 2\mathrm{S}} = k_{\mathrm{S}}|\langle\uparrow\Uparrow|\mathrm{S}\rangle|^2, \tag{2.18}$$

where k_{S} is the singlet exciton formation rate. The spin projection factors between energy eigenstates of two sites and the singlet and triplet states on a single site are listed in Table 2.2 on the following page. The same spin projection factors are used for dissociation of an exciton or bipolaron or for ionization of a dopant.

These hopping rates between energy eigenstates allow us to model spin-dependent processes with simple rate equations. It also makes it possible to perform Monte Carlo simulations of multiple-polaron systems. Those will be discussed in the next section.

$\lvert\langle\cdot\rvert\cdot\rangle\rvert^2$	$\langle\uparrow\rvert$	$\langle\downarrow\rvert$
$\lvert\Uparrow\rangle$	$\cos^2(\theta/2)$	$\sin^2(\theta/2)$
$\lvert\Downarrow\rangle$	$\sin^2(\theta/2)$	$\cos^2(\theta/2)$

Table 2.1 Spin projection factors between the spin eigenstates of two sites, whose effective magnetic fields make a mutual angle θ.

$\lvert\langle\cdot\rvert\cdot\rangle\rvert^2$	$\langle S\rvert$	$\langle T_-\rvert$	$\langle T_0\rvert$	$\langle T_+\rvert$
$\lvert\uparrow\Uparrow\rangle$	$\frac{1}{2}\sin^2(\theta/2)$	0	$\frac{1}{2}\sin^2(\theta/2)$	$\cos^2(\theta/2)$
$\lvert\uparrow\Downarrow\rangle$	$\frac{1}{2}\cos^2(\theta/2)$	$\sin^2(\theta/2)$	$\frac{1}{2}\cos^2(\theta/2)$	0
$\lvert\downarrow\Uparrow\rangle$	$\frac{1}{2}\cos^2(\theta/2)$	0	$\frac{1}{2}\cos^2(\theta/2)$	$\sin^2(\theta/2)$
$\lvert\downarrow\Downarrow\rangle$	$\frac{1}{2}\sin^2(\theta/2)$	$\cos^2(\theta/2)$	$\frac{1}{2}\sin^2(\theta/2)$	0

Table 2.2 Spin projection factors between the spin eigenstates of two sites, whose effective magnetic fields make a mutual angle θ, and the singlet and triplets states of the second site.

2.3 Monte Carlo simulations

Monte Carlo methods are computational methods that use statistical sampling to calculate some property.[76] When ENIAC, the first electronic general-purpose computer, was finished just after the second world war, Stanisław Ulam quickly realized that it could be used to apply statistical sampling techniques to the problem of neutron diffusion in fissionable materials.[¶] Although ENIAC was developed to calculate artillery firing tables for the army, it was flexible enough to do other calculations and John von Neumann was able to convince the owners to use it for calculations of nuclear fission and fusion for nuclear weapons. It was Nicholas Metropolis who came up with the name Monte Carlo, because Ulam's uncle used to go to Monte Carlo to gamble and the new method also relied on chance.[75] Since then, Monte Carlo methods have become more sophisticated and have found many other applications in physics, biology, economics, and other fields.

In this thesis, we are interested in following the time evolution of charges in an organic semiconductor to find properties like the current. To get such 'kinetic' properties, the Kinetic Monte Carlo method was developed by Young, Elcock and others in the late 1960s.[119,130] Essentially the same method was derived independently by other authors and named Dynamical Monte Carlo,[72] the n-fold way,[18] and Gillespie algorithm.[39] The first time this method was used to study charge transport in organic semiconductors was in 1981 by Bässler and coworkers, although that was for single polarons only.[7,104] Simulations with multiple polarons (including Coulomb interactions) were done for the first time by Houili *et al.*[47] for interfaces between organic semiconductors and later by Zhou *et al.*[136] for a bulk organic semiconductor.

In the rest of this thesis, the kinetic Monte Carlo method described below will simply be called "Monte Carlo", as is usual in the field of organic semiconductors.

[¶] Already in the 1930s, Enrico Fermi applied a 'Monte Carlo' method to the same neutron diffusion problem using only a "small mechanical adding machine" whenever he suffered from insomnia.[75]

2.3.1 Description of the Monte Carlo method

Below, the steps of a single Monte Carlo simulation as used in our research are listed. Steps 1 to 3 are used to set up the simulation. After that, steps 4 to 8 constitute, what is called, one *time step*. At each time step, one single event is chosen and performed. Finally, in the last step, the output is written to a file.

This procedure is used both to calculate the current in the presence of an electric field as well as to simulate the diffusion of a single polaron in absence of an electric field.

Often, the system is equilibrated for a certain number of time steps, after which the simulation of the quasi-equilibrium state continues and the properties of interest are measured. Sometimes, for example for single-polaron simulations, equilibration happens so fast that the equilibration phase can be omitted.

The different steps in the Monte Carlo method are:

1. A *disorder configuration* is made: A lattice of sites is made and each site gets an energy taken from a Gaussian distribution with standard deviation σ and a hyperfine field taken from a three-dimensional Gaussian distribution with standard deviation B_{hf}.
2. A number of polarons, according to the desired charge concentration, is placed on their (usually random) initial positions in a random spin state.
3. The simulation time, counters for the number of hops (in different directions) and all other counters are set to zero.
4. The first time this step occurs, the rates, k_i, of all events are calculated. In all following occurrences, only those rates that might have changed are recalculated. Depending on the system of interest, the following events are possible: Hopping of a charge, bipolaron formation, bipolaron dissociation, ionisation of a dopant, and recombination of a charge with an ionised dopant. Combinations might also be possible: For example, a bipolaron next to a charge might dissociate while forming a new bipolaron with the charge. The rates are calculated as described in Section 2.2.3.
5. An event is chosen at random, weighted by its rate k_i. The probability that event i is chosen is: $k_i / \sum_j k_j$. A binary tree of all hopping rates is maintained to make choosing an event fast.
6. The chosen event is performed. Depending on what type of event happened, the corresponding counters are updated.
7. The simulation time is increased by a random time taken from the distribution:

$$f(t) = k_{\mathrm{tot}} e^{k_{\mathrm{tot}} t} \tag{2.19}$$

where k_{tot} is the sum of all rates.

8. When equilibrating: If the desired number of equilibration steps has been taken, go to **step 3**, otherwise go to **step 4**. When equilibration was already finished or not used: If the total prescribed number of time steps has not yet been reached or the final simulation end time has not been reached, go to **step 4**. Otherwise, continue to the next step.
9. Output the final simulation time, the values of the counters (e.g., number of hops to the left, number of bipolarons formed), and values derived from that (e.g., the current). Often, also during the simulation output is written to a file to monitor the progress and to judge whether convergence has been reached.

To calculate a magnetic field effect, the steps listed above are performed for $B = 0$. After that, the charges are removed from the system and all steps except for step 1 are repeated for other values of the magnetic field for the same disorder configuration. The currents (or any other property of interest) found from the runs for the same disorder configuration are then used to calculate the magnetic field dependence.

This procedure is repeated for many different disorder configurations and an average is calculated of all properties. The number of disorder configurations is chosen such that the variance of the mean is small enough. Usually the variance is smaller than 1%.

2.4 Resistor network

In 1971, Ambegaokar and coworkers[1] have shown that the calculation of the current through a network of sites where electrons can hop from site to site can be simplified by mapping of the hopping problem onto the problem of finding the current through a resistor network. The derivation below follows the derivation by Ambegaokar *et al.* as rephrased by Cottaar *et al.*[29]

The average transition rate between sites i and j is given by:

$$\Gamma_{ij} = \langle n_i(1 - n_j)k_{i\to j}\rangle, \tag{2.20}$$

where $k_{i\to j}$ is the hopping rate from site i to site j, n_i is the occupation number of site i and the factor $(1 - n_j)$ appears because a site can be occupied by at most a single electron (or hole). We ignore the possibility of bipolaron formation.

We first consider thermal equilibrium. In this case, the occupation numbers for sites i are given by the Fermi-Dirac distribution:

$$\langle n_i\rangle = n_i^{\mathrm{eq}} = \frac{1}{1 + e^{(E_i - E_\mathrm{F})/k_\mathrm{B}T}}, \tag{2.21}$$

where E_i and E_j are the energies of sites i and j, $k_\mathrm{B}T$ is the thermal energy, and E_F is the Fermi energy. The Fermi energy is determined by the temperature and charge density n of the system as $n = \sum_i n_i$. Furthermore, we assume that the

occupation numbers are statistically independent: $\langle n_i n_j \rangle = \langle n_i \rangle \langle n_j \rangle$ for $i \neq j$. This assumption is only exact in the limit of vanishing charge concentration.[28] We will, however, only use the mapping described in this section in that limit (See Section 5.2 on page 59). The transition rate from site i to site j can now be found by filling Equation 2.21 into Equation 2.20, yielding:

$$\Gamma_{ij}^{\mathrm{eq}} = k_{i\to j}^{\mathrm{symm}} \frac{1}{4\cosh[(E_i - E_\mathrm{F})/2k_\mathrm{B}T]\cosh[(E_j - E_\mathrm{F})/2k_\mathrm{B}T]} \tag{2.22}$$

$$\approx k_{i\to j}^{\mathrm{symm}} \exp\left(\frac{E_\mathrm{F}}{k_\mathrm{B}T} - \frac{E_i + E_j}{2k_\mathrm{B}T}\right). \tag{2.23}$$

Here, we have factored the hopping rate $k_{i\to j}$ in a part that is symmetric in the energy difference, $\Delta E_{ij} = E_j - E_i$, between sites i and j and a part that is antisymmetric in ΔE_{ij} as follows:

$$k_{i\to j} = k_{i\to j}^{\mathrm{symm}} e^{-\Delta E_{ij}/2k_\mathrm{B}T}, \tag{2.24}$$

where the symmetric part $k_{i\to j}^{\mathrm{symm}}$ depends on the particular hopping rate.[29] We have also used the fact that the hopping rates $k_{i\to j}$ must satisfy *detailed balance*, resulting in:[‖]

$$\frac{k_{i\to j}}{k_{j\to i}} = e^{(E_i - E_j)/k_\mathrm{B}T}, \tag{2.25}$$

or, in this case, $k_{i\to j}^{\mathrm{symm}} = k_{j\to i}^{\mathrm{symm}}$. Both Miller-Abrahams and Marcus hopping rates (see Section 1.1.1 on page 3) satisfy this condition, both being proper physical hopping rates. Note that $\Gamma_{ij}^{\mathrm{eq}}$ is symmetric under exchange of i and j: $\Gamma_{ij}^{\mathrm{eq}} = \Gamma_{ji}^{\mathrm{eq}}$. This means that there is no net charge flow between sites i and j, as should be the case in equilibrium.

If now a small electric field F is applied, it can be treated as a perturbation, giving rise to small perturbations $\delta k_{i\to j}$ and δn_i in the hopping rates, $k_{i\to j}$, and occupation numbers, n_i. Using detailed balance and the symmetry of $\Gamma_{ij}^{\mathrm{eq}}$, the current I_{ij} between sites i and j can written in terms of those perturbations (in first order):

$$I_{ij} = e(\Gamma_{ij} - \Gamma_{ji}) \tag{2.26}$$

$$= e\Gamma_{ij}^{\mathrm{eq}} \left(\frac{\delta k_{i\to j}}{k_{i\to j}} - \frac{\delta k_{j\to i}}{k_{j\to i}} + \frac{\delta n_i}{n_i(1-n_i)} - \frac{\delta n_j}{n_j(1-n_j)}\right) \tag{2.27}$$

$$= \frac{e}{k_\mathrm{B}T}\Gamma_{ij}^{\mathrm{eq}} \left(e\mathbf{R}_{ij}\cdot\mathbf{F} + \delta\mu_i - \delta\mu_j\right) \tag{2.28}$$

$$\equiv G_{ij}V_{ij}, \tag{2.29}$$

where $\mathbf{R}_{ij}$ is the distance between sites i and j and V_{ij} is the potential between *nodes* i and j of the resistor network, which needs not be the same as the potential

[‖] Detailed balance means that every elementary processes must be equilibrated by its reverse process. For fermions that means: $n_i(1-n_j)k_{i\to j} = n_j(1-n_i)k_{j\to i}$. The factor $1-n_i$ results from the Pauli exclusion principle, which states that two fermions cannot occupy the same state. Using this relation and the fact that in equilibrium fermions must obey the Fermi-Dirac distribution yields Equation 2.25.

difference between sites i and j of the original hopping problem. It follows directly that the current between those two sites is the same as through a resistor with a conductivity,

$$G_{ij} = \frac{e^2}{k_B T} \Gamma_{ij}^{\mathrm{eq}} \tag{2.30}$$

$$= \frac{e^2}{k_B T} k_{i \to j}^{\mathrm{symm}} \exp\left(\frac{E_F}{k_B T} - \frac{E_i + E_j}{2 k_B T} \right). \tag{2.31}$$

This means that the current resulting from hops between the sites of the original problem is the same as the current through a network of resistors given by Equation 2.31.

3

Modelling exciton formation using a two-site model

We explore the magneto-electroluminescence of organic light-emitting diodes by evaluating the magnetic-field dependent fraction of singlet excitons formed. We use a two-site model with spin mixing by hyperfine fields and different singlet and triplet exciton formation rates. When the hopping rate is comparable to or smaller than the hyperfine frequency, we find a deviation from the statistical fraction of 25% *singlet excitons as well as a magnetic-field effect of the fraction. A huge magneto-electroluminescence is predicted when exciton formation is in competition with spin mixing and when the triplet exciton formation rate is significantly larger than the singlet exciton formation rate. This competition also leads to a low-field structure in the magneto-electroluminescence that is in agreement with recent experiments.*

3.1 Introduction

Surprisingly large magnetic field effects of several percents on the electroluminescence and current in organic light-emitting diodes (OLEDs) have been found in recent years.[32,36,48,53,92] Intensive experimental and theoretical research is presently going on to unravel the mechanism behind these effects. The small field scale of a few millitesla at which the effects occur points at the role of hyperfine fields. Several mechanisms to explain the effects were proposed, involving excitons[32,92] or bipolarons.[16] These mechanisms rely on the suppression by an applied magnetic field of the hyperfine-induced spin mixing within a pair of polarons prior to

This chapter was adapted with permission from:

S. P. Kersten, A. J. Schellekens, B. Koopmans, and P. A. Bobbert. *Magnetic-Field Dependence of the Electroluminescence of Organic Light-Emitting Diodes: A Competition between Exciton Formation and Spin Mixing*. Phys. Rev. Lett. **106**, 197402 (2011).

exciton or bipolaron formation. Magnetocurrent measurements on organic donor-acceptor and single-carrier devices suggest that both exciton and bipolaron mechanisms can be operative.[124]

The importance of hyperfine coupling for spin mixing in organic semiconductors was demonstrated explicitly by experiments in which magnetic field effects occurring in a deuterated conjugated polymer were compared to those in the undeuterated polymer.[83] In identical OLEDs, the deuterated polymer yields a narrower lineshape of the magneto-electroluminescence, i.e., the magnetic-field dependence of the electroluminescence. This is in agreement with the smaller magnetic moment of a deuteron as compared to a proton. Interestingly, the magneto-electroluminescence curves of Reference 83 show an additional structure at low field. Finding the cause of this structure is important for establishing the precise mechanism responsible for the magneto-electroluminescence and possibly other magnetic field effects.

Closely related to the discussion about magnetic field effects is the question if the quantum-statistical 1:3 ratio for the formation of singlet vs. triplet excitons in OLEDs is violated. There are experimental claims of either a larger[22,33,98,126,127] or smaller[23,106,129] ratio. This question has great technological relevance, since a larger than statistical ratio would break the 25% efficiency limit of OLEDs based on fluorescence. Establishing the origin of magnetic field effects in OLEDs is expected to provide an answer to this question. Since the magneto-electroluminescence of OLEDs quantifies the change in the number of singlet excitons formed when a magnetic field is applied, it is an important tool to address this question.

In this chapter we investigate the effects of spin mixing by hyperfine coupling on the fraction of singlet excitons formed in OLEDs. These effects have until now only been described in qualitative terms.[32,53,92,129] Moreover, only the case was considered where exciton formation from a pair of polarons is slow as compared to spin mixing by hyperfine coupling.[129] However, modeling of charge transport in two derivatives of PPV* shows[89] that the rate of polaron hopping is larger than the rate of spin mixing.[17] Since exciton formation is essentially a process in which one charge hops to the site of an opposite charge, exciton formation is not expected to be slow as compared to spin mixing. We therefore consider general exciton formation and spin mixing rates. We demonstrate that unexpected effects occur when there is *competition between exciton formation and spin mixing*. We predict that huge magneto-electroluminescence effects can then occur. Furthermore, we show that this competition leads to a low-field structure in the magneto-electroluminescence curves comparable to that of Reference 83.

3.2 Two-site model

We start our considerations with the two-site model shown in Figure 3.1 on the next page. The two sites α and β represent localized states in a disordered organic

*PPV: poly(*p*-phenylene vinylene)

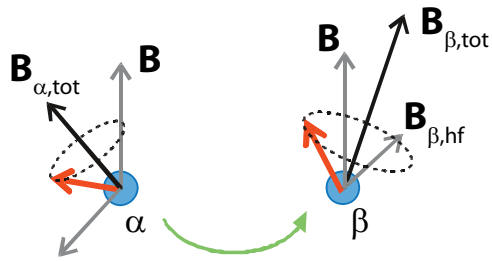

Figure 3.1 Two-site model, with an electron at site β at which an exciton will be formed by hopping of a hole at site α to β. The total effective magnetic field $\mathbf{B}_{\alpha(\beta),\mathrm{tot}}$ is the sum of a random hyperfine field $\mathbf{B}_{\alpha(\beta),\mathrm{hf}}$ and an applied field $\mathbf{B}$. Spin mixing occurs by precession of the spins (red arrows) around $\mathbf{B}_{\alpha(\beta),\mathrm{tot}}$.

semiconductor. A hole-polaron at site α and an electron-polaron at site β together form a "polaron pair", a precursor to an exciton. In the polaron pair state the exchange coupling and the possible dipolar coupling between the spins of the electron and hole are small with respect to the hyperfine and Zeeman coupling, which means that the spins are free to evolve independently.

We treat the hyperfine coupling at both sites within a semi-classical approach, with coupling of each polaron spin to a random hyperfine field $\mathbf{B}_{\alpha(\beta),\mathrm{hf}}$. This field is drawn from a three-dimensional Gaussian distribution with a standard deviation B_{hf}. This treatment is correct for the typical situation that coupling of the π-electron spin to several hydrogen nuclear spins occurs.[105] The total effective magnetic field $\mathbf{B}_{\alpha(\beta),\mathrm{tot}}$ at each site is the sum of its hyperfine field and an externally applied magnetic field $\mathbf{B} = B\hat{z}$.

Exciton formation in this model takes place by hopping of the hole from site α to site β, resulting in the formation of a singlet or one of the triplet (T_0, T_+, T_-) excitons. We assume that in the exciton states the exchange coupling is dominant with respect to the coupling to $\mathbf{B}_{\alpha(\beta),\mathrm{eff}}$. Because of the steep exponential decay of the exchange coupling with distance one should expect that there is always a step in the exciton formation process where this coupling changes from subdominant in the polaron pair state to dominant in the exciton state. We note that the exciton states after the hopping are not necessarily the states with the lowest energy. Further relaxation within the singlet or triplet exciton manifold can take place, but we assume that the exchange splitting prevents spin mixing during this process.

Because of their different energies and wave functions, the formation of singlet and triplet excitons occurs with different rates k_{S} and $k_{\mathrm{T}_0,\mathrm{T}_-,\mathrm{T}_+} = k_{\mathrm{T}}$, with a ratio $\gamma \equiv k_{\mathrm{S}}/k_{\mathrm{T}}$. We also introduce the *relative hopping rate* $r \equiv k_{\mathrm{S}}/\omega_{\mathrm{hf}}$ as a parameter, with $\omega_{\mathrm{hf}} = g\mu_{\mathrm{B}}B_{\mathrm{hf}}/\hbar$ the typical hyperfine frequency; $r \gg 1$ ($r \ll 1$) corresponds to "fast" ("slow") singlet exciton formation, as compared to the hyperfine precession time $2\pi/\omega_{\mathrm{hf}}$ (≈ 35 ns for $B_{\mathrm{hf}} \approx 1$ mT). The rates k_{S} and k_{T} are determined by material-specific details of the exciton formation process. Values for these rates could be obtained form *ab initio* calculations or by fitting of experimental data;

however, this goes beyond the present work. We therefore treat γ and r as parameters. We will assume that unbinding of the excitons is prevented by a large energy difference between the polaron pair and exciton states.

There are two positional configurations in this model: the polaron pair state (PP), where both sites are occupied by one polaron, and the exciton state (X), where site α is empty and site β is occupied by a exciton. For simplicity, we will assume that the exciton states do not evolve in time, therefore $H_X = 0$. The Hamiltonian for the PP configurations is given by:

$$H_{PP} = g\mu_B \mathbf{B}_{\alpha,\text{eff}} \cdot \mathbf{S}_1/\hbar + g\mu_B \mathbf{B}_{\beta,\text{eff}} \cdot \mathbf{S}_2/\hbar \tag{3.1}$$

where g is the g-factor, μ_B is the Bohr magneton, $\mathbf{S}_{1(2)}$ is the spin operator for polaron 1(2). Because of the small spin-orbit coupling in organic materials we have for the g-factor $g \approx 2$; we take this factor equal for electrons and holes.

The combination of the coherent time evolution of the spin state of the polaron pair and the incoherent formation of an exciton on site β is described by a Stochastic Liouville equation, as described in Section 2.2 on page 24. The time evolution of the polaron pair and exciton density operators ρ_{PP} and ρ_X is given by:

$$\frac{\partial \rho_{PP}}{\partial t} = -\frac{i}{\hbar}[H, \rho_{PP}] - \frac{1}{2}\{\Lambda, \rho_{PP}\} \tag{3.2}$$

$$\frac{\partial \rho_X}{\partial t} = \sum_\lambda k_\lambda |\lambda\rangle\langle\lambda|\rho_{PP}|\lambda\rangle\langle\lambda|, \tag{3.3}$$

where $\Lambda = \sum_\lambda k_\lambda |\lambda\rangle\langle\lambda|$ for $\lambda = S, T_-, T_0, T_+$.

We take $\rho_X(0) = 0$ and for $\rho_{PP}(0)$ we take a density operator corresponding to equal populations of the polaron pair spin states as initial conditions. Equation 3.3 is solved as described in Section 2.2.2 on page 27. The final singlet and triplet exciton fractions χ_S (*singlet fraction*) and $\chi_T = 1 - \chi_S$ are obtained from $\rho_X(t \to \infty)$. For all the results presented in this chapter, a numerical average has been taken over the hyperfine fields.

3.3 Time dependence

We start by considering the time evolution of the system that was just described for $\gamma = 10$ in the fast and slow-hopping limits. For simplicity, the standard deviations B_{hf} were taken equal for electrons and holes. Figure 3.2(a) shows the occupation probability of the polaron pair state and the singlet and triplet exciton states in the fast hopping limit ($r = 10^2$). Because $\gamma > 1$, initially more singlet than triplet excitons are formed. However, exciton formation happens too fast for spin mixing to take place, so in the final state the statistical ratio of singlet to triplet excitons is recovered. This behavior is also reflected in the singlet character, $\chi_{PP,S} = \text{Tr}[\rho_{PP}|S\rangle\langle S|]$, and triplet character, $\chi_{PP,T} = 1 - \chi_{PP,S}$, of the polaron pair state, see the dashed curves. While the initial polaron pair state consists of 25% singlets,

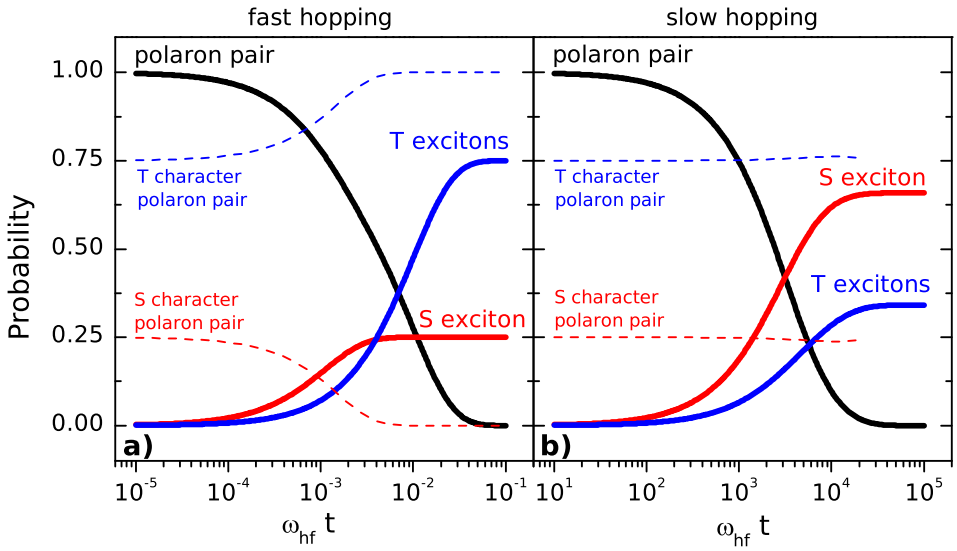

Figure 3.2 Occupation probabilities of the polaron-pair (black curve) and exciton states (blue and red curves) as a function of time in the two-site model for $\gamma = 10$ in (a) the fast hopping limit ($r = 10^2$) and (b) in the slow-hopping limit ($r = 10^{-2}$). The dashed curves indicate the singlet and triplet character of the polaron pair state.

this fraction quickly reduces to zero as singlet excitons are formed faster than triplets excitons. After all singlet polaron pairs have formed singlet excitons, the remaining 75% polaron pairs are triplets and will form triplet excitons.

Figure 3.2(b) shows the results for slow hopping ($r = 10^{-2}$). In this case, spin mixing takes place which keeps the singlet and triplet character of the polaron pair state constant throughout the exciton formation process, see the dashed lines. Now, singlet excitons keep being formed at the faster rate, resulting in more singlet than triplet excitons being formed—a clear deviation from the statistical singlet fraction of 1/4. *We conjecture that the mechanism presented here is the generic mechanism behind violations of the statistical S:T ratio in* OLEDs.

3.4 Magneto-electroluminescence

Figure 3.3(a) shows the dependence of the singlet fraction $\chi_S(B = 0)$ on γ and r. A deviation from the statistical ratio is found when $\gamma \neq 1$. This deviation disappears in the fast hopping limit $r \to \infty$, where the effect of the hyperfine fields is quenched. As expected, the largest deviation occurs in the slow-hopping limit $r \to 0$.

Figure 3.3(b) shows the dependence of the magnetic field effect $\mathrm{MFE}(B) = [\chi_S(B) - \chi_S(0)]/\chi_S(0)$ for $B \to \infty$ (MFE for short) on γ and r. We see that in the slow-hopping limit $r \to 0$ a substantial magnetic field effect occurs. In this limit, χ_S and its

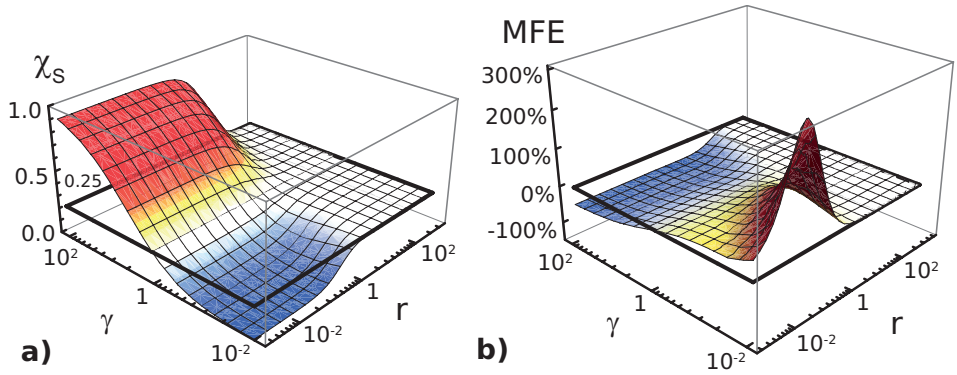

Figure 3.3 (a) Fraction of formed singlet excitons χ_S and (b) magnetic field effect (MFE) of χ_S as a function γ and r for the two-site model. The statistical ratio of 0.25 (and the corresponding absence of a magnetic field effect) is shown as a black frame.

magnetic field effect can be calculated analytically, as will be shown in the next section.

The magnetic field dependence arises from the *alignment* of the effective magnetic fields as the applied magnetic field is increased. As explained in the previous section, the deviation from the statistical ratio depends on the amount of spin mixing. The amount of spin mixing decreases when the mutual angle between the two effective magnetic fields decreases.

In the slow-hopping limit, this is the only mechanism by which the applied magnetic field affects the amount of spin mixing. However, as we will see in Section 3.5.1 on page 43 and in Chapter 7, at intermediate hopping rates there are other ways in which the applied magnetic field can affect the amount of spin mixing.

3.4.1 Analytical derivation

As explained in Section 2.2.3, in the slow-hopping limit it is sufficient to know the eigenstates of the Hamiltonian and their projections onto the singlet and triplet spin subspaces in order to calculate χ_S. These projections are only determined by the angle $\theta \in [0, \pi]$ between $\mathbf{B}_{\alpha,\text{eff}}$ and $\mathbf{B}_{\beta,\text{eff}}$, see Table 2.2 on page 30.

The four eigenstates of the Hamiltonian can be categorized into two pairs: two *parallel* (P) eigenstates, for which the spins at α and β are either both parallel or both antiparallel to $\mathbf{B}_{\alpha,\text{eff}}$ and $\mathbf{B}_{\beta,\text{eff}}$, and two *anti-parallel* (AP) eigenstates, for which the spin at α is parallel to $\mathbf{B}_{\alpha,\text{eff}}$ and the spin at β is antiparallel to $\mathbf{B}_{\beta,\text{eff}}$, or vice versa. The rates for exciton formation are equal to the spin-independent formation rates times the spin projection factor, see Section 2.2.3 on page 27. For the P eigenstates, one can easily derive that the rates of singlet and triplet exciton formation are equal to $\frac{1}{2}k_S \sin^2(\theta/2)$ and $k_T\left[\frac{1}{2}\sin^2(\theta/2) + \cos^2(\theta/2)\right]$, while for the AP eigenstates

these rates are $\frac{1}{2}k_S\cos^2(\theta/2)$ and $k_T\left[\frac{1}{2}\cos^2(\theta/2)+\sin^2(\theta/2)\right]$, respectively. For a fixed angle θ, the fraction of produced singlet excitons is therefore

$$\chi_S = \frac{1}{2}\left\{\frac{k_S\frac{1}{2}\sin^2(\theta/2)}{k_S\frac{1}{2}\sin^2(\theta/2)+k_T\left[\frac{1}{2}\sin^2(\theta/2)+\cos^2(\theta/2)\right]} + \frac{k_S\frac{1}{2}\cos^2(\theta/2)}{k_S\frac{1}{2}\cos^2(\theta/2)+k_T\left[\frac{1}{2}\cos^2(\theta/2)+\sin^2(\theta/2)\right]}\right\}. \tag{3.4}$$

The factor $1/2$ comes from the initial occupation of the P and AP states, which are equally occupied and must add up to unity. Since, in the limit $B\to\infty$ the two effective magnetic fields are aligned, we have $\theta=0$ and we find therefore that

$$\chi_S(B\to\infty)=\frac{\gamma}{2(\gamma+1)}. \tag{3.5}$$

For $B=0$ the directions of $\mathbf{B}_{\alpha,\mathrm{eff}}$ and $\mathbf{B}_{\beta,\mathrm{eff}}$ are isotropically distributed. Taking an angular average of Equation 3.4 then results in

$$\chi_S(B=0)=\frac{\gamma\left\{\gamma-1-\ln\left[\frac{1}{4}(1+\gamma)^2\right]\right\}}{(\gamma-1)^2}. \tag{3.6}$$

From the last two equations it follows straightforwardly that MFE $\to -1/2$ for $\gamma\to\infty$, whereas MFE $\to 3-4\ln 2 = +0.227$ for $\gamma\to 0$. These results are in agreement with the numerical results shown in Figure 3.3.

We note that the above result is valid for any isotropic distribution of the hyperfine fields. In particular, the standard deviations of the hyperfine fields at α and β may be different.

3.4.2 Prediction of extremely large magneto-electroluminescence

Quite surprisingly, however, the largest magnetic field effect does not occur for $r\to 0$, but for *intermediate* values of r and small γ ($k_T \gg k_S$), see Figure 3.3(b). The reason for this is the competition between exciton formation and spin mixing. For large r the effect of the hyperfine fields is quenched and the singlet fraction is equal to 0.25. When r decreases the singlet fraction decreases too. However, this decrease happens faster for $B=0$ than for $B\gg B_{\mathrm{hf}}$, see Figure 3.4(a). In Chapter 7, an expression is derived for χ_S as a function of r and γ for $B\to\infty$, which is shown in Equation 7.7 on page 90. From that equation it can be found that χ_S behaves as a power law in r with exponent 1 for $r\approx 1$. For intermediate r, the singlet fraction for $B=0$ can be fitted with a power law as well with an exponent of $\sim$1.9. The magnetic field effect would therefore increase indefinitely for decreasing r as a power law in r with exponent ~ -0.9. However, depending on γ, a maximal magnetic field effect is reached as the singlet fraction saturates to the value for the slow-hopping limit, as given by Equations 3.5 and 3.6. This leads to a pronounced

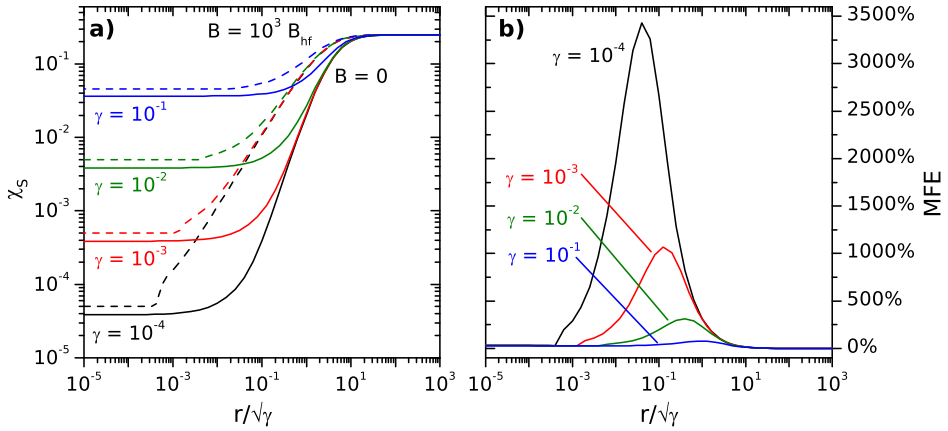

Figure 3.4 (a) The singlet fraction χ_S and (b) its magnetic field effect as a function of $r/\sqrt{\gamma}$ for $B = 0$ (solid curves) and $B = 10^3 B_{hf}$ (dashed curves) for different values of γ. Around $r = 1$, χ_S varies as a power law of r with exponents ~ 1.9 for $B = 0$ and 1 for $B \to \infty$. The magnetic field effect is independent of γ when r is small.

peak in MFE(r) that grows indefinitely with decreasing γ, see Figure 3.4(b). This means that it should be possible to obtain a huge magneto-electroluminescence if the parameters of the organic material can be appropriately tuned. As an example, for $\gamma = 0.1$ and $r = 0.3$ an magnetic field effect of 75% can be obtained, with an singlet exciton fraction of 10% at large field.

3.5 Lineshapes

We also investigated the lineshapes of $\chi_S(B)$. We always found Lorentzian lineshapes with a width of a few times B_{hf}. Lineshapes for $\gamma = 10$ are shown in Figure 3.5. The linewidths B_0 (see Section 1.2.1 on page 8) increase from $3.1B_{hf}$ for slow hopping to $8.3B_{hf}$ for $r = 10$. These lineshape and linewidths are in agreement with those measured experimentally, see Section 1.2.1 on page 8.

The experimentally observed *increase* of the magneto-electroluminescence with magnetic field by Nguyen *et al.*,[83] see Figure 3.6(b), and others[96] points at a larger triplet than singlet formation rate, that is, $\gamma < 1$. This is in agreement with the claim of Segal *et al.* that in PPV the singlet fraction is *lower* than 25%.[106] With $\gamma \approx 0.7$ we can reproduce the value of $20 \pm 4\%$ reported by these authors.

We have modelled the exciton formation in the deuterated and undeuterated PPV derivatives that were investigated by Nguyen *et al.*[83] The results for the magnetic field effects shown in Figure 3.6(a) were obtained with the two-site model by taking $\gamma = 0.7$ and $B_{hf,e} = 3B_{hf,h}$,[†] as found by electrically detected magnetic resonance measurements on a related PPV-derivative.[68] We took $r = k_S/\omega_{hf,h} = 1.5$ (black squares) and 4.886 (red discs). The factor $4.886/1.5 = 3.257$ accounts for the

[†]There is no reason to assume that the electron's hyperfine field is the larger of the two. However, in our model it does not matter whether the electron's or hole's hyperfine field is larger than the other.

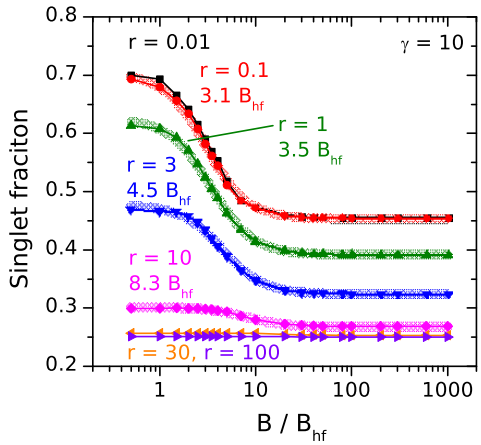

Figure 3.5 The lineshapes of the singlet fraction as a function of the applied magnetic field for $\gamma = 10$ and relative hopping rates ranging from slow hopping to fast hopping. Lorentzian fits (thick, shaded curves) and the corresponding values for B_0 are shown.

difference in hyperfine fields between the deuterated and undeutared polymer, resulting from the different spins and gyromagnetic ratios (267.51 and 41.07 rad/sT) of the proton and deuteron. With these values of r, the ratio of the sizes of the low-field structure [discussed in the next section; see Figures 3.6(c) and (d)] for the deuterated and undeuterated case is approximately equal for the predicted and measured results. The decrease in linewidth of the magneto-electroluminescence of the deuterated polymer compared with the undeuterated polymer caused by its smaller hyperfine field is partially countered by the increase due to the larger r, see Figure 3.5. That explains why the difference in linewidths for the deuterated and undeuterated polymers is smaller than the factor 3.257 difference between the gyromagnetic ratios of the proton and deuteron. Considering the large uncertainty in the parameters, the overall agreement with the magneto-electroluminescence experiments is quite remarkable.

3.5.1 Ultra-small-magnetic-field effect

For intermediate r we generically found an additional feature at a field scale smaller than or comparable to the hyperfine field, as in the magneto-electroluminescence experiments of Reference 83, see Figure 3.6(c) and (d). The structure has been named *ultra-small-magnetic-field effect*. In Reference 83 the magneto-electroluminescence curves were modeled with a coupling of the spins of the polaron pair to a single nuclear spin at each of the two sites of the polaron pair (spin-1/2 for the undeuterated and spin-1 for the deuterated polymer). However, as explained in Section 1.2.2 on page 11, it should be expected that in reality coupling to many nuclear spins occurs, in accordance with our semi-classical treatment.

When the magnetic field is increased, two things happen to the effective magnetic fields: their magnitudes increase and they become more aligned. The alignment leads to less spin mixing as explained in Section 3.4. The increase in magnitude

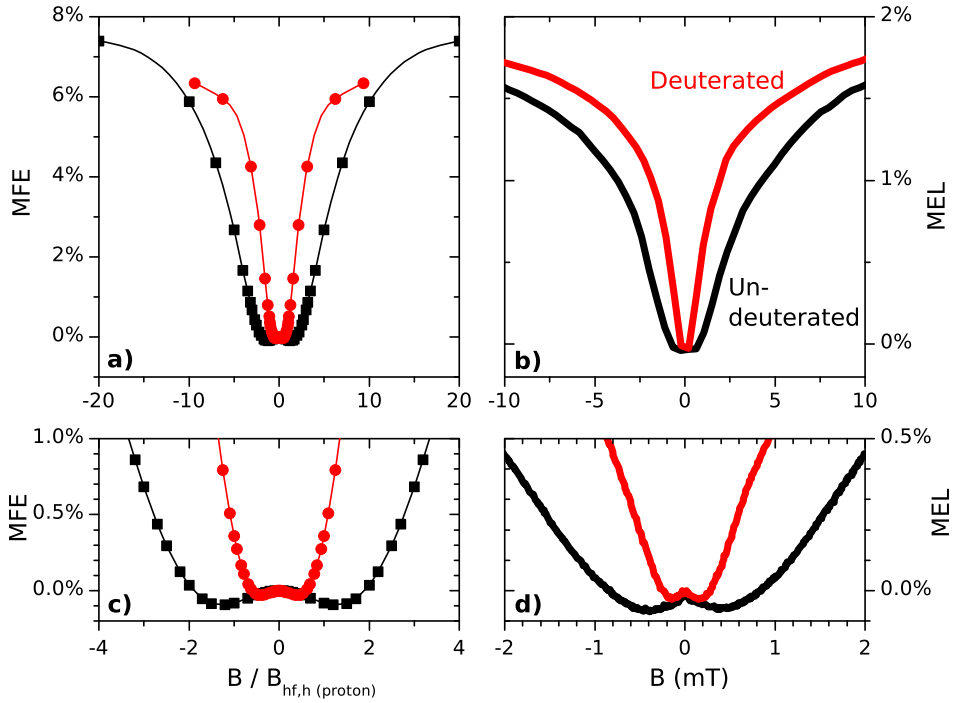

Figure 3.6 (a) Magnetic field dependence MFE(B) of the singlet exciton fraction χ_S in the two-site model for $\gamma = 0.7$ and $B_{hf,e} = 3B_{hf,h}$. Black squares: $r = 1.5$ (protons). Red circles: $r = 4.886 = 3.257 \times 1.5$ and hyperfine fields divided by 3.257 (deuterons). The field axis is scaled with $B_{hf,h}$ for protons. (b) Magneto-electroluminescence of OLEDs of a deuterated and undeuterated PPV-derivative, reproduced from Reference 83. (c) and (d) zoom in to the effects occurring at low field.

of the effective magnetic fields leads to faster precession. If the hopping rate is comparable to or faster than the hyperfine frequency, no complete spin mixing takes place and an increase in the precession frequency leads to more spin mixing. There is, therefore, a competition between an increase in spin mixing due to the increase in magnitude of the effective magnetic fields and a decrease in spin mixing due to their alignment.

This can be seen clearly when the difference between the two hyperfine fields is large. For illustrative purposes, the singlet fraction is shown in Figure 3.7 as a function of the applied magnetic field B for $\gamma = 10$ and $B_{hf,\beta} = 100B_{hf,\alpha}$. Results are shown for slow hopping (blue discs) and intermediate hopping rate $r = 30$ (black squares), where the "ultra-small-magnetic-field" effect is visible for $B < 100B_{hf,\alpha}$. When B increases between $B_{hf,\alpha}$ and $B_{hf,\beta}$, the precession frequency increases, leading to more spin mixing and a larger deviation of 0.25 for the singlet fraction. Around $B = 300B_{hf,\alpha}$ the value for slow hopping (where the maximum amount of mixing takes place) is approached.

Figure 3.8(a) shows the singlet fraction as a function of the magnetic field B and the relative hopping rate r with $B_{hf,e} = 3B_{hf,h}$. For r between 10^{-2} and 10, the

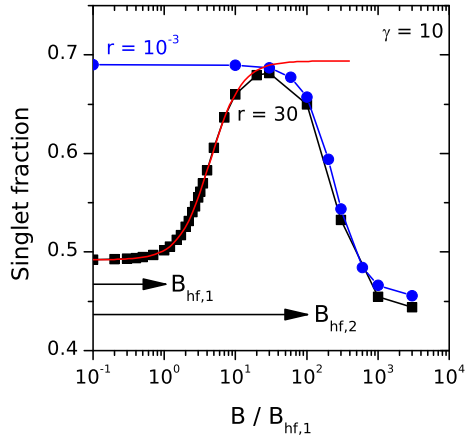

Figure 3.7 Singlet fraction as a function of $B/B_{\mathrm{hf},\alpha}$ for $\gamma = 10$ for slow hopping (blue discs) and $r = 30$ (black squares). The ratio between the two hyperfine fields $B_{\mathrm{hf},,\alpha}$ and $B_{\mathrm{hf},,\beta}$ (indicated as arrows) is 100. The ultra-small-magnetic-field effect can be fitted with a Lorentzian (red curve).

singlet fraction increases for $B < 2B_{\mathrm{hf,h}}$ before decreasing for larger B, that is, the ultra-small-magnetic-field effect is observed. Figure 3.8(b) again shows the singlet fraction as a function of B and r. However, now the magnitude of the effective magnetic fields is kept constant: $\mathbf{B}_{\mathrm{eff}} = B_{\mathrm{hf}}(\mathbf{B}_{\mathrm{hf}} + \mathbf{B})/\|\mathbf{B}_{\mathrm{hf}} + \mathbf{B}\|$. (This is done per hyperfine field configuration, before averaging.) In this case, the singlet fraction decreases monotonically with B. This shows that indeed, the increase in precession frequency is the cause of the ultra-small-magnetic-field effect.

Although not essential for obtaining the low-field structure, taking different standard deviations for the hyperfine fields of electrons and holes makes the structure more prominent. This is easy to understand, as the applied magnetic field needs only to be larger than the smallest hyperfine field to increase the precession frequency, while alignment of the effective magnetic fields occurs when the applied field is larger than the largest hyperfine field. The larger the difference between the two hyperfine fields, the larger is the size and the magnetic field range of the ultra-small-magnetic-field effect.

Finally, we remark that similar low-field structures as found in the magneto-electroluminescence were very recently also found in the magnetoconductance of OLEDs as well as single-carrier devices.[82] The low-field structure in the magnetoconductance of OLEDs could very well be related to that in the magneto-electroluminescence. However, in the single-carrier devices no exciton formation should take place, leaving the bipolaron mechanism[16] as candidate for the description of the magnetoconductance. By taking very large values of γ in the two-site model, reflecting suppression of triplet bipolaron formation,[16] we checked that the low-field structure for intermediate r then also appears. This demonstrates the similarity of the physics involved in exciton and bipolaron formation.

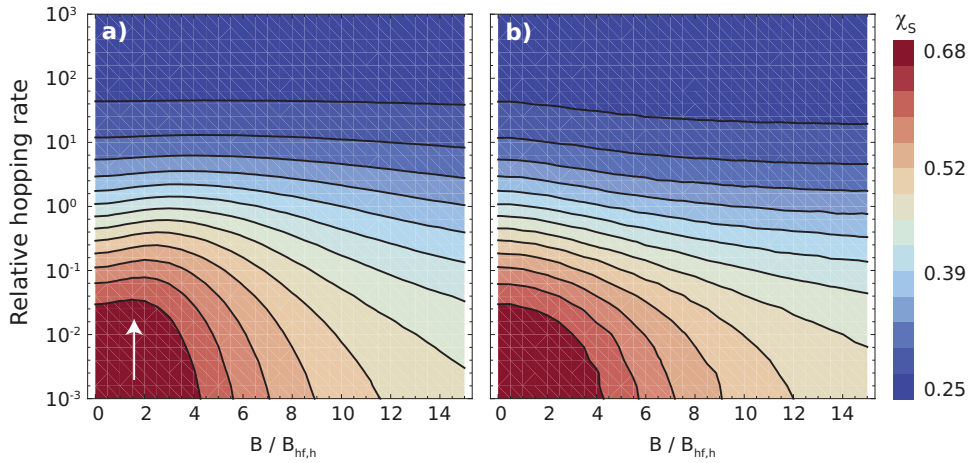

Figure 3.8 (a) The singlet fraction as a function of the magnetic field $B/B_{\mathrm{hf,h}}$ and the relative hopping rate r. At constant r, the singlet fraction first increases as a function of B due to faster spin precession before decreasing due to alignment of the effective magnetic fields. This gives rise to the ultra-small-magnetic-field effect (indicated by the arrow). (b) The singlet fraction for the same parameter range, but the magnitude of the effective magnetic fields is kept constant as B increases. There is no ultra-small-magnetic-field effect in this case.

3.6 Conclusions

We have found that the magnetic field dependence of the efficiency of an OLED proves that the statistical singlet-to-triplet ratio of 1:3 is violated. The observation that the efficiency of a PPV OLED increases when a magnetic field is applied indicates that triplet excitons are formed faster than singlet excitons—in agreement with measurements of the efficiency. Furthermore, we have shown that the recently observed ultra-small-magnetic-field effect can be explained as a competition between an increase in spin mixing due to faster spin precession and a decrease due to alignment of the effective magnetic fields. An important conclusion is that our study of magneto-electroluminescence curves provides valuable information about the magnitude and ratio of the triplet and singlet exciton formation rates in OLEDs. Finally, we could explain why the difference in linewidth for the deuterated and undeuterated polymer as measured by Nguyen *et al.* is smaller than expected: The small hyperfine field for the deuterated polymer leads to slower spin precession and thus a faster relative hopping rate, for which the lineshape is broader.

We thank Dr. T. D. Nguyen for providing us with the experimental data in Figure 3.6, which is published in Reference 82.

4

Investigating the effect of Coulomb interaction and energetic disorder on exciton formation

In the previous chapter, the fraction of singlet excitons and its magnetic field effect was investigated using a two-site model. In this chapter, the effect of Coulomb interaction between the electron and hole and the effect of energetic disorder on exciton formation is studied for lattices of up to 9×9×9 sites. A violation of the statistical singlet-triplet ratio and a magnetic field effect occur at much faster hopping rates than in the two-site model.

4.1 Introduction

In the previous chapter, only the last step of the exciton formation process was considered. It was assumed that only exciton formation could take place; the electron and hole could not hop to other sites. However, in reality, a nearest-neighbor electron-hole pair might temporarily break up by hopping of the electron or hole (or both) to other sites before forming an exciton. In this chapter, we will consider exciton formation in a more realistic system consisting of a box of up to 9×9×9 sites. We take the Coulomb attraction between electron and hole into account as well as energetic disorder.

Parts of this chapter were adapted with permission from:

S. P. Kersten, A. J. Schellekens, B. Koopmans, and P. A. Bobbert. *Magnetic-Field Dependence of the Electroluminescence of Organic Light-Emitting Diodes: A Competition between Exciton Formation and Spin Mixing*. Phys. Rev. Lett. **106**, 197402 (2011).

S. P. Kersten, A. J. Schellekens, B. Koopmans, and P. A. Bobbert. *Effect of hyperfine interactions on exciton formation in organic semiconductors*. Synth. Met. **161**, 613 (2011).

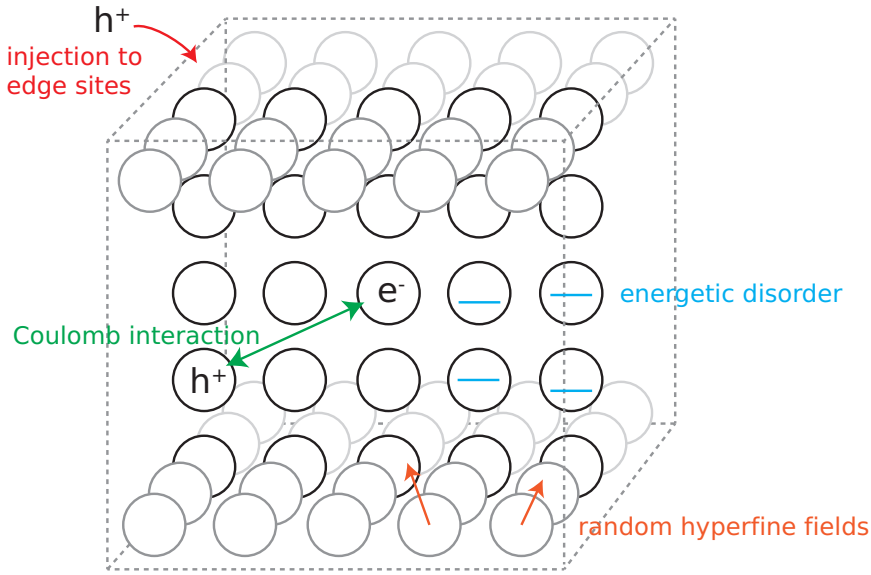

Figure 4.1 Exciton formation in a box of 5×5×5 sites. An electron is fixed in the middle of the box. The sites have energetic disorder and at each site there is a random hyperfine field. A hole is injected at the edge sites with a random spin and can hop around until it forms an exciton with the electron. The Coulomb interaction between the electron and hole is taken into account. For clarity, not all sites are shown.

It has become clear that the hopping rate relative to the hyperfine frequency, the relative hopping rate r, is an important parameter determining the size of the magnetic field effect. Only when hopping is slower than or comparable to the hyperfine frequency—that is, $r \lesssim 1$—spin mixing and magnetic field effects can occur. However, studies[89] of hole-only devices made of OC$_1$C$_{10}$-PPV* indicate that r is of the order of 10–1000.[17] That seems to be at odds with the fact that a magnetic field effect have been observed in the similar DOO-PPV† polymers.[83] On the other hand, in an analysis by Baker and coworkers[4] a relative hopping rate of $r = 0.1$ is found in MEH-PPV‡. While differences between materials can result in a variation in hopping rates and thus in the occurrence of a magnetic field effect in one material but not in another, the results presented in this chapter show that even at relative hopping rates much larger than unity a magnetic field effect can be found.

4.2 Multi-site model

In order to study situations closer to reality than the two-site model, we simulated recombination in a three-dimensional box of $N \times N \times N$ sites separated by a distance a, see Figure 4.1. The sites have a random energy E_i, taken from a Gaussian

*OC$_1$C$_{10}$-PPV: poly[2-methoxy-5-(30,70-dimethyloctyloxy)-*p*-phenylene vinylene]
†DOO-PPV: poly[2,5-dioctyloxy-1,4-*p*-phenylene vinylene]
‡MEH-PPV: poly[2-methoxy-5-(2′-ethylhexyloxy)-*p*-phenylene vinylene]

distribution with standard deviation σ. An electron is fixed in the middle on site X, while a hole with random spin is injected at the boundary sites and can hop around on the lattice. Since electrons are severely trapped compared to holes in PPV,[11] it is indeed reasonable to assume that the electron remains fixed while the hole moves. Due to the Coulomb interaction, the hole is attracted to the electron and will eventually recombine with it, forming a singlet or triplet exciton.

The energy due to the Coulomb interaction between an electron and hole on sites i and j is given by:

$$\frac{-e^2}{4\pi\epsilon_r\epsilon_0 R_{ij}} \equiv \frac{-V}{r_{ij}}, \tag{4.1}$$

where R_{ij} is the distance between the particles, e is the elementary charge, ϵ_0 is the vacuum permittivity, and ϵ_r is the relative permittivity constant. We have defined the dimensionless distance between two sites as $r_{ij} \equiv R_{ij}/a$ and the strength of the Coulomb interaction as $V = e^2/4\pi a\epsilon_r\epsilon_0$. We take typical values $a = 2$ nm and $\epsilon_r = 3$, giving us $V = 0.24$ eV. Because the electron is kept fixed in the middle, the Coulomb potential the hole feels due to the electron can be added to the site energies: The hole energy for site i is then equal to $E_i - V/r_{iX}$.

It is straightforward to generalize the Hamiltonian Equation 3.1 on page 38 and the Stochastic Liouville equation Equation 3.3 on page 38 to this case as is described in Section 2.2.1 on page 25. Since we keep the electron fixed in the middle on site X, the positional configuration (i, X) of the system is determined by the site i at which the hole is located. We will therefore use i to label the configuration (i, X). This results in the following Hamiltonian for the polaron-pair states with the hole on site $i \neq X$:

$$H_i = g\mu_B \mathbf{B}_{i,\text{eff}} \cdot \mathbf{S}_h/\hbar + g\mu_B \mathbf{B}_{X,\text{eff}} \cdot \mathbf{S}_e/\hbar, \tag{4.2}$$

where g is the g-factor, μ_B is the Bohr magneton, $\mathbf{S}_{e(h)}$ is the spin operator for the electron (hole), and $\mathbf{B}_{i(X),\text{eff}}$ is the effective magnetic field on site i (site X). We take $g = 2$ for the electron and hole and for all sites. As in the previous chapter, we will ignore the coherent evolution of the exciton states, when the hole is on site X, so $H_X = 0$.

The density matrix ρ_i for the case that the hole is on site $i \neq X$ evolves according to the Stochastic Liouville equation:

$$\begin{aligned} \frac{\partial \rho_i}{\partial t} &= -\frac{i}{\hbar}[H_i, \rho_i] - \frac{1}{2}\{\Lambda_i, \rho_i\} + \Gamma_i & (4.3)\\ &= -\frac{i}{\hbar}[H_i, \rho_i] + \sum_{\substack{j \in \text{NN}(i) \\ j \neq X}} \left(\rho_j k_{j\to i} - \rho_i k_{i\to j}\right) \\ &\qquad -\frac{1}{2}\left\{\sum_\lambda k_\lambda |\lambda\rangle\langle\lambda|, \rho_i\right\} \delta_{i\in \text{NN(X)}}, & (4.4) \end{aligned}$$

where $\lambda = S, T_-, T_0, T_+$ (in the basis of site X), $\text{NN}(i)$ are the nearest neighbors of site i, and $\delta_{i\in\text{NN(X)}}$ is 1 if i is a nearest-neighbor of X and zero otherwise.

The second term on the right-hand side of Equation 4.4 accounts for hops from nearest-neighbor sites of site i to site i (and vice versa). The third term is only non-zero when site i is a nearest-neighbor of site X and accounts for the decrease in occupation probability of site i due to exciton formation. As in the previous chapter, we take for the singlet exciton formation rate $k_S = k_{hop}$ and for the triplet exciton formation rates $k_{T_0,T_-,T_+} = k_T = k_S/\gamma$. Since exciton formation is an energetically downward process that occurs by hopping of a hole to the electron, it is reasonable to assume that k_S and k_T are comparable in magnitude to k_{hop}. The density matrix for the exciton states' time dependence is given by:

$$\frac{\partial \rho_X}{\partial t} = \sum_{j \in NN(X)} \sum_{\lambda} k_\lambda |\lambda\rangle\langle\lambda|\rho_j|\lambda\rangle\langle\lambda|. \tag{4.5}$$

In addition to these physical rates, we add an artificial rate for a spin-randomizing flow from the exciton states to the edge sites of the lattice. This rate corresponds to the physical process of decay of excitons and the formation of new polaron pairs. We add this rate such that there is an equilibrium solution of Equations 4.4 and 4.5, which is easier to determine than the time-dependent solution, see Section 2.2.2 on page 27. While the magnitude of this rate affects the occupation probability of site X compared to that of the other sites, it does not affect the fraction of singlet and triplet excitons formed. The additional source term for the N_{edge} edge sites is $k_{eq,i} \operatorname{Tr}[\rho_X] \, I/4$, where I is the identity operator. The rate $k_{eq,i}$ is taken proportional to $\exp(-E_i/k_B T)$ in order to get the right occupation probability of edge site i. To the Liouville equation for site X we then simply add a term $-\sum_{i \in Edge} k_{eq,i} \rho_X$.

For all data presented in this chapter, averages were taken over different energetic and hyperfine disorder configurations until the statistical error was of the order of the size of the symbols shown. Results are shown for $\gamma = k_S/k_T = 10$. We expect that the behavior of the singlet fraction and the magnetic field effect as a function of other parameters is not much affected by the choice of γ. With the chosen value of γ, this behavior is easier to study than for more realistic values of γ close to unity.

4.3 Results

Let us start by considering the effect of the box's size in absence of energetic disorder and Coulomb interactions. The singlet fraction χ_S of the excitons that are formed as a function of the relative hopping rate r is shown in Figure 4.2 for boxes of different sizes and for the two-site model (open symbols). The first thing to notice is that the maximal obtainable singlet fraction is larger than for the two-site model. In fact, it is close to the singlet fraction that would result if complete spin mixing would take place between the polaron pair's spin states:[107] $k_S/(k_S + 3k_T) = \gamma/(\gamma + 3)$ (dashed line in the figure), where the factor 3 comes from the fact that there are three triplets. Clearly, no complete spin mixing can take place in the two-site model, where only two hyperfine fields can change the

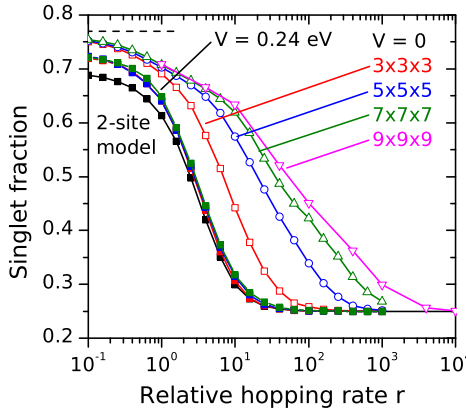

Figure 4.2 The singlet fraction as a function of the relative hopping rate for $\gamma = 10$ and $B = 0$. Results are shown for boxes with 3×3×3 (red), 5×5×5 (blue), 7×7×7 (green), and 9×9×9 (purple) sites and with (filled symbols) and without (open symbols) Coulomb interaction of $V = 0.24$ eV. The results for the two-site model are shown for comparison (black). The dashed line at $\chi_S = 0.769$ indicates the singlet fraction that would result if complete mixing would take place between all electron-hole-pair spin states.

spin configuration of the pair. When the hole can hop away from the electron it can experience different hyperfine fields and the pair's spin configuration will be more effectively mixed.

The second observation is that the transition from slow to fast hopping is shifted to faster hopping rates as compared to the two-site model and shifts further as the box size increases. The reason for this is the following. When the hole reaches the electron, electron-hole pairs with predominantly singlet character will recombine faster than pairs with predominantly triplet character (since $\gamma > 1$). If no recombination occurs, the pair will separate by hopping of the hole. Of those pairs that separate, more than 25% will be triplets. The hole will make a random walk through the box and will return after some time. During this time, the spin configuration of the pair gets mixed by the hyperfine fields, increasing the singlet character (back towards 25%). The amount of spin mixing increases with the time it took the hole to return, which is longer in a larger box.

When Coulomb interaction ($V = 0.24$ eV) is included, the singlet fraction is the same as for the two-site model irrespective of the box size, except for the larger value at slow hopping rates, see the filled symbols in Figure 4.2. The hole is now strongly attracted to the electron and does not have much chance to hop around. Clearly, Coulomb interactions are important for exciton formation and should be included in theoretical considerations involving more than two sites.

Figure 4.3(a) shows the singlet fraction for a 5×5×5 box[§] with Coulomb interaction and energetic disorder strengths of $\sigma = 0$, 0.05, 0.1, and 0.15 eV. The corresponding

[§]The largest box that is computationally feasible when including energetic disorder. As explained in Section 2.2.2 on page 27, to calculate the singlet fraction involves solving a matrix equation. The dimension of that matrix is equal to the dimension of the density matrix of a single configuration ($2^{2n} = 16$ for $n = 2$ particles) times the number of configurations ($N^3 - 1$): $16(N^3 - 1)$.

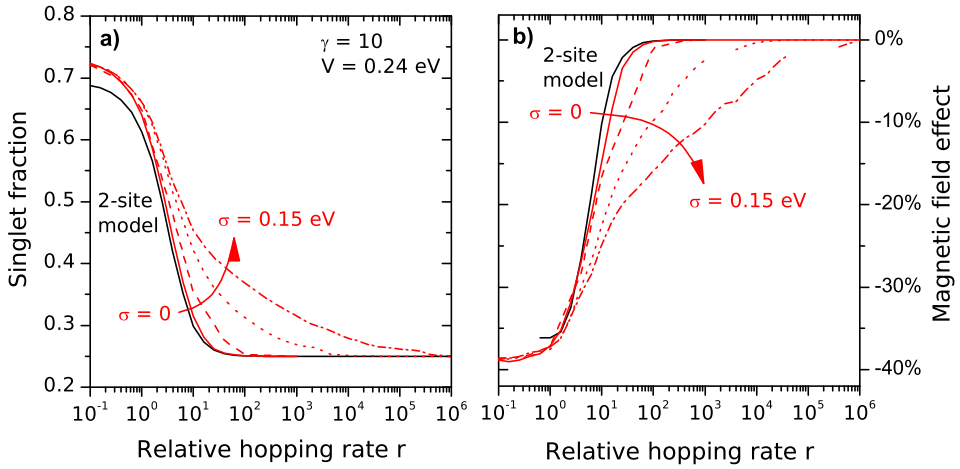

Figure 4.3 (a) Singlet fraction χ_S and (b) its magnetic field effect $[\chi_S(B) - \chi_S(0)]/\chi_S(0)$ as a function of the relative hopping rate in a box of 5×5×5 sites for $\gamma = 10$ and $V = 0.24$ eV (red). Results are shown for different energetic disorder strengths $\sigma = 0$ (solid), 0.05 (dashed), 0.1 (dotted), and 0.15 eV (dash-dotted). The results for the two-site mode (black) are shown for comparison.

magnetic field effects are shown in Figure 4.3(b). The presence of energetic disorder results in a deviation from the statistical singlet fraction of 25% and a magnetic field effect at much higher relative hopping rates than without energetic disorder or for the two-site model. For $\sigma = 0.15$ eV, a magnetic field effect is found for a relative hopping rate up to 10^6, even higher than for the case where no Coulomb interaction was present. Energetic disorder makes some hops away from the central site easier and some hops towards the central site more difficult. The time spent by the hole between the first encounter and the second encounter is thereby increased. As the amount of spin mixing is proportional to this time, the spin mixing increased as well.

4.3.1 Open box

The results presented sofar are for a *closed box*, that is, the hole cannot hop over the boundary of the box. In reality, many electron-hole pairs will be present in an organic semiconductor and a hole can hop out off the Coulomb potential well of one electron into that of another nearby electron. The escaping of a hole to another electron is more likely if the electron-hole pair is a triplet than if it is a singlet, because singlets recombine faster (for $\gamma > 1$). The spin configuration of the hole with the electron it has escaped to is again completely random, that is, with a probability of 0.25 singlet and 0.75 triplet. In this way, the statistical singlet-triplet ratio can be violated even without a spin-mixing mechanism. Consequently, the resulting violation is not magnetic field dependent. The deviation from the statistical ratio resulting from this mechanism depends (besides γ) only on the ratio between the recombination rate and the rate of the hole hopping out of the electron's Coulomb well once the electron and hole have become nearest neigh-

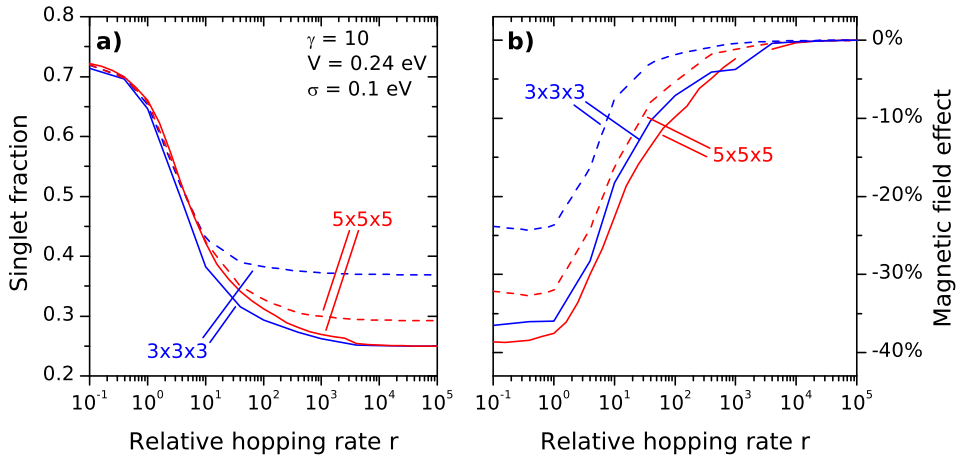

Figure 4.4 (a) The singlet fraction and (b) its magnetic field effect as a function of the relative hopping rate in boxes with (dashed curves, *open box*) and without (solid curves, *closed box*) periodic boundary conditions. Results are shown for box sizes of 3×3×3 (blue) and 5×5×5 (red) sites for $\gamma = 10$, $\sigma = 0.1$ eV, and $V = 0.24$ eV. Boxes of 3×3×3 and 5×5×5 sites corresponds to an electron (or hole) density of, respectively, 3.7% and 0.8%.

bors. The deviation from the statistical ratio from this mechanism increases with increasing charge concentration: The higher the charge concentration the smaller the distance between two electrons and the easier it is for the hole to hop out of the Coulomb well of one electron into that of another. As mentioned, This mechanism does not rely on spin mixing by hyperfine fields (or otherwise) and has therefore no magnetic field dependence.

While it is not feasible to treat more than two particles (electrons or holes) with our stochastic Liouville method, we can approximate the effect described in the previous paragraph by using periodic boundary conditions. Whenever the hole hops over the boundary of this *open box*, we randomize the spin configuration of the electron-hole pair. Hopping over the boundary by the hole corresponds then to the physical process where one hole leaves the electron's Coulomb well while at the same time another hole (with random spin) enters the Coulomb well. In this way, several effects are ignored, for example, the possibility of two holes in the Coulomb well of a single electron or the fact that a new hole might still be correlated with the electron from a previous encounter. Nevertheless, we can gain some insight from this model.

Figure 4.4(a) shows the singlet fraction as a function of the relative hopping rate for a *open box* of 5×5×5 sites for $\sigma = 0.1$ eV and $V = 0.24$ eV. With one electron (and hole) per box this corresponds to an electron (hole) concentration of $1/5^3 = 0.8\%$. When $r \lesssim 1$, there is no difference in the singlet fraction between the open and closed boxes, because in either case the maximal amount of spin mixing takes place. However, for $r \gtrsim 1$, the singlet fraction is larger for the open box. Moreover, the singlet fraction remains larger that the statistical value even in the limit $r \to \infty$. The magnetic field effect is shown in Figure 4.4(b)

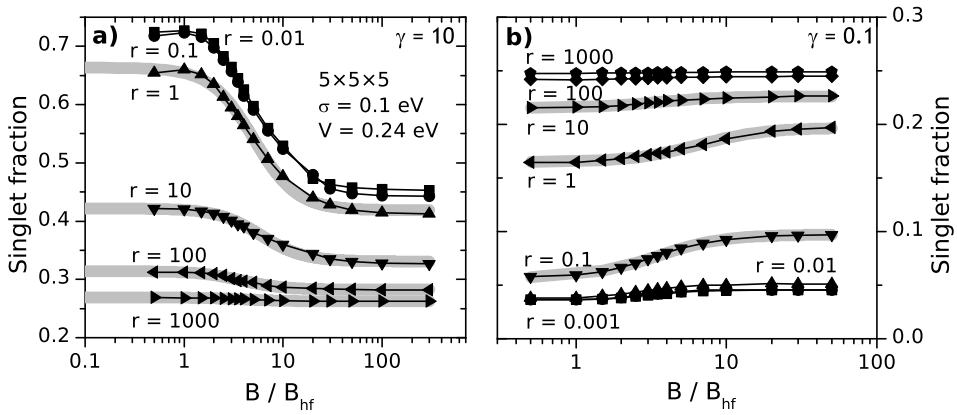

Figure 4.5 Magnetic field dependence MFE(B) of the singlet exciton fraction χ_S calculated for the multi-site model with a box of 5×5×5 sites for (a) $\gamma = 10$ and (b) $\gamma = 0.1$, both for $\sigma = 0.1$ eV and $V = 0.24$ eV. Results are shown for a relative hopping rate r ranging from 0.001 to 1000. Lorentzian fits are shown as thick shaded curves with widths B_0 that are $4 - 6B_{hf}$ for $\gamma = 10$ and $3.5 - 6.5B_{hf}$ for $\gamma = 0.1$. The standard deviations of the hyperfine fields of electrons and holes were taken to be equal.

4.4 Lineshapes

Figure 4.5(a) shows the singlet fraction as a function of the applied magnetic field for $\gamma = 10$, $\sigma = 0.1$ eV, $V = 0.24$ eV, and several relative hopping rates ranging from fast hopping to slow hopping. All lineshapes are Lorentzian with widths B_0 (see Section 1.2.1 on page 8) that increase from $4B_{hf}$ for slow hopping to $6B_{hf}$ for $r = 10^3$, see the fits in the figure. Results for $\gamma = 0.1$ are shown in Figure 4.5(b). These lineshapes are Lorentzian too, with B_0 ranging from $3.5B_{hf}$ for $r = 0.1$ to $6.5B_{hf}$ for $r = 100$. The linewidths are comparable to those of the two-site model, see Figure 3.5. Even the ultra-small-magnetic-field effect might be visible for $r = 0.1$ and 1 for $\gamma = 10$, although it is comparable in size to the error margins.

4.5 Conclusions

Without taking Coulomb interactions into account, a deviation from the statistical singlet-triplet exciton ratio (and thus a magnetic field effect) occurs at relative hopping rates that are more than an order of magnitude larger for exciton formation on a lattice of 3×3×3 sites (and larger) than for the two-site model. However, with Coulomb interactions, the results are close to each other when there is only a small amount of energetic disorder (less than 0.05 eV). It is therefore important to include Coulomb interaction when considering the magnetic field effect on the singlet-triplet ratio.

For larger energetic disorder, though, the transition from slow hopping, where the statistical ratio can be violated, to fast hopping, where it cannot, is much more spread out. For a realistic energetic disorder strength of 0.15 eV, a violation of the statistical ratio is found for relative hopping rates up to 10^6 for $\gamma = 10$. This could be an explanation for the observation of magnetic field effects in materials where the hopping rate might not be much slower than the hyperfine frequency. The lineshapes with Coulomb interaction and a realistic amount of energetic disorder can be fitted by a Lorentzian with a width B_0 of 3.5 to 6.5 times the hyperfine field, comparable to the lineshapes of the two-site model.

We conclude that, while the two-site model gives comparable lineshapes, to accurately model the formation of excitons, a multi-site model should be used. The two-site model underestimates the amount of spin mixing in the slow-hopping limit but especially for relative hopping rates larger than unity when the amount of energetic disorder is larger than 0.05 eV.

5

Prediction of a giant magneto-conductance in doped polymers

Room-temperature magnetoconductance of the order of 10% *has been observed in organic semiconductors. We predict that even larger magnetoconductance can be realized in suitably synthesized doped conjugated polymers. In such polymers, ionization of dopants creates free charges that recombine with a rate governed by a competition between an applied magnetic field and random hyperfine fields. This leads to a spin-blocking effect that depends on the magnetic field. We show that the combined effects of spin blocking and charge blocking, the fact that two free charges cannot occupy the same site, lead to a magnetoconductance of more than* 90%. *This magnetoconductance occurs even at vanishing electric field and is therefore a quasi-equilibrium effect. The influences of the dopant strength, energetic disorder, and interchain hopping are investigated. We find that the dopant strength and energetic disorder have only little influence on the magnetoconductance. Interchain hopping strongly decreases the magnetoconductance because it can lift spin-blocking and charge-blocking configurations that occur in strictly one-dimensional transport. We provide suggestions for realization of polymers that should show this magnetoconductance.*

5.1 Introduction

In the last decade, large room-temperature magnetic field effects in the current and in the electroluminescence of devices made of organic semiconductors have been found.[13,32,36,48,53,82,83,86,92,124] The precise mechanisms behind these effects are still debated, but agreement is arising that the effects are caused by the magnetic-field

This chapter was adapted with permission from:

S. P. Kersten, S. C. J. Meskers, and P. A. Bobbert. *Route towards huge magnetoresistance in doped polymers*. Phys. Rev. B **86**, 045210 (2012).

sensitivity of spin-selective reactions between spin-carrying electronic excitations (electrons, holes, triplet excitons). Striking analogies exist with mechanisms known in the field of spin chemistry.[111] The involvement of hyperfine fields has recently been demonstrated by the occurrence of isotope effects.[82,83] Isotope substitution in organic semiconductors—the replacement of hydrogen by deuterium or carbon-12 by carbon-13 leads to different nuclear magnetic moments and therefore to a different hyperfine interaction between the nuclei and spin-carrying excitations, while leaving all other electronic properties of the semiconductor unchanged. It has been shown that the magnetic field dependence scales accordingly.[82,83]

The electronic spin in an organic semiconductor interacts with many (typically of the order of ten or more) nuclear spins. As a consequence, this interaction can be quite well described by assuming that the electronic spin experiences a classical, quasi-static, and random hyperfine field, having a Gaussian distribution with a standard deviation B_{hf} of the order of a millitesla.[15,105] The evolution of the spin state of a pair of spin-carrying excitations is then determined by the sum of an externally applied magnetic field B and the local hyperfine fields, which are different for the two excitations. If the reaction between the two excitations is spin-selective, the reaction rate changes when the magnitude of B surpasses B_{hf}, giving rise to a B-dependent reaction rate. Magnetic field effects in the current of unipolar organic devices have been explained by a mechanism in which two electrons or holes react to form a singlet bipolaron.[16] Magnetic field effects in the electroluminescence of bipolar devices have been explained by a mechanism in which electrons and holes react to form singlet or triplet excitons with different rates.[58,82,83] Spin-selective reactions between electrons and holes as well as between electrons or holes and triplet excitons have also been suggested to be responsible for magnetic field effects in the current.[32,48,92]

A magnetic field effect in the current is usually interpreted as a magnetoresistance. The reported magnetoresistance of present organic devices is of the order of 10% at rather high electric fields.[73] With the insight that magnetic field effects in organic semiconductors are caused by spin-selective reactions between spin-carrying excitations one may ask the question if it is possible to *design* organic materials with even higher magnetoresistance at a low electric field. The manufacturing of an organic material with very large magnetoresistance at low magnetic and electric field, to be used in highly sensitive magnetic sensors or maybe even magnetic switches, would be of large technological interest. Such sensors could be integrated with other cheap and flexible organic electronics. The present chapter is concerned with a theoretical survey of this possibility.

The route we propose towards high magnetoresistance at low electric field is the use of doped π-conjugated polymers with specific properties. Doped polymers have been investigated in great detail because of their conducting properties. In these polymers free charges created by ionization of dopants move along the polymer chains. Our present interest is in the concurrent creation of *free spins*, carried by the free charges and the ionized dopants. We will consider the case of *intrinsically doped polymers*, where the dopants are part of the polymer chains themselves.

To obtain a large magnetoresistance it is important that the coupling between the monomeric units of the polymers is small, such that the hopping transport between these units takes place with a rate that is smaller than the hyperfine precession rate. This makes the proposed polymers different from commonly used conjugated polymers, where charges can delocalize over several monomers. We propose to achieve the required small hopping rate by inserting spacer units in between the monomers. Under this condition, the recombination rate of a free charge with an ionized dopant will become magnetic-field-dependent, leading to magnetoresistance. Another important condition for obtaining large magnetoresistance is that the charge transport is one-dimensional. In this case, free charges contributing to transport are forced to regularly recombine with the ionized dopants. In principle, polymers are ideal in this respect, because charge transport mainly takes place along the polymer chain. However, interchain hopping can also take place, and this may allow a free charge to hop around a dopant. In order to obtain a large magnetoresistance, interchain hopping will therefore have to be suppressed. Suppression of interchain hopping can be achieved by introducing side groups that keep individual polymer chains sufficiently separated from each other.

This chapter is built up as follows. In Section 5.2 we will introduce our model system for a doped polymer. We will show that in the case of low density of free charges in the system the problem of finding its conductivity can be mapped onto that of a resistor model. The latter problem can be easily solved. In this case, the magnetoresistance is solely caused by a spin-blocking effect in the recombination of a free charge with a dopant. In the general case of high free electron density we find the conductivity from Monte Carlo simulations. In these simulations the effect of charge blocking is included, that is, the effect that two free charges are not allowed to occupy the same site due to their Coulomb repulsion. In Section 5.3 we present the results of the resistor model and those of the Monte Carlo simulations. The influences of the dopant strength, energetic disorder, and interchain hopping are investigated. In Section 5.4 we discuss how the envisaged doped polymers could be realized. Section 5.5 contains a summary and the main conclusions.

5.2 Model

We model a polymer chain as a sequence of sites along which nearest-neighbor hopping of localized charges occurs; see Figure 5.1. For simplicity, we assume that dopant sites are distributed periodically within the chain, with a period of n sites. Because of the one-dimensionality, the case of arbitrarily distributed dopants follows from combining the results of periodically doped chains with appropriate weights for different n. We consider the case of donors—the case of acceptors is completely equivalent—with a highest occupied molecular orbital (HOMO) that lies a small energy Δ below the lowest unoccupied molecular orbital (LUMO) of the host sites. (Δ is negative if the host's LUMO is lower in energy than the donor's HOMO.) In that case, ionization of a donor can take place at thermal conditions by hopping of an electron from the donor to a neighboring host site. With the unionized donor being a spin singlet, the combination of the free electron and the

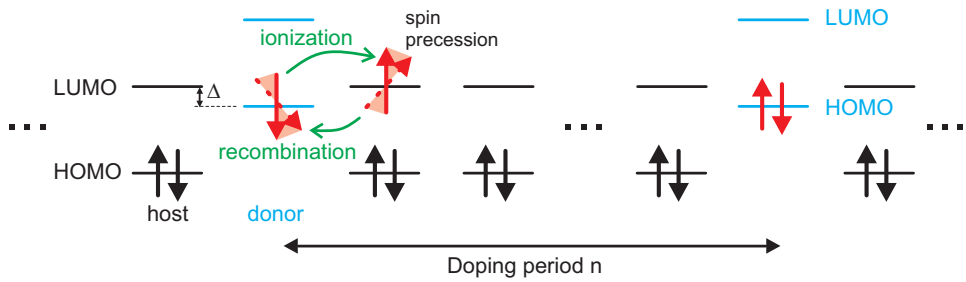

Figure 5.1 Doped polymer chain containing donor sites with period n. A small energy difference Δ between donor HOMO and host LUMO allows ionization of donors, followed by precession of the donor spin and the free-electron spin (red arrows). Recombination occurs back to the spin-singlet unionized donor state.

ionized donor, both having spin $\frac{1}{2}$, will initially also be a spin singlet. However, the different hyperfine fields at the positions of the free electron and ionized donor mixes in triplet character, which reduces the recombination rate back to the singlet state of the unionized donor. Spin mixing also changes the recombination rate of the free electron with other ionized donors. The spins of the free electron and the ionized donor might happen to be in a triplet configuration, for which recombination would not be allowed. Spin mixing by the random hyperfine fields will then raise the recombination rate by mixing in singlet character. An applied magnetic field suppresses the spin mixing and hence the recombination. In both cases, a magnetic field-dependent *spin blocking* occurs that leads to magnetoresistance, even at vanishing electric field.

The combination of incoherent spin-selective hopping and coherent spin evolution can be described with the stochastic Liouville equation, see Section 2.2 on page 24. It follows from this equation that when the hopping rate k_{hop} is much larger than the hyperfine frequency ω_{hf} of typically 10^8 s^{-1} ($\omega_{\text{hf}} = \gamma B_{\text{hf}}$, with γ the gyromagnetic ratio) the effects of the hyperfine fields will be quenched and no magnetoresistance occurs. The largest magnetoresistance occurs when k_{hop} is much smaller than ω_{hf} and this "slow-hopping" case is the case we consider from now on.* The observation of large magnetic field effects in organic semiconductors[13,32,36,48,53,82,83,86,92,124] indicates that the hopping rate can indeed be smaller than or at least comparable to the hyperfine frequency. Because coherent effects between eigenstates of the spin Hamiltonian vanish in the limit of slow hopping, we only need to consider the occupancy of the (localized) spin eigenstates and hopping between these states, see Section 2.2.3 on page 27.

5.2.1 Resistor model

In Figure 5.2(a) we consider a part of the chain for the simplest situation, with periodically a donor and a host site, corresponding to a period $n = 2$ in Figure 5.1.

*The extremely large magnetic field effect that was found for intermediate hopping rates in Chapter 3 occurs only when $k_{\text{S}} \ll k_{\text{T}}$. Recombination with a dopant can be mapped onto the exciton formation problem where $k_{\text{S}} > k_{\text{T}}$, see Appendix A.

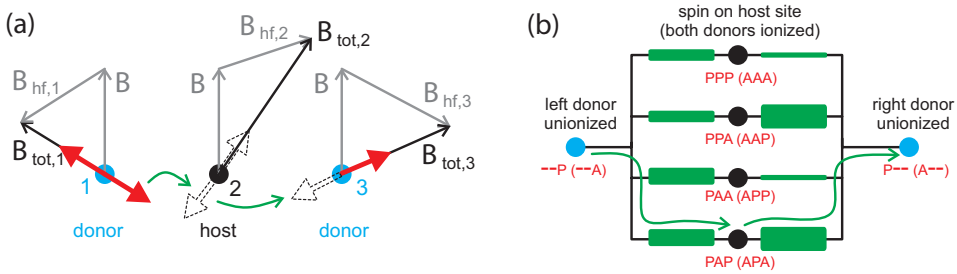

Figure 5.2 (a) Donor-host-donor sequence $i = 1, 2, 3$ for the case $n = 2$. The spin eigenstates are indicated by the red and dashed arrows. The total effective magnetic fields $\mathbf{B}_{\mathrm{tot},i}$ are the sums of the external field $\mathbf{B}$ and local random hyperfine fields $\mathbf{B}_{\mathrm{hf},i}$. Two possible consecutive hopping events are shown, corresponding to ionization at the left donor and recombination at the right donor. (b) Resistor network corresponding to hopping between the spin eigenstates of (a), with conductances indicated by the thickness of the drawn resistors. The arrows show the current flow corresponding to the two hopping events in (a). The labeling of the states indicates whether the spins on the three sites are parallel (P) or antiparallel (A) to the local effective magnetic field or whether there is no spin-1/2 (−) on that site.

To demonstrate the essence of the magnetoresistance occurring in this system, we take $\Delta = 0$ and first consider what we will call a "low electron density", corresponding to at most one *free electron* on the chain. In this case, there is either only one donor unionized—the free electron is at that donor site—and no electrons on host sites, or all donors are ionized and there is only one free electron on a host site. Since an ionized donor site is positively charged, that means that the whole chain is positively charged due to the absence of compensating electrons.[†] In the donor-host-donor sequence of Figure 5.2(a) the free electron can be on one of the three sites $i = 1, 2, 3$. If the electron is on either of the donor sites ($i = 1, 3$), that donor is unionized, while the other is ionized. The spin eigenstates then correspond to a spin at the ionized donor that can be either parallel (P) or anti-parallel (A) to the total effective magnetic field $\mathbf{B}_{\mathrm{tot},i}$ at that donor, which is the sum of the external magnetic field $\mathbf{B}$ and the local random hyperfine field $\mathbf{B}_{\mathrm{hf},i}$. We label these eigenstates as $--$P, $--$A, P$--$, and A$--$. If the electron is on the host site $i = 2$, there are spins at all three sites and the corresponding eigenstates are labeled as PPP, AAA, APP, PAA, PAP, APA, PPA, and AAP. In Figure 5.2(a) two consecutive hops are indicated, corresponding to $--\mathrm{P} \to \mathrm{PAP} \to \mathrm{P}--$.

In presence of a vanishingly small electric field F the current through the hopping network can be calculated from a mapping onto a resistor network as derived by Ambegaokar and coworkers,[1] see Section 2.4 on page 32. The same mapping is also possible between a resistor network and the energetic spin eigenstates that have been introduced above, where the above eigenstates correspond to the nodes of the network. Generalizing the result of Reference 1, the conductance between

[†]This situation might be realized by applying a large negative gate voltage in a FET-like device that forces out almost all electrons.

nodes p and q is given by

$$\tilde{G}_{pq} = \frac{e^2 \tilde{k}_{pq}^{\text{symm}}}{k_B T} \exp\left(\frac{E_F^{\text{network}}}{k_B T} - \frac{E_p + E_q}{2 k_B T} \right), \tag{5.1}$$

where $k_B T$ is the thermal energy and e the electronic charge. E_p and E_q are the energies associated with nodes p and q of the network, and E_F^{network} is the Fermi energy of the network, which determines the number of extra charges on the chain (more on that below). $\tilde{k}_{pq}^{\text{symm}}$ is a symmetrized hopping rate: $\tilde{k}_{pq}^{\text{symm}} \equiv (\tilde{k}_{pq}\tilde{k}_{qp})^{1/2}$. The rates $\tilde{k}_{pq}$ are equal to a spin-independent rate k_{pq} multiplied by a spin projection factor P_{pq}: $\tilde{k}_{pq} \equiv P_{pq} k_{pq}$, see Section 2.2.3 on page 27. For hops of the electron between two host sites we have $P_{pq} = \cos^2(\theta_{pq}/2)$ ($\sin^2(\theta_{pq}/2)$) for hops between eigenstates for which the spin keeps (changes) its orientation with respect to the direction of the local effective magnetic field, where θ_{pq} is the angle between the effective magnetic fields of the two sites. For recombination from or ionization to a state for which the dopant spin is parallel and the electron spin antiparallel to the local effective magnetic field, or vice versa, we have $P_{pq} = \frac{1}{2}\cos^2(\theta_{pq}/2)$. If both spins are parallel or antiparallel to the local effective magnetic field we have $P_{pq} = \frac{1}{2}\sin^2(\theta_{pq}/2)$. The latter factors are the projections onto the spin-singlet subspace. The resistor network corresponding to Figure 5.2(a) for the case $\Delta = 0$, $n = 2$, and $k_{pq} = k_{\text{hop}}$ for all allowed hops is given in Figure 5.2(b), where the thickness of the drawn resistors indicates their conductance. We note that reversing all spins leaves the network unchanged, which is indicated by the labels between brackets. It is straightforward to set up resistor networks for larger values of n, but their complexity increases rapidly with increasing n.

The requirement, for the mapping onto a resistor network, that the occupation probabilities of any two site be independent restricts us to the case where there is only a single electron in the resistor network. If there were more than one electron in the network, the occupation of the states PPP, AAA, APP, etc. would not be independent: Those states cannot be occupied by an electron if any other of those states is occupied by another electron, because two electrons cannot be on the same site. The resistor model, therefore, only models our doped polymer correctly in the limit of low electron densities, where interactions between two electrons are not important.

The Fermi energy that appears in Equation 5.1 is not the same as the Fermi energy of the original doped chain. In the derivation given in Section 2.4 on page 32, every site was mapped to a node of the resistor network. However, in this section we have mapped every site between two donor sites to four nodes of the resistor network, corresponding to the four possible (unique) spin states of the donor sites. The number of charges in the chain of sites is equal to

$$N_{\text{donors}} n e^{E_F / k_B T}, \tag{5.2}$$

where N_{donors} is the number of donors in the chain, n is the doping period, and E_F is the Fermi energy of the real system. This number must be equal to the number

of charges in the resistor network, which is given by

$$N_{\text{donors}}(4n-3)e^{E_{\text{F}}^{\text{network}}/k_{\text{B}}T}. \tag{5.3}$$

This leads to the following relation between the two Fermi energies:

$$\frac{n}{4n-3}e^{E_{\text{F}}/k_{\text{B}}T} = e^{E_{\text{F}}^{\text{network}}/k_{\text{B}}T}. \tag{5.4}$$

The charge-carrier mobility can be obtained from the resistance $R(B)$ of a chain of $N \gg 1$ sites by $\mu(B) = \exp(-E_{\text{F}}/k_{\text{B}}T)Na^2/eR(B)$, where a is the inter-site distance. The resistance $R(B)$ is the sum of the resistances of many of the above resistor networks with random hyperfine fields and is obtained by a hyperfine-field average of the resistance of such a network. For simplicity we assume equal standard deviations B_{hf} for the Gaussian distributions of the donor and host hyperfine fields, and equal gyromagnetic ratios. If donor and acceptor have different B_{hf} this will only change the results for non-zero finite B but not the total magnetoresistance.

5.2.2 Monte-Carlo simulations

As explained, the resistor model is limited to the case of low electron densities. When the electron density is high, electrons interact with each other. While in principle two electrons could form a bipolaron, see Section 1.2.4 on page 12, we assume in this chapter that the bipolaron formation energy is so high that bipolaron formation does not happen. (The magnetoconductance resulting from bipolaron formation in a one-dimensional system is investigated in the next chapter.) Therefore, the main effect of those interactions in a one-dimensional system is that an electron cannot get past another electron. In other words, an electron can be blocked by another. We call this *charge blocking*. We take this effect into account in Monte Carlo simulations that we performed for long chains. In these simulations hops are chosen randomly with weights proportional to the rates $\tilde{k}_{pq}$ discussed above, where now two free electrons are not allowed to occupy the same site. After each hop the time is increased with a random time step drawn from an exponential distribution with a decay time equal to the inverse of the sum of the rates of all possible hops, see Section 2.3 on page 30. A small electric field F is applied that leads to a net drift of the electrons along the chain by decreasing the rate of the up-field hops by a factor $\exp(-eaF/k_{\text{B}}T)$. The mobility is obtained from the average electron drift velocity $v(B)$ by $\mu(B) = v(B)/F$. We take F small enough to be in the regime where $v(B)$ is linear in F, yet large enough to obtain a sufficient accuracy in $\mu(B)$.

We considered the charge-neutral case of "high electron density", where the number of free electrons is equal to the number of ionized donors. The typical chain lengths that we took were 2×10^5 ($n = 2$) up to 3×10^6 ($n = 30$) sites. Steady-state situations were obtained after 2×10^9 hops, after which $v(B)$ was calculated for

2×10^9 ($n = 2$) up to 3×10^{10} ($n = 30$) hops. Averages were taken over 10 ($n = 30$) up to 200 ($n = 2$) hyperfine-field configurations.

Monte Carlo simulations were also performed for the case of low electron density. In that case the mobility can alternatively be obtained by using Einstein's relation $\mu(B) = eD(B)/k_{\mathrm{B}}T$, and calculating the diffusion constant $D(B)$ from Monte Carlo simulations of diffusion of a single electron along a chain in absence of an electric field. The chain lengths that we took were the same as for the case of high electron density. The number of hops in the calculation of the diffusion constant were 2×10^6 ($n = 30$) up to 8×10^6 ($n = 2$). Averages were taken over 10^3 ($n = 10$) up to 3.5×10^3 ($n = 2$) hyperfine-field configurations.

5.3 Results

The results of the resistor model and the Monte Carlo simulations are discussed in the next two subsections for low and high electron density. After that, lineshapes and the effects of relaxing some requirements we have made so far are discussed.

5.3.1 Low electron density

We start by considering the case of low electron density, where there is at most one free electron on the chain. The results for the mobility obtained from the resistor model are shown in Figure 5.3(a). In the limit $B \to \infty$ we obtain $\mu(\infty) = [n^2/(4n - 3)(n + 2)]ek_{\mathrm{hop}}a^2/k_{\mathrm{B}}T$ (crosses). Results for $\mu(0)$ were evaluated for networks up to $n = 5$ (plusses). For $n \to \infty$ and finite B the effect of the presence of the donors vanishes and we thus obtain $\mu(0) = ek_{\mathrm{hop}}a^2/k_{\mathrm{B}}T$. The results for the mobility using the Einstein relation, with the diffusion constant obtained from Monte Carlo simulations in absence of an electric field, are also displayed ($B = 0$: filled circles, $B \to \infty$: open circles). The agreement with the results of the resistor model and with the mobility obtained directly from the Monte Carlo simulations with a small electric field (not shown) is perfect. These results demonstrate explicitly that the magnetic field effect occurs even in absence of an electric field, namely as *magnetodiffusion*.

The magnetic field effect in the mobility, defined as $\mathrm{MFE} \equiv \mathrm{MFE}(\infty)$, where $\mathrm{MFE}(B) \equiv [\mu(B) - \mu(0)]/\mu(0)$, is shown in Figure 5.3(c) (half-filled circles). For $n = 2$ we obtain a magnetic field effect of -37%, which grows to -75% in the limit $n \to \infty$. The physical reason for the magnetic field effect is the spin blocking that occurs in the case of large B due to the occurrence of spin configurations where the spin of the electron has the same orientation as that of a neighboring ionized donor site, preventing recombination and further transport. The reason why the magnetic field effect increases for increasing doping period n is that spin blocking then becomes more effective. At short doping period a spin-blocking situation of a free charge and an ionized donor in a configuration with parallel spins can be lifted not only by spin mixing by hyperfine fields, but also by return of the free charge to the ionized donor that was last visited. Recombination at this donor

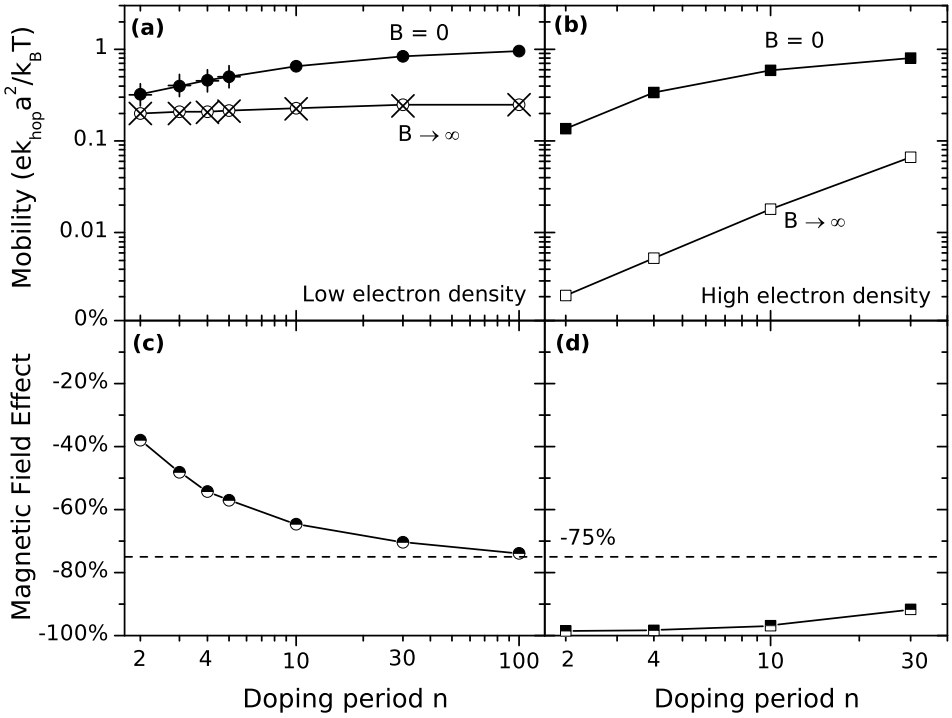

Figure 5.3 Mobility as a function of doping period n for $B = 0$ and $B \to \infty$ for low (a) electron density as found from the resistor model (plusses and crosses) and from Monte Carlo simulations (discs) and (b) for high electron density found from Monte Carlo simulations. Magnetic field effect in the mobility for (c) low and (d) high electron density. The horizontal line shows the asymptotic magnetic field effect of -75% in absence of interaction. The error in the Monte Carlo results is smaller than or equal to the size of the symbols.

and subsequent re-ionization of this donor randomizes the spin of the free charge, which can lift the spin blocking. This process becomes more unlikely for a longer doping period.

We checked that in the Monte Carlo simulations at zero electric field the equilibrium occupancies of all states are equal. This should be the case because the hyperfine energy scale of μeV of energy differences between the states is orders of magnitude smaller than the thermal energy scale of 10 meV. A magnetic field of the order of the hyperfine fields therefore cannot lead to a change of equilibrium occupancies. We note that existing explanations of magnetic field effects involve driven reactions between spin-carrying excitations and therefore assume a non-equilibrium situation. By contrast, *the present magnetoresistance is a quasi-equilibrium effect*, that occurs in the diffusion constant even in absence of an electric field.

5.3.2 High electron density

We now consider the case of high electron density, where the number of free electrons is equal to the number of ionized donors and the chain is electrically neutral. The results for the mobility and the magnetic field effect in the mobility

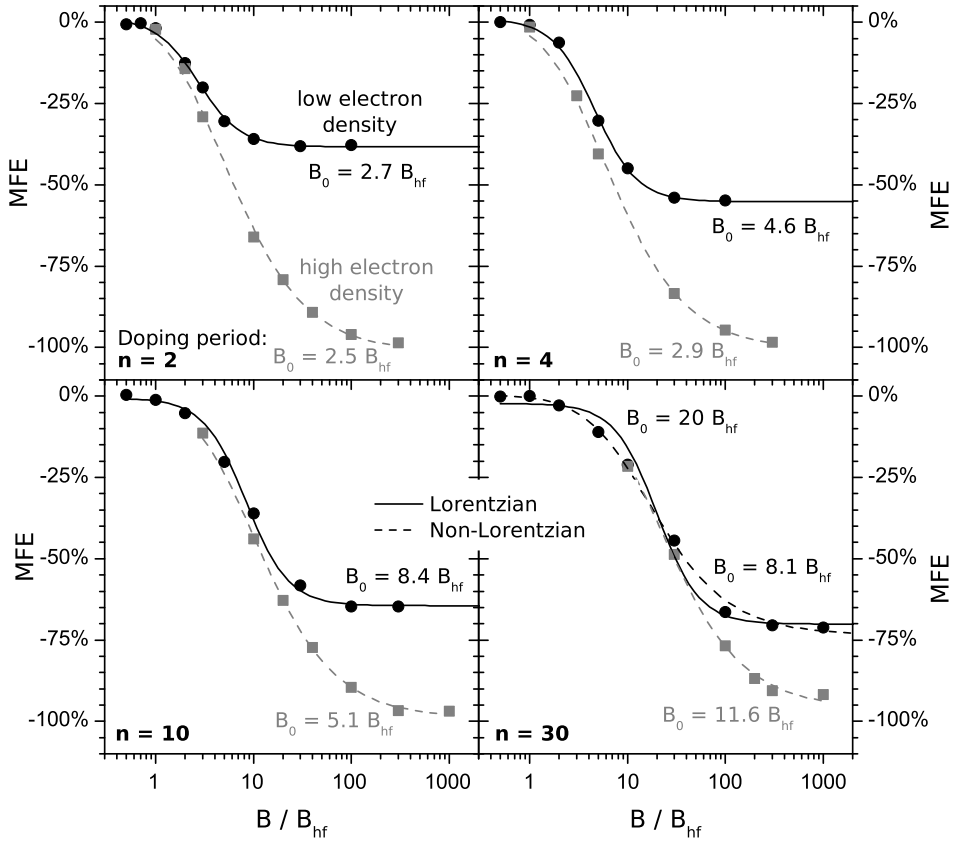

Figure 5.4 Lineshapes of MFE(B) at low (circles) and high (squares) electron density, for four different doping periods. Lorentzian ($B^2/[B^2 + B_0^2]$, solid line) and non-Lorentzian ($B^2/[|B| + B_0]^2$, dashed line) fits are shown with the corresponding values of B_0.

as obtained from Monte Carlo simulations for this case are shown in Figures 5.3(b) and (d). For large doping period n the results approach the case of low electron density, as expected. Contrary to that case, however, we now see that the size of the magnetic field effect increases with decreasing n. For $n = 2$ a magnetic field effect of $-98.5 \pm 0.3\%$ is found, corresponding to a magnetoresistance of almost two orders of magnitude. Figure 5.3(b) shows that the main cause for this huge magnetoresistance is a dramatic drop in the mobility for $B \to \infty$ at low doping period. The reason for this huge magnetoresistance is that the spin blocking is now enhanced by *charge blocking*: since two electrons cannot occupy the same site, a single spin-blocked electron blocks all electrons that would otherwise be able to pass it.

5.3.3 Lineshapes

Figure 5.4 shows MFE(B) for several doping periods, for low (circles) and high (squares) electron density. For low electron density, the lineshape is Lorentzian for small n, but changes to the non-Lorentzian between $n = 10$ and 30. For high

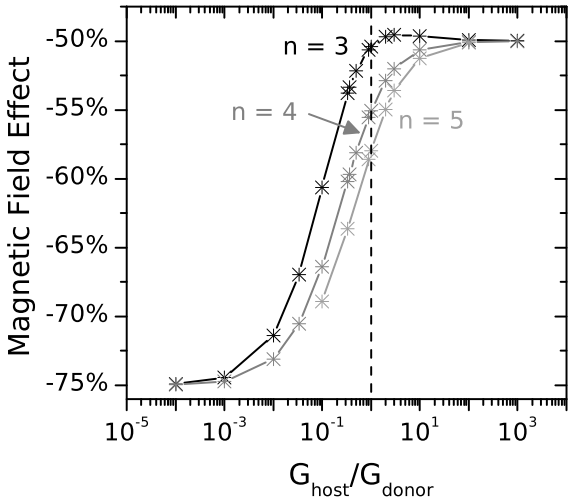

Figure 5.5 Magnetic field effect in the mobility at low electron density as a function of the ratio between G_{host} and G_{donor}, for doping periods $n = 3$, 4, and 5. Points lying on the dashed line correspond to the data shown in Figure 5.3.

electron density, the lineshapes are always non-Lorentzian and broader than for low electron density.

5.3.4 Influences of the dopant strength and energetic disorder

We investigated the influences of the donor-host HOMO-LUMO energy offset $\Delta = E_{\text{host}}^{\text{LUMO}} - E_{\text{donor}}^{\text{HOMO}}$, which is a measure of the dopant strength of the donor, and of energetic disorder in the site energies of donor and host. For simplicity we considered only the case of low electron density. We expect that the conclusions drawn will qualitatively also hold for high electron density.

In the resistor model, the effect of a finite Δ manifests itself in a difference between the spin-independents part of the conductance between two host sites, G_{host}, and the conductance between a donor and a host site, G_{donor}. We note that the relevant dimensionless parameter is $\Delta/k_{\text{B}}T$. Since for the case of a doping period $n = 2$ there are only hops between donor and host sites, all hops are affected equally by a change in Δ and there is thus no dependence of the magnetic field effect on Δ for this case. For doping periods $n = 3$, 4, and 5, the magnetic field effect in the mobility as a function of the ratio $G_{\text{host}}/G_{\text{donor}}$ is shown in Figure 5.5. (The effect of Δ on G_{host} and G_{donor} will be discussed later in this section.) The results shown earlier for low electron density in Figure 5.3 correspond to $G_{\text{host}} = G_{\text{donor}}$ and lie on the dashed line in Figure 5.5. We see in Figure 5.5 that there is a gradual decrease in the magnitude of the magnetic field effect from 75% when $G_{\text{host}} \ll G_{\text{donor}}$ to 50% when $G_{\text{host}} \gg G_{\text{donor}}$. Except for a small region in $G_{\text{host}}/G_{\text{donor}}$ for $n = 3$, the magnitude of the magnetic field effect never gets smaller than 50%. *The largest magnetic field effect is found when the hops that determine the current—the slowest hops—are the magnetic-field-dependent hops.*

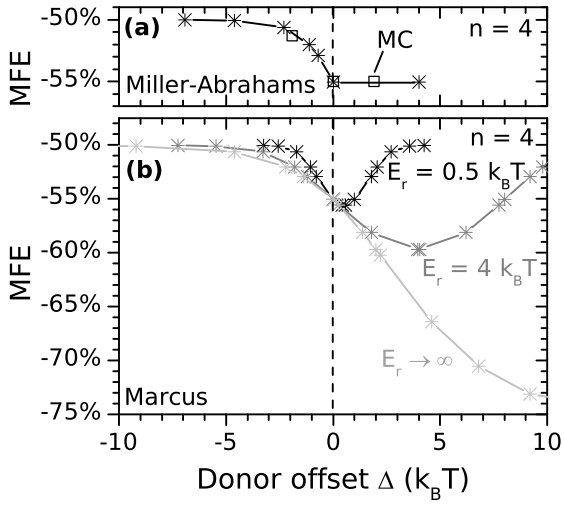

Figure 5.6 Magnetic field effect (MFE) in the mobility at low electron density as a function of energy offset Δ for $n = 4$, for (a) Miller-Abrahams hopping and (b) Marcus hopping. The asterisks are calculated with the resistor model while the squares are obtained with Monte Carlo simulations. In the case of Marcus hopping, results are shown for three values of the reorganization energy. The dashed line corresponds to the case considered in Figure 5.3.

The dependence of $G_{\text{host}}/G_{\text{donor}}$ on Δ is determined by the specific hopping model. In modeling studies of charge transport in organic semiconductors usually Miller-Abrahams[77] or Marcus[66] hopping models are used, see Section 1.1.1 on page 3. For Miller-Abrahams hopping we find:

$$\frac{G_{\text{host}}}{G_{\text{donor}}} = \begin{cases} \exp(-\Delta/k_{\text{B}}T) & \text{if } \Delta \leq 0 \\ 1 & \text{if } \Delta > 0 \end{cases}, \tag{5.5}$$

while for Marcus hopping we find:

$$\frac{G_{\text{host}}}{G_{\text{donor}}} = \exp\left(\frac{-\Delta + \Delta^2/2E_{\text{r}}}{2k_{\text{B}}T}\right). \tag{5.6}$$

Here, E_{r} is the reorganization energy, which is typically of the order of 0.1 eV (approximately $4k_{\text{B}}T$ at room temperature).[109]

Figure 5.6 shows the magnetic field effect in the mobility as a function of the offset Δ for doping period $n = 4$, for both (a) Miller-Abrahams and (b) Marcus hopping. It is clear from Figure 5.6 that the type of hopping determines the effect of Δ on the magnetic field effect. While for Miller-Abrahams hopping the magnetic field effect is constant for $\Delta > 0$, for Marcus hopping the magnitude of the effect can both decrease or increase as a function of Δ for realistic E_{r}. For Miller-Abrahams hopping, we also calculated the magnetic field effect using Monte Carlo simulations to confirm the results of the resistor model. The agreement is perfect; see the squares in Figure 5.6(a).

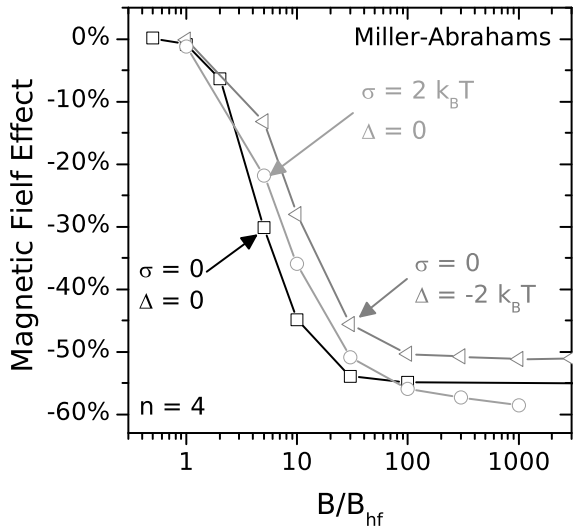

Figure 5.7 MFE(B) found from Monte Carlo simulations at low electron density for $n = 4$ and different combinations of the energy offset Δ and strength of the energetic disorder σ.

We also studied the effect of energetic disorder, again for the case of low electron density. We took Gaussian energetic disorder with a standard deviation σ both for the HOMO energies of the donor sites and the LUMO energies of the host sites. The relevant dimensionless parameter is $\sigma/k_{\mathrm{B}}T$. For the special case $n = 2$ there are two types of conductances within each donor-host-donor sequence: the ones between the middle host site and the left donor site, and the ones between the middle host site and the right donor site. A change in the ratio between the spin-independent parts of those two types of conductances with respect to unity increases the magnitude of the magnetic field effect in the mobility from 37% at a ratio of unity (the case considered in Section 5.3.1) to 50% at an infinite or zero ratio. For $n > 2$, a difference between the energies of neighboring host sites decreases G_{host}, while an energy difference between a host and a donor site can both increase or decrease G_{donor}, depending on Δ and, in the case of Marcus hopping, E_{r}. Figure 5.7 compares MFE(B) when $\sigma = \Delta = 0$ (the case considered in Section 5.3.1) to the case $\Delta = -2k_{\mathrm{B}}T$ (that is, the donor level above the host level) and $\sigma = 0$, and to the case $\Delta = 0$ and $\sigma = 2k_{\mathrm{B}}T$, for Miller-Abrahams hopping. The results in Figure 5.7 were obtained from Monte Carlo simulations. The case of positive Δ is identical to that of $\Delta = 0$ for Miller-Abrahams hopping; see Figure 5.6(a). It is clear from Figure 5.7 that neither non-zero Δ nor non-zero σ changes the magnetic field effect significantly.

The conclusion of our analysis is that the predicted magnetoresistance is very robust against a non-zero energy offset Δ and the presence of energetic disorder. Since the relevant dimensionless parameters are $\Delta/k_{\mathrm{B}}T$ and $\sigma/k_{\mathrm{B}}T$, this also means that the magnetoresistance is robust against a change in the temperature. We do note that a non-zero Δ or σ creates energy barriers in the transport and that therefore the mobility itself strongly decreases with increasing $|\Delta|$ or σ.

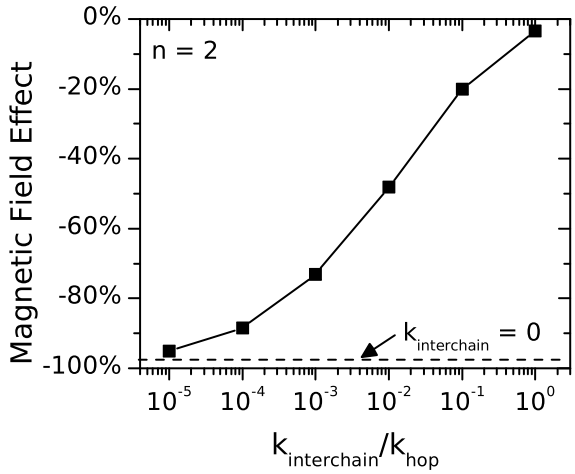

Figure 5.8 Magnetic field effect in the mobility as a function of the interchain hopping rate, $k_{\text{interchain}}$, for doping period $n = 2$, energy offset $\Delta = 0$, no disorder, and high electron density. The dashed line indicates the result for $k_{\text{interchain}} = 0$.

5.3.5 Influence of interchain hopping

The huge magnetoresistance in doped polymers predicted in this work crucially depends on the effects of spin and charge blocking, which are only optimal for one-dimensional charge transport. However, in reality it might be difficult to separate individual chains far enough to completely prevent interchain hopping. We investigated the adverse effect of interchain hopping on the magnetoresistance by Monte Carlo simulations at high electron density, for $\Delta = 0$ and no energetic disorder. In these simulations interchain hopping is modeled by allowing every electron to hop to a randomly chosen empty host site or to an ionized donor site within the chain with a rate $k_{\text{interchain}}$.

Figure 5.8 shows the magnetic field effect in the mobility as a function of the ratio $k_{\text{interchain}}/k_{\text{hop}}$ for doping period $n = 2$. The size of the magnetic field effect decreases strongly with increasing $k_{\text{interchain}}$ to a very small value when $k_{\text{interchain}}/k_{\text{hop}} > 1$. This result demonstrates that if the interchain hopping rate is not small enough, spin and charge blocking are not effective anymore, since electrons can hop to another chain when confronted with a spin-blocking or charge-blocking configuration.

5.4 Realization of suitable systems

We now come to the discussion of the possible realization of suitable systems that would show the predicted magnetoresistance. Two important conditions should be fulfilled: (1) The charges should be localized on monomers, with a hopping rate between monomers, k_{hop}, that is smaller than the hyperfine frequency, ω_{hf};

(2) Charge transport should be essentially one-dimensional, which means that the interchain hopping rate must be much lower than the intrachain hopping rate.

Condition (1) could be fulfilled by inserting spacer units in between the monomers. We propose to use phenyl spacer units for this. It has been shown that with a single phenyl spacer the exchange coupling between a hole at a donor and an electron at an acceptor unit can be reduced to a value corresponding to a millitesla, while with more phenyl spacers the coupling decreases exponentially with the number of phenyl units.[30] In the optimal case of vanishing Δ, the condition that k_{hop} is smaller than ω_{hf} means that the intrachain mobility (in absence of an external magnetic field and for $n = 2$) should not exceed $0.1e\omega_{\mathrm{hf}}a^2/k_{\mathrm{B}}T$; see Figure 5.3(a). With the typical values $\omega_{\mathrm{hf}} = 10^8\ \mathrm{s}^{-1}$ and $a = 1$ nm this leads to a maximal room-temperature mobility $\mu \approx 4 \times 10^{-6}\ \mathrm{cm}^2/\mathrm{Vs}$. While this is not a very high mobility, the high charge density still leads to an appreciable current. Taking for the case $n = 2$ half an electron per monomer unit with a volume of 1 nm^3, such a mobility leads to a conductivity of about 0.3 $\mathrm{S/cm}^{-1}$. This is not more than one order of magnitude lower than the conductivity of a conducting doped polymer like PEDOT:PSS[‡].

Condition (2) could be fulfilled by adding side groups to the polymer such that polymer chains are far enough apart to prevent interchain hopping. Another interesting option might be blending with a non-conducting polymer. It has been shown that blends of P3HT[§] with non-conducting commodity polymers can show excellent conduction even at P3HT weight percentages of only a few percent.[40]

A starting point for realizing the case $n = 2$ could be the copolymerization of monomeric units with strongly electron-accepting and electron-donating properties. The onset of the optical transition for charge transfer in these polymers marks the energy needed to generate free charge carriers and has been made as low as $\Delta = 0.5$ eV.[44,110] The mobility for these copolymers has been measured to be in the range 10^{-5}–$10^{-3}\ \mathrm{cm}^2/\mathrm{Vs}$,[110] which is too large to find a substantial magnetic field effect. Localization of the charges to the monomeric units and a sufficiently low hopping rate could be achieved by inserting spacer units in between the monomers, as discussed above.

Although a small value of the energy offset Δ is not needed to obtain a large magnetoresistance, it is an important condition for obtaining an appreciable mobility. It is interesting to note that the condition $\Delta \approx 0$ has been realized in molecularly doped organic semiconductors. An example is F_4-TCNQ:ZnPc,[¶] which is used as hole-injection material in organic light-emitting diodes.[122] In this system the LUMO energy of the acceptor (F_4-TCNQ) and the HOMO energy of the host (ZnPc) are nearly identical. The conduction in these systems is not one-dimensional, so that the blocking effects discussed above will not be optimal. However, the existence of these systems shows that synthesis of π-conjugated organic units with $\Delta \approx 0$ should be possible.

[‡] PEDOT:PSS: poly(3,4-ethylenedioxythiophene):poly(styrenesulfonate)
[§] P3HT: poly(3-hexylthiophene)
[¶] F_4-TCNQ:ZnPc: tetrafluorotetracyanoquinodimethane:zinc phthalocyanine

We finally remark that a small magnetoresistance has been found in devices of PEDOT:PSS.[84] It would be very interesting to investigate if the magnetoresistance in this polymer is of the type proposed in the present work. If this is the case, one could try to optimize the magnetoresistance along the route described in this chapter.

5.5 Summary and conclusions

In summary, we have investigated the magnetic field dependence of the charge mobility in a doped conjugated polymer by analytical and numerical methods. We considered the case of an electron donor in a host polymer in the slow-hopping limit. The largest magnetic field effect in the mobility of $-98.5 \pm 0.3\%$ was found for high doping concentration (equal amounts of donor and host sites) and high electron density (equal amounts of free electrons and ionized donors). The magnetic field effect arises because of the spin dependence of the recombination of an electron with an ionized donor (spin blocking) and the suppression of hyperfine-induced spin mixing by an external magnetic field. The increased effect at high electron density occurs because a single free electron-ionized donor pair in a spin-blocking configuration can block the current through the whole polymer chain (charge blocking). In addition, we found that energetic disorder and an imperfect alignment of the HOMO energy of the donor and the LUMO energy of the host polymer have only a minimal influence on the effect. The interchain hopping rate, however, does have a significant influence and should be low in order to obtain a large effect. We have suggested promising ways of realizing polymers that show the effect.

6

Modelling the giant magneto-conductance in molecular wires

Very large magnetoconduction with a size larger than −90% has been observed in molecular wires in zeolite crystals. Spin blocking by bipolaron formation between a trapped and free electron is proposed as the mechanism behind those magnetic field effects. It is shown that trapping caused by just the energetic disorder explains neither the size of the effect nor its electric field dependence. We propose that the inhomogeneous distribution of the positive ions that are present in the zeolite leads to traps sites. With those traps it is possible to correctly explain the size, the electric field dependence, and the lineshapes of the magnetoconduction.

6.1 Introduction

In the previous chapter, very large magnetic field effects are predicted in doped, one-dimensional systems. The (ionized) donors, which have fixed positions in the chain, can block the current through the chain. An electron behind one of the donors cannot recombine with it if their spin configuration is a triplet. The same spin-blocking effect can result between a trapped electron and a free electron. In that case, bipolaron formation plays the same role as recombination between an electron and and ionized donor does in the doped systems: the current is blocked when no bipolaron can be formed because the spins of the two electrons are in a triplet configuration. While the bipolaron mechanism in three dimensions yields only a small magnetic field effect of a few percent—see Section 1.2.4 on page 12—the spin-blocking effect is greatly enhanced in a one-dimensional system. Unlike for dopant sites, however, spin blocking by a trapped electron can be lifted because the trapped electron can detrap. How likely that is to happen depends on

The data presented in this chapter are part of a manuscript that is submitted for publication.[65] S.P.K. contributed to the modelling of the experimental results in that publication.

the bipolaron formation energy, the trap depth, and the size of the applied electric field. In addition, the number and positions of trapped electrons are not constant but depend on the charge concentration and the electric field. These dependencies will be investigated in this chapter.

A very large magnetoconduction has recently been measured in molecular wires by Mahato and coworkers.[65] The wires consist of DXP* molecules embedded in the channels of a zeolite L crystal. We propose that the potassium ions that are present in the zeolite (see below) lead to the trap sites that are necessary to explain the large magnetoconductance that is observed.

In the next section, the experimental results on the DXP wires will be briefly described. The model we use to describe the results is introduced in Section 6.3. We assume in this model that the current is only carried by electrons, that is, we assume unipolar transport. In Section 6.4 we discuss the results from the model and compare them to the experimental results. Some remarks are made about the relation between the hopping rate and the charge concentration in Section 6.5. In Section 6.6 we comment on the validity of our model in the case that charge transport through the wires is not unipolar. We end with the main conclusions of this chapter in Section 6.7.

6.2 Experiments

One-dimensional molecular wires of DXP molecules were created by inserting DXP molecules in a zeolite L crystal. Zeolite L is an aluminosilicate with straight channels along its *c*-axis with a diameter varying between 0.71 nm and 1.26 nm along each channel, see Figure 6.1. The aluminosilicate structure is negatively charged. To compensate this charge, (mobile) potassium ions are present in the channels.

When DXP molecules, which are rod-shaped with their smallest dimension close to the channel diameter and a length of 2.2 nm, fill those channels, wires are formed of uniaxially oriented molecules, see Figure 6.1. The length of the wires is determined by the height of the zeolite crystals, which was varied between 30 and 90 nm. A loading degree of 86% of the unit cells filled with DXP was achieved.

The wires are contacted at the bottom by a PEDOT:PSS† layer on top an ITO‡ electrode and at the top by the PtSi tip of a conducting-probe atomic force microscope (CP-AFM). The tip radius is $\sim$10 nm, such that in the order of 100 wires are contacted at the same time. The current through the wires was measured as a function of the applied voltage at an applied magnetic field of up to 14 mT. The applied magnetic field is perpendicular to the molecular wires.

*DXP: N,N′-bis(2,6-dimethylphenyl)-perylene-3,4,9,10-tetracarboxylic diimide
†PEDOT:PSS: poly(3,4-ethylenedioxythiophene):poly(styrenesulfonate)
‡ITO: Indium tin oxide

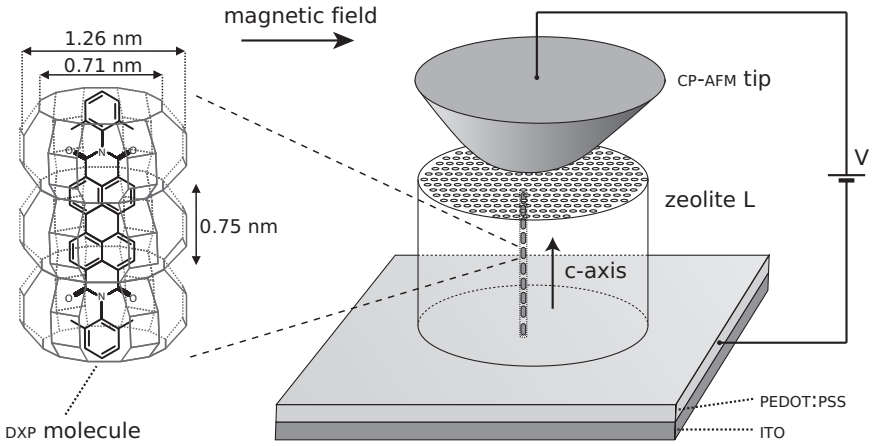

Figure 6.1 The experimental setup used to measure the magnetoconduction of molecular DXP wires in a zeolite crystal. The zeolite crystal contains channels (only a single channel is shown) in which DXP molecules are inserted. Part of a channel is magnified at the left. The DXP molecules only fit in the channels with their long axes oriented along the channel. The conductivity of about 100 wires at the same time is measured between the ITO electrode and the tip of a conducting-probe atomic force microscope (CP-AFM). A magnetic field is applied perpendicular to the direction of the channels. Adapted from Reference 65.

The work functions of both contacts are about -5 eV.[8,79] That is in the middle between the HOMO and LUMO of DXP, which are -6.0 eV and -3.9 eV.[61] However, the potassium ions in the zeolite channels are closer to the DXP molecules than the equally, but oppositely, charged aluminosilicate around them. That will lower the electrical potential for electrons in the wire and raise it for holes. We believe therefore that charge injection and transport is (mostly) by electrons. But even if holes are injected as well, the modelling of the magnetic field effect in this chapter remains valid, as will be discussed in Section 6.6 on page 82.

6.2.1 Results

Figure 6.2(a) shows the measured magnetoconduction of a 60 nm thick zeolite crystal loaded with DXP molecules as a function of the applied magnetic field for voltages over the zeolite between 2 V and 9 V. A maximal magnetoconductance of -93% is observed at 2 V. This value is comparable to the values predicted for doped polymers in the previous chapter and much larger than what has so far been reported in the literature on organic materials at room temperature. The lineshapes seem to be fitted slightly better with a non-Lorentzian than with a Lorentzian, although these two lineshapes are hard to distinguish over the available magnetic field range. The linewidths B_0 that are found from fitting the lineshapes are between 2 and 6 mT and do not have a clear voltage or length dependence. Figure 6.2(b) shows the maximal magnetoconductance $\mathrm{MC}_{\max} \equiv \mathrm{MC}(14\ \mathrm{mT})$ as a function of the applied voltage for wires with lengths between 30 nm and 90 nm. The magnetoconductance is found to decrease with increasing applied voltage.

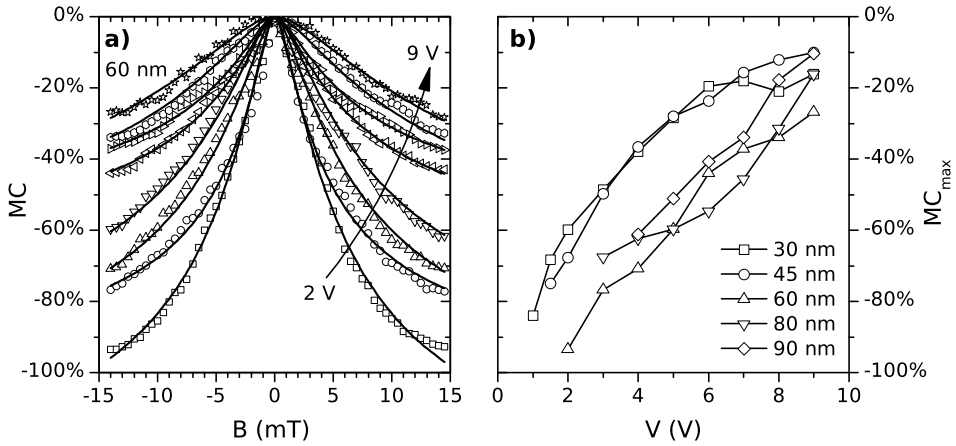

Figure 6.2 (a) The measured magnetoconductance (MC) of molecular wires in a 60 nm thick zeolite crystal as a function of the applied magnetic field B for applied voltages between 2 V and 9 V. (b) The maximal magnetoconductance $\mathrm{MC}_{\mathrm{max}} \equiv \mathrm{MC}(14\ \mathrm{mT})$ as a function of the applied voltage V for wires of different lengths. Adapted from Reference 65.

The importance of the one-dimensionality of the DXP wires for observing the large magnetic field effect was demonstrated by two control experiments. Firstly, when the magnetoconduction of a $\sim$40 nm DXP film was measured with the same CP-AFM tip, an effect of about -20% was found. When the dimensionality was increased by using a platinum wire with a diameter of 250 μm instead of the AFM tip, the magnetoconduction decreased to about -5%.[65] A voltage of 0.5 V was used. At lower voltages there was too much noise to measure the magnetoconductance.

6.3 Model

The measured lineshapes have a non-Lorentzian shape with a width of a few millitesla, which is typical for magnetic field effects that arise from spin-dependent reactions between particles (electrons or holes) when spin mixing takes place by hyperfine fields. This is, together with the apparent importance of the one-dimensionality of the charge transport on the size of the measured magnetic field effect, a strong indication that similar physics as described in the previous chapter takes place.

While in the doped polymers the magnetoconductance arises due to spin-dependent reactions between free electrons (or holes) and ionized dopants, we propose that, in the DXP wires, spin-dependent reactions take place between free electrons and trapped electrons. That is, magnetoconduction results from magnetic-field-dependent bipolaron formation, see Section 1.2.4 on page 12. An electron can get trapped in an energetically low-lying site in the Gaussian density of states. It will be conjectured that more effective trapping can happen due to an inhomogeneous distribution of the mobile potassium ions that are present in the zeolite. A local

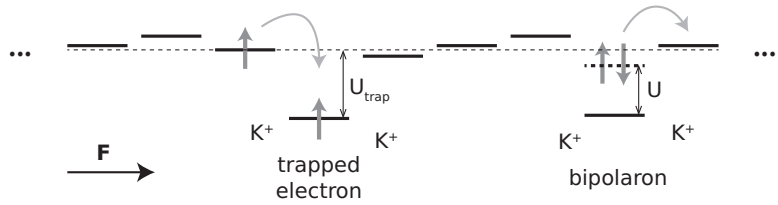

Figure 6.3 A chain of sites as a model of a wire of DXP molecules. At random locations, electron trap sites are formed with an energy U_{trap} below the LUMO of the host sites due to a local concentration of potassium ions. When an electron is trapped, a second electron can only pass that site by first forming a bipolaron at the cost of an energy penalty U (the bipolaron formation energy). An electric field **F** is applied along the chain.

concentration of potassium ions lowers the energy of an electron on a nearby DXP molecule, creating a trap site.

We model the DXP wire as a chain of $N = 100$ sites, see Figure 6.3. The site energies are taken from a Gaussian distribution with standard deviation σ. At every site there is a random hyperfine field, which is taken from a three-dimensional Gaussian distribution with standard deviation B_{hf}. The potassium ions are much less mobile than electrons, so their distribution can be considered stationary on the time scale of an electron passing through the wire. We assume that the presence of the ions leads to randomly located trap sites. Traps are added to the chain with a concentration c_{trap} and an energy U_{trap} below the middle of the Gaussian density of states. The trap concentration and trap energy are treated as parameters.

In the model, electrons can hop between nearest-neighbor sites with Miller-Abrahams hopping rates, see Section 1.1.1 on page 3. When two nearest-neighbor sites are both occupied by an electron, one of the electrons can hop to the other site, forming a bipolaron. Bipolaron formation happens with an energy penalty U (the bipolaron formation energy), which we take to be 0.2 eV as found from cyclic voltammetry measurements on DXP.[61] Bipolaron formation is only possible to the singlet state and happens, therefore, with a rate that is proportional to the spin projection factor onto the singlet space, see Section 2.2.3 on page 27. We use periodic boundary conditions, which avoids the complication of considering the injection and collection of charges by the electrodes.

The current through the chain is determined as a function of the applied magnetic field in the slow-hopping limit by Monte Carlo simulations, see Section 2.3 on page 30. In reality, this limit might not be reached, so the size of the magnetic field effect that we find will be an upper boundary for what will happen in reality. After calculating the magnetoconductance per disorder configuration, an average is taken over 30 to 100 disorder configurations to reach a relative statistical error in the magnetoconductance smaller than 1%, see Section 2.3 on page 30. Incidentally, the number of disorder configurations we average over is similar to the number of DXP wires that is contacted at the same time by the CP-AFM probe, see Section 6.2 on page 74.

The experimental voltage range of the data shown in Figure 6.2 on page 76(a) is 2 V to 9 V. If we assume that this voltage falls entirely over the 60 nm wire, this voltage range translates to electric fields between 0.07 V/hop and 0.33 V/hop. (For the wires of lengths of 30 nm and 90 nm, the ranges corresponding to the voltage range in Figure 6.2(b) are, respectively, 0.07–0.66 V/hop and 0.10–0.22 V/hop.)

6.4 Results

Let us start by considering a wire without traps and only a typical amount of energetic disorder with strength $\sigma = 0.1$ eV. The magnetoconduction as a function of the applied magnetic field is shown in Figure 6.4(a) (black squares) for an electric field $F = 0.1$ V/hop and a charge concentration $c = 0.3$. (A justification of this large charge concentration will be given in Section 6.5 on page 81.) Like the experimentally obtained lineshapes, the lineshape we find is best fitted by a non-Lorentzian and comparing the linewidth to the experimentally obtained values yields a reasonable value of $\sim$1 mT for the hyperfine fields. However, the magnitude of the effect, about 65%, is not quite as large as in the experiments, which is $> 90\%$. Figure 6.5 shows the dependence of the maximal magnetoconduction $\mathrm{MC}_{\mathrm{max}} \equiv \mathrm{MC}(B = 100 B_{\mathrm{hf}})$ on the charge concentration. While the magnitude increases with increasing charge concentration, it saturates at about 70%. Even if the bipolaron energy would be 0.3 eV, the magnitude never reaches 90%. Increasing the amount of energetic disorder to $\sigma = 0.15$ eV leads to a small decrease of the magnetoconduction from -64% to -56% for $F = 0.1$ V/hop, $c = 0.3$. When the energetic disorder is decreased to $\sigma = 0.05$ eV, the magnetoconduction decreases to -45%. (The magnetoconduction is less than 1% for $\sigma = 0$.)

Apart from the disagreement in the size, the experimental magnetic field effect is found to increase with decreasing voltage, while we find a decrease with decreasing electric field from our simulations for the range of electric fields that correspond to the voltages used in the experiments, see the black squares in Figure 6.4(b). We conclude, therefore, that the trapping caused by just the Gaussian energetic disorder of organic materials is unlikely to be the origin of the measured magnetic field effects.

6.4.1 Magnetoconduction with traps

As mentioned before, positively charged potassium ions are present in the zeolite channels. An inhomogeneous distribution of those ions can give rise to trap sites. Figure 6.6(a) shows the magnetic field effect $\mathrm{MC}_{\mathrm{max}}$ as a function of the trap concentration c_{trap} for several trap depths between $U_{\mathrm{trap}} = 0.1$ eV to 0.4 eV for a charge concentration $c = 0.3$ and electric field $F = 0.1$ V/hop. In order to focus exclusively on the effect of traps we took $\sigma = 0$.

The magnetic field effect is largest when c_{trap} is slightly larger than half the charge concentration. As we have seen in Section 5.3.4 on page 67, the magnetic field effect is largest when the current is determined by the magnetic-field-dependent

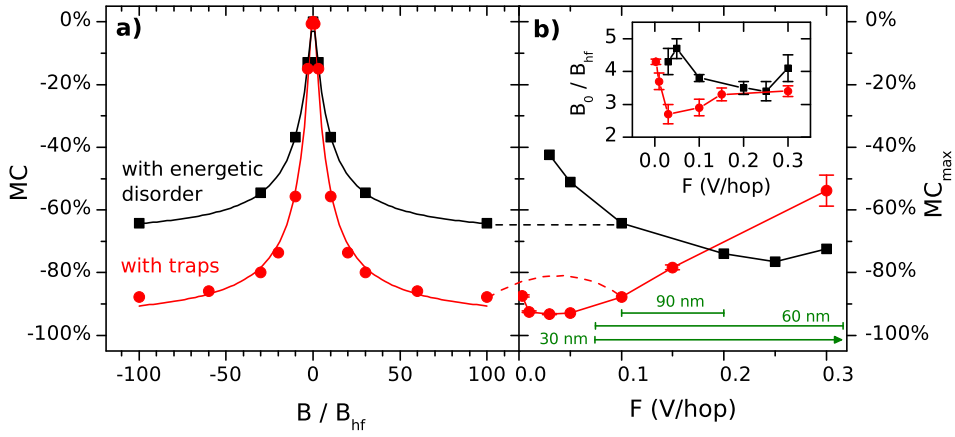

Figure 6.4 (a) The magnetoconductance (MC) as a function of the applied magnetic field B for a charge concentration $c = 0.3$. Results are shown for a wire with energetic disorder $\sigma = 0.1$ eV (black squares) and a wire with traps with a concentration $c_{\text{trap}} = 0.15$ and trap depth $U_{\text{trap}} = 0.2$ eV equal to the bipolaron formation energy (red discs). Both curves are best fitted with a non-Lorentzian lineshape. (b) The maximal magnetic field effect $\text{MC}_{\text{max}} \equiv \text{MC}(B = 100B_{\text{hf}})$ as a function of the electric field F. The green bars indicate the approximate electric field range corresponding to the voltage range used in the experiments for wires of length 30 nm, 60 nm, and 90 nm (see Figure 6.2 and the main text). The linewidths B_0 of fits with a non-Lorentzian as a function of the electric field are shown in the inset.

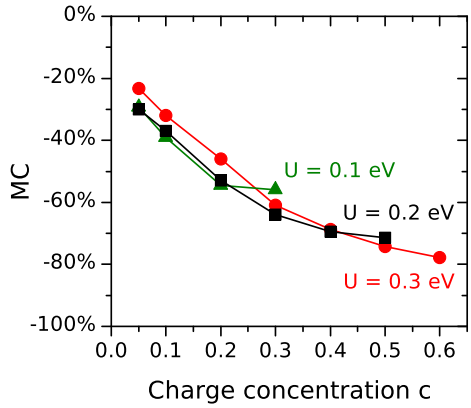

Figure 6.5 The maximal magnetoconduction MC_{max} of a wire as a function of the charge concentration for energetic disorder $\sigma = 0.1$ eV, electric field $F = 0.1$ V/hop and bipolaron formation energies $U = 0.1$ (green), 0.2 (black), and 0.3 (red).

hops. That is, an electron moving through the chain should spend most of its time making magnetic-field-dependent hops. It has also become clear in the previous chapter that the magnetoconductance is larger for high rather than for low dopant (trap) and free-electron densities, because only a single electron has to be blocked to block the whole current and electrons spend less time between recombinations/bipolaron formations if the dopants/traps are closer together. Those two effects explain the dependence of the magnetoconductance on the trap concentration. When the trap concentration is increased from zero, initially, the magnetoconductance increases due to the increased blocking by the increased number of trapped electrons. However, if the trap concentration increases beyond $c/2$, the effect of decreasing free-electron concentration dominates and the magnetoconductance decreases. Another way of looking at this is that the number of spin-blocked electrons is proportional to both the number of trapped charges and the number of free charges: $c_{\mathrm{trap}}(1 - c_{\mathrm{trap}})$, assuming that almost all traps are filled with electrons. The number of spin-blocked electrons is therefore maximal for $c_{\mathrm{trap}} = c/2$.

The effect of U_{trap} on the magnetoconduction is less straightforward: When less than half of all electrons are trapped for $c_{\mathrm{trap}} < 0.15$ (again assuming that all traps are filled), there is an optimal trap depth of 0.2 eV, equal to the bipolaron formation energy. For $c_{\mathrm{trap}} \gg c$, the magnetoconductance increases as a function of the trap depth. A likely reason for this is that, with increasing trap concentration, it becomes more probable to find two traps next to each other: The magnetic field effect is largest when the hop that is magnetic field dependent—bipolaron formation—is slow, such that a change in the rate of that hop—due to the magnetic field—affects the current significantly, see Section 5.3.4 on page 67. In addition, the blocking electron should have a small detrapping rate, otherwise it would just detrap instead of forming a bipolaron with the blocked electron. Those two conditions can be fulfilled when two traps are located next to each other, see the inset in Figure 6.6 on the facing page. The right electron in the figure cannot easily detrap because of the energy penalty U_{trap} and bipolaron formation happens with an energy penalty U.

From now on we set $U_{\mathrm{trap}} = 0.2$ eV. Figure 6.6(b) shows the dependence of the magnetoconductance on the charge concentration for $F = 0.1$ V/hop and $c_{\mathrm{trap}} = 0.05$ (green triangles), 0.1 (red discs), and 0.15 (black squares). For small c, the magnetoconductance increases as a function of c. However, when c is larger than $\sim c_{\mathrm{trap}}$, when all traps are filled with electrons, the magnetoconductance is almost independent of c.

The magnetic field dependence of the magnetoconductance for this case is shown in Figure 6.4(a) (red discs) for $c = 0.3$ and $c_{\mathrm{trap}} = c/2 = 0.15$. Again, a non-Lorentzian lineshape is found. However, the magnetoconductance, -88% at $B = 100B_{\mathrm{hf}}$, is much larger than that for the case without traps. The electric field dependence is shown in Figure 6.4(b). The decrease of the magnetoconductance's magnitude with increasing electric field that we find (for $F > 0.3$ V/hop) is in agreement with the experiments. While the charge concentration and possibly the

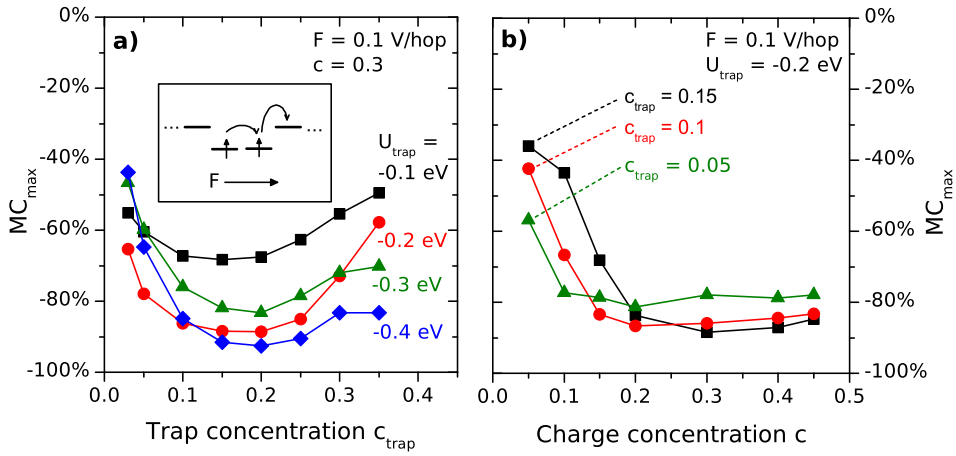

Figure 6.6 (a) Magnetoconduction as a function of the concentration of traps c_{trap} for a charge concentration $c = 0.3$ and trap depths $U_{\text{trap}} = 0.1$ (black squares), 0.2 (red discs), 0.3 (green triangles), and 0.4 eV (blue diamonds). The inset shows two trap sites next to each other, both with a trapped electron on them. In the presence of a strong electric field, either the left electron will form a bipolaron by hopping to the right or the right electron will detrap. (b) Magnetoconduction as a function of c for $c_{\text{trap}} = 0.15$ (black squares), 0.1 (red discs), and 0.05 (green triangles). All results are for electric field $F = 0.1$ V/hop.

trap concentration in the experiment depend on the electric field as well, the magnetoconductance does not depend strongly on those quantities for the parameters we have chosen. The experimental and simulated electric field dependencies can therefore be compared with each other. The largest magnetoconductance of -93% is found for $F = 0.3$ V/hop and is equal to the experimentally found maximal magnetoconductance.

We have found no—that is, less than the error margin of 1%—direct dependence of the magnetoconduction on the wire length N between 60 and 140 for $c = 0.3$ and $c_{\text{trap}} = 0.15$. The experimentally observed length dependence is therefore likely indirect, resulting from a length-dependent charge concentration, trap depth and/or concentration, electric field, or from an effect due to the injection and/or collection. More-detailed simulations, incorporating charge injection and the dynamics of the potassium ions, have to be done to investigate the length dependence.

6.5 Charge concentration and hopping rate

To get an estimation for the charge concentration, we take the measured current $I = 50$ nA for the 60 nm thick zeolite crystal at 9 V. As mentioned in Section 6.2 on page 74, the CP-AFM tip contacts in the order of 100 wires. We assume that all hops are with the electric field—not unreasonable given the fact that the Boltzmann factor for hopping against an electric field of 9 V/60 nm is $\sim 10^{-5}$. Using these data, we find the relation $rc \approx 4$ between the relative hopping rate and the charge concentration. The presence of energetic disorder leads to sizable magnetic field

effects even for relative hopping rates comparable to unity, see Chapter 4. However, the large magnetoconductance that was measured is comparable to the values we find from our simulations, r must be comparable to or smaller than unity—only for small r does enough spin mixing take place to yield large magnetic field effects. Furthermore, by ignoring energetic disorder or traps, the presence of which lowers the current, we have underestimated rc. As a consequence, the charge concentration c must be close to unity. In addition, the magnetoconductance that we find for lower charge concentrations is much lower than what is found experimentally. This justifies the large values for c that we have used in this chapter, provided our model is correct.

6.6 The assumption of unipolarity

We have assumed above that there are only electrons in the DXP wire and no holes. However, even if holes are injected into the wire, our model keeps most of its validity. When electrons are injected form one side and hole from the other side, they will meet somewhere in a wire and form excitons. However, at both sides of the place where excitons are formed the wire will be unipolar. In the electron-only part of the device, the magnetic field effects we have described in this chapter will occur and will lead to a large magnetoconductance.

A magnetic field effect might also arise at the point where the electron-only and hole-only parts of the wire meet. However, we do not expect this magnetic field effect to be as large as those experimentally observed. The exciton formation process could be magnetic-field dependent, as is described in Chapter 3. However, to get the experimentally observed large magnetic field effect requires an unrealistically low (or high) ratio between the singlet and triplet exciton formation rates (γ).

Only magnetic-field-dependent charge blocking is expected to give the large magnetic field effects that were measured. Triplet excitons have a long life time and could lead to charge blocking. This blocking is magnetic field dependent, because a magnetic-field-dependent triplet-charge interaction can make the triplet decay, thereby clearing the blockage. However, the linewidth of the magnetic-field dependence of the triplet-charge interaction is determined by the zero-field splitting,[103] which is typically about 100 mT.[38,87] Thus, this mechanism cannot explain the measured lineshapes.

6.7 Discussion and conclusions

We have simulated the magnetoconductance resulting from bipolaron formation in an experimentally studied system of wires of DXP molecules in a zeolite crystal in the slow-hopping limit using Monte Carlo simulations. The magnetoconductance emerges due to blocking of the current by trapped electrons, which can be overcome by magnetic-field-dependent bipolaron formation. The trapping resulting from energetic disorder does not yield a magnetic field effect as large as

measured in DXP wires. Moreover, the electric field dependence of the magnetoconduction is the opposite of what was experimentally found. Potassium ions that are present in the zeolite could lead to trap sites. With those traps the simulated magnetoconductance is as large as the experimentally found values and has the right electric field dependence. We suggest that this is the mechanism behind the large magnetoconductance that was measured.

What is not understood yet is the dependence of the magnetoconductance on the wire length. The largest magnetoconductance is measured for the 60 nm long wires; longer or shorter wires show a smaller magnetoconductance. Our simulations, on the other hand, show no length dependence. Possible explanations for the length dependence found in the experiment are: a different distribution of DXP molecules in wires of different length; a trap concentration and trap depth that depend on the wire length; or an inhomogeneous charge distribution (and, consequently, a position-dependent electric field), for example, due to charge accumulation at the contacts. More insight could be gained by including injection from and collection by the contacts in the model (instead of using periodic boundary conditions) and explicitly including the potassium ions and their dynamics.

7

Spin mixing by fringe fields

When all effective magnetic fields are completely aligned due to the presence of a large applied magnetic field, spin mixing still takes place between the singlet and T_0 triplet states of polaron pairs. This spin mixing is analytically investigated in this chapter. The amount of spin mixing is found to depend on both the difference in magnitude of the effective magnetic fields at different sites and the relative hopping rate. We conclude that this so-called ΔB-mechanism is the likely mechanism behind the magnetoconductance that was measured in a device with a single magnetic electrode. The magnetic-field-dependent magnetization of that magnetic electrode leads to magnetic-field-dependent fringe fields. Those fringe fields are the source of the difference in effective magnetic fields at different sites.

7.1 Introduction

All magnetic field effects discussed in this thesis, except for the ultra-small-magnetic-field effect (see Section 3.5.1 on page 43), rely on spin mixing by local hyperfine fields and the suppression of this mixing by applying an external magnetic field. However, there are also other sources of spin mixing. In particular, the (inhomogeneous) fringe fields emerging from magnetic nanoparticles could play a role similar to that of hyperfine fields, as was proposed by Cohen.[27]

Relying on hyperfine fields offers only very little control over the amount of spin mixing: They are determined by the organic material and vary only little between different materials. Moreover, they cannot be changed once a device has been made. Fringe fields, on the other hand, result from the properties of a magnetic layer or nanoparticles. By using different materials or by patterning the magnetic layer differently, control could be exerted over the fringe fields. Furthermore, the presence of fringe fields depends on the magnetization of the magnetic layer, which can be controlled by an applied magnetic field.

Using fringe fields as a source of spin mixing is interesting from both a scientific and technological standpoint. In principle, fringe fields could be controlled such that the amount of spin mixing depends on the position within the device, possibly giving insight into where magnetic-field-dependent processes, like exciton or bipolaron formation, take place.

Recently, this idea was applied to organic semiconductors by Wang and coworkers.[123] They have measured a magnetoconduction of up to 5% in an OLED with a magnetic layer as bottom electrode. Control experiments—where the magnetic layer is present, but charge injection takes place from a layer above the magnetic layer—proved that the observed effect is not related to injection from a magnetic electrode. Furthermore, a model in which the fringe fields suppress spin mixing in the same way as an external magnetic field does in, for example, the two-site model of Chapter 3, was unable to explain the experimental linewidth or lineshapes. The magnetic field scale for which the magnetoconduction was measured coincides with the field scale over which the magnetic layer switches its magnetization.[64] These are strong indications that the fringe fields—which are only present during the switching of the magnetic layer—are the cause of spin mixing. However, the exact mechanism by which this happens remained unclear.

In the next section of this chapter, the measurements by Wang and coworkers are briefly discussed. In Section 7.3 we propose a mechanism in which the difference in magnitude of the (effective) magnetic fields of two sites is the dominant source of spin mixing. An analytical proof of principle is given for how this can lead to a magnetic field effect. How spin mixing due to a difference in magnitude of the effective magnetic fields could lead to a magnetic field effect in the experiments by Wang and coworkers is explained in Section 7.4. This chapter ends with conclusions and an outlook.

7.2 Fringe field device

The structure of the device on which measurements are reported by Wang and coworkers in Reference 123 is shown in Figure 7.1(a). An Alq_3 layer and a PEDOT hole-injection layer are sandwiched between a magnetic and a non-magnetic electrode. The Alq_3 layer has a thickness of 30 nm, while the thickness d of the PEDOT layer is varied between 12 nm and 84 nm. The magnetic electrode consists of alternating layers of cobalt and platinum and has perpendicular magnetic anisotropy. The magnetization of the magnetic layer as a function of the applied magnetic field is shown in Figure 7.1(b). When the magnetization of the layer switches, a domain structure appears, with domains of about 200 nm when the magnetization is zero, see Figure 7.1(c). The magnetization of these domains is perpendicular to the layer. As a result of this domain structure, fringe fields appear above the magnetic layer. Variation in thickness of the magnetic layer may also give rise to fringe fields.

The magnetoconduction of the device is measured as a function of the applied magnetic field, see Figure 7.1(d). It is clear that the lowest current is measured

for magnetic fields for which the magnetic layer's magnetization is switching and fringe fields are present. As the thickness d of the spacer layer increases, the magnetic field effect on the 100 mT scale decreases and only the ordinary magnetic field effect at the hyperfine field scale remains. Since the gradient in the fringe fields decreases with the distance from the magnetic layer [see Figure 1(d) in Reference 123], this suggests that the presence of the fringe fields leads to additional spin mixing.*

An explanation along the lines of two-site models in the slow-hopping limit, like in Reference 121, was dismissed by the authors because the correlation length of the fringe fields is too large and results in effective magnetic fields on neighboring sites that are almost completely aligned. However, slow-hopping models assume that complete mixing takes place between the singlet and T_0 triplet of a polaron pair, while at intermediate (and more realistic) hopping rates, mixing between those states depends on the difference in precession frequency of the two spins. The measurements can be explained when that effect is taken into account correctly, as will be shown in the rest of this chapter.

7.3 ΔB-mechanism

The dominant source of the magnetic field effects so far discussed in this thesis is the alignment of the effective magnetic fields of two sites when an external magnetic field is applied. Due to this alignment, the spin mixing for a polaron pair between the singlet and T_0 triplet with the T_- and T_+ triplets is suppressed. However, even when the two effective magnetic fields are completely aligned, spin mixing will still take place between the singlet and T_0 triplet polaron-pair states, because the precession frequencies of the polarons' spins will differ—due to a difference in g-factor or a difference in magnitude of the effective magnetic fields at the polarons' sites.

When the reaction rate is much slower than the difference in precession frequency, complete mixing between the singlet and T_0 triplet takes place. When that is not the case, the amount of spin mixing depends on the difference in precession frequencies. For the Δg-mechanism, which was discussed in Section 1.2.5 on page 16, the difference in g-factor between the two polarons' spins leads to a magnetic-field-dependent difference in precession frequency proportional to $\Delta g B$, where B is the applied magnetic field. When there is a gradient in the magnetic field, for example, due to fringe fields, a similar difference in precession frequency occurs, which is proportional to $g\Delta B$, where ΔB is the difference in the magnetic fields at the sites of the two polarons and where the g-factors are assumed to be equal. In analogy to the Δg-mechanism, we call this the *ΔB-mechanism*.

Consider an electron and a hole that are about to form an exciton. For simplicity, we assume that both have the same g-factor and that their effective magnetic fields

*Note that the charge mobility in PEDOT is much higher than that in Alq_3. Consequently, the current and, therefore, the magnetoconduction is determined by what happens in the Alq_3 layer.

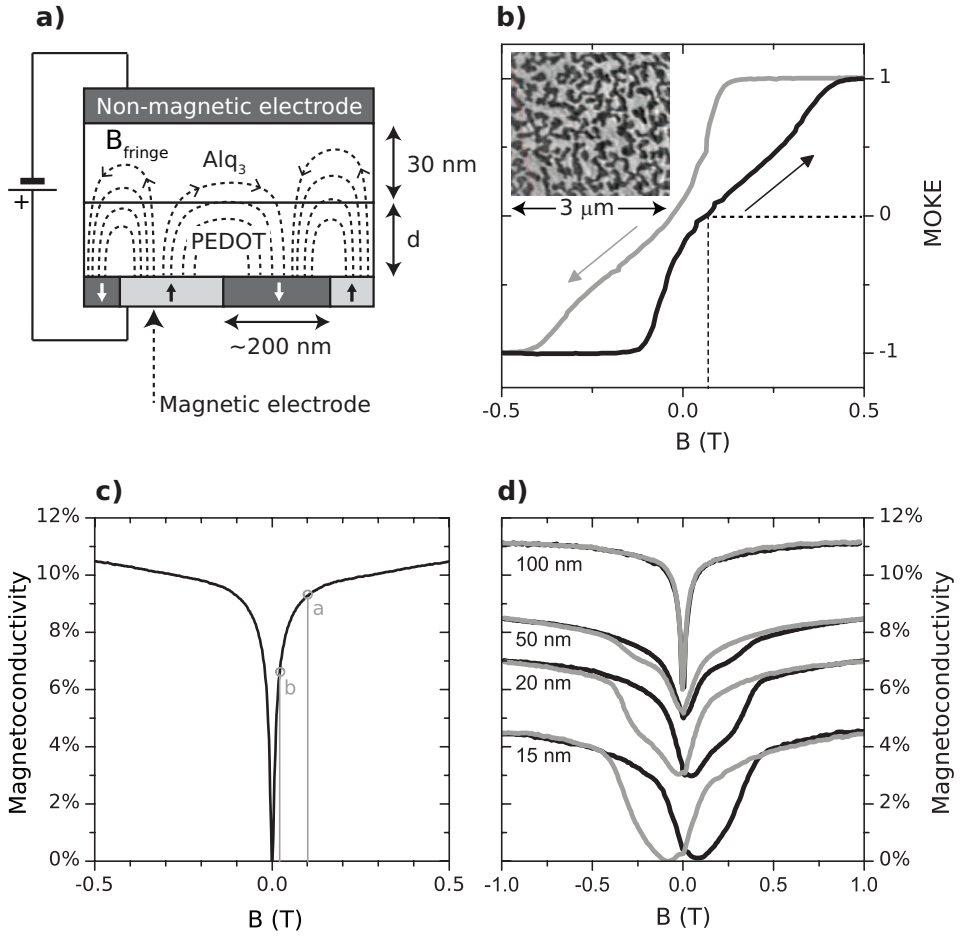

Figure 7.1 (a) A simplified schematic of the fringe-field device from Reference 123. An 30 nm thick Alq_3 layer and a PEDOT hole-transport layer with a width d are sandwiched between a magnetic and a non-magnetic electrode. (b) Schematic magnetization of the magnetic layer as a function of the applied magnetic field. When the magnetization is switching between -1 and 1, magnetic domains will emerge (shown in the inset) in the magnetic electrode, causing fringe fields (B_{fringe}) above the electrode [indicated as dashed lines in (a)]. (c) The magnetoconduction as a function of the applied magnetic field for a device similar as shown in (a) but without magnetic layers. (d) Magnetoconduction of the device as a function of the applied magnetic field for $d = 15$, 20, 50, and 100 nm. Figures (b), (c), and (d) are adapted from Reference 123.

are completely aligned, as would be the case when a large external magnetic field is applied (pointing in the z-direction). The electron and hole feel effective magnetic fields B_e and $B_\mathrm{h} = B_\mathrm{e} + \Delta B$ respectively. The Hamiltonian of this system is given by,

$$H = g\mu_\mathrm{B} B_\mathrm{e} S_{z,\mathrm{e}}/\hbar + g\mu_\mathrm{B} B_\mathrm{h} S_{z,\mathrm{h}}/\hbar, \tag{7.1}$$

where μ_B is the Bohr magneton, and $S_{z,\mathrm{e(h)}}$ is the spin operator in the z-direction for the electron (hole).

As a model for all spin-dependent reactions between two spin-1/2 particles, we consider the steady-state fraction of singlet excitons that is formed, χ_S, when polaron pairs are formed with a rate k_u from which singlet and triplet excitons are formed with rates k_S and k_T respectively. We will use a stochastic Liouville equation to find the singlet fraction, see Section 3.2 on page 36. The steady-state density operator is found by demanding:

$$0 = \frac{\partial \rho}{\partial t} = -\frac{i}{\hbar}\big[H, \rho\big] - \frac{1}{2}\big\{\Lambda, \rho\big\} + \Gamma, \tag{7.2}$$

where $\Lambda = \sum_\lambda k_\lambda |\lambda\rangle\langle\lambda|$, with $\lambda = \mathrm{S}, \mathrm{T}_0, \mathrm{T}_-, \mathrm{T}_+$, and $\Gamma = k_\mathrm{u}\mathrm{I}/4$, where I is the identity operator. For the formation rates, we take $k_\mathrm{T} = k_{\mathrm{T}_0} = k_{\mathrm{T}_-} = k_{\mathrm{T}_+} = k_\mathrm{hop}/\gamma$ and $k_\mathrm{S} = k_\mathrm{hop}$.

We find the density matrix that is a solution to Equation 7.2 as described in Section 2.2.2 on page 27. The non-zero elements of this matrix are:

$$\rho_{\uparrow\uparrow,\uparrow\uparrow} = \rho_{\downarrow\downarrow,\downarrow\downarrow} = \frac{\gamma k_\mathrm{u}}{4k_\mathrm{hop}} \tag{7.3}$$

$$\rho_{\uparrow\downarrow,\uparrow\downarrow} = \rho_{\downarrow\uparrow,\downarrow\uparrow} = \frac{\gamma k_\mathrm{u}}{k_\mathrm{hop}} \frac{(4g\mu_\mathrm{B}\Delta B\gamma/k_\mathrm{hop}\hbar)^2 + (1+\gamma)^2}{8(1+\gamma)[(2g\mu_\mathrm{B}\Delta B\gamma/k_\mathrm{hop}\hbar)^2 + \gamma]} \tag{7.4}$$

$$\rho_{\uparrow\downarrow,\downarrow\uparrow} = \rho^*_{\downarrow\uparrow,\uparrow\downarrow} = \frac{\gamma k_\mathrm{u}}{k_\mathrm{hop}} \frac{\gamma - 1}{(2g\mu_\mathrm{B}\Delta B\gamma/k_\mathrm{hop}\hbar)^2 + \gamma} \left(\frac{1}{8} + i\frac{g\mu_\mathrm{B}\Delta B\gamma/k_\mathrm{hop}\hbar}{2(1+\gamma)}\right) \tag{7.5}$$

From this density matrix, it is easy to get the singlet exciton fraction, which is given by,

$$\chi_\mathrm{S} = \frac{\gamma}{1+\gamma}\frac{1}{4}\left(2 - \frac{\gamma - 1}{(2g\mu_\mathrm{B}\Delta B\gamma/k_\mathrm{hop}\hbar)^2 + \gamma}\right). \tag{7.6}$$

The singlet fraction as a function of the relative hopping rate is shown in Figure 7.2(a) for $\Delta B = 10B_\mathrm{hf}$ and $\gamma = 1/2$ (solid curve). When the exciton formation rate is slower than the difference in precession frequencies, a deviation from the statistical singlet fraction of 0.25 is found. The transition occurs around $k_\mathrm{hop} = 2g\mu_\mathrm{B}\Delta B\sqrt{\gamma}/\hbar$. If we define the relative hopping rate as $r = k_\mathrm{hop}/\omega_\mathrm{hf}$, with the hyperfine frequency $\omega_\mathrm{hf} = g\mu_\mathrm{B}B_\mathrm{hf}/\hbar$, the transition occurs around $r = 2\Delta B\sqrt{\gamma}/B_\mathrm{hf}$.

When no fringe fields are present and only an external magnetic field $B\tilde{\mathbf{z}}$ that is much larger than the hyperfine fields, ΔB is equal to the difference of the z-components of the hyperfine fields. That means that ΔB is distributed according

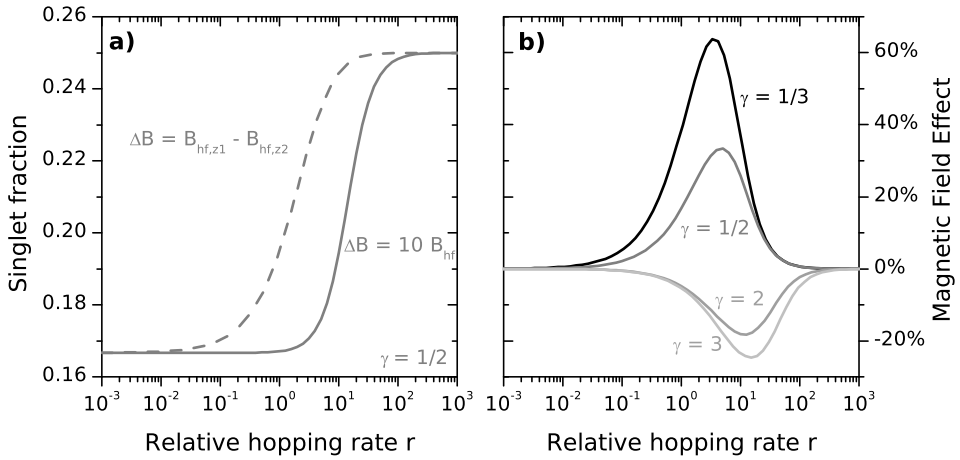

Figure 7.2 (a) The singlet fraction as a function of the relative hopping rate for $\gamma = 1/2$ resulting from the ΔB-mechanism, where ΔB is either $10B_{\rm hf}$ ($\chi_{\rm S,fringe}$, solid curve) or the difference between the z-components of two random hyperfine fields ($\chi_{\rm S,hf}$, dashed curve). For the latter, an average over all hyperfine fields was taken. (b) The resulting magnetic field effect, defined as $(\chi_{\rm S,hf} - \chi_{\rm S,fringe})/\chi_{\rm S,fringe}$ for $\gamma = 1/3$, $1/2$, 2, and 3.

to a Gaussian distribution with standard deviation $2B_{\rm hf}$. Taking an average over the hyperfine fields yields the following expression:

$$\langle \chi_{\rm S} \rangle_{\rm hf} = \frac{\gamma}{1+\gamma}\frac{1}{4}\left(2 - \frac{e^{r^2/32\gamma}(\gamma-1)r\sqrt{\pi/2}\left[1-\mathrm{erf}(r/\sqrt{32\gamma})\right]}{4\gamma^{3/2}}\right), \qquad (7.7)$$

where $\mathrm{erf}(x)$ is the error function. In Figure 7.2(a), $\langle \chi_{\rm S} \rangle_{\rm hf}$ is shown as a dashed curve. The transition from fast to slow hopping is slightly broader compared to the case where ΔB has a fixed value (solid curve).

The derivation in this section is for the case of exciton formation. However, the same physics applies to other reactions where spin mixing by hyperfine fields plays a role, such as bipolaron formation.

7.4 Magnetic field effect

For magnetoconductance to arise in the fringe field device that was described in Section 7.2 on page 86, the difference in magnitude of the fringe fields at two neighboring site must be larger than the difference between the hyperfine fields for at least a significant fraction of sites that determine the current. For illustrative purposes, assume that the difference in fringe fields is $10B_{\rm hf}$. We also assume that the fringe fields are static on the time scale of exciton formation. In that case, the singlet fractions with (solid curve) and without (dashed curve) fringe fields are given in Figure 7.2(a) for $\gamma = 1/2$. (For simplicity, the effects of the smaller hyperfine fields are neglected for the former case.) It is clear from this figure that, for relative hopping rates between 10^{-1} and 10^2, the singlet fraction in

the presence of fringe fields is different from the singlet fraction without fringe fields. Therefore, "turning off" the fringe fields by saturating the magnetization of the magnetic layer with an external magnetic field leads to an increase in the singlet fraction. That is, the singlet fraction—or indeed any other quantity that depends on spin mixing—is magnetic field dependent. The resulting magnetic field effect is shown as a function of the relative hopping rate for several values of γ in Figure 7.2(b).

This behavior is indeed what is seen in the experiments by Wang and coworkers[64,123] that were described in Section 7.2, see Figures 7.1(b) and (d). Let us start by considering the case of $d = 15$ nm. At that distance above the magnetic layer, the fringe fields are larger than 0.1 T (see Figure 1(d) in Reference 123). In a device without a magnetic layer and the resulting fringe fields, the magnetoconductance is almost saturated for magnetic fields of that size and larger, see the point labeled a in Figure 7.1(c). Since the magnetoconductance in such a device is caused by the alignment of the effective magnetic fields when an external magnetic field is applied, we conclude that at 0.1 T and larger the effective magnetic fields are aligned. The assumption made in the previous section that the effective magnetic fields are aligned and only the differences in magnitude of the effective magnetic fields lead to spin mixing is therefore justified for the case of $d = 15$ nm.

Let us now consider what happens as a function of the applied magnetic field. At high applied magnetic fields (> 0.5 T), no fringe fields are present and only the difference in magnitude of the hyperfine fields leads to spin mixing. When the applied magnetic field gets smaller than $\sim$0.2 T, the magnetization of the magnetic layer starts to become smaller than its saturation value and fringe fields appear. The resulting increase in spin mixing leads (in this case) to a decrease of the current. The current reaches a minimum when the maximal amount of spin mixing is attained—the largest gradients in the fringe fields. That happens when the magnetization is zero, that is at $B \approx -0.1$ T, see Figures 7.1(b) and (d). When decreasing the applied magnetic field further, the magnetization increases again (with the opposite sign), the gradient in the fringe fields decreases, and the current increases back to the initial value.

For larger d, the gradients in the fringe fields are smaller, as is the magnitude of the fringe fields. The former—the decrease of the gradient—results in a smaller amount of spin mixing at applied magnetic fields (between 0.1 and 0.5 T) for which the fringe fields are present, see Figure 7.1(d). The smaller fringe fields result in effective magnetic fields that are not fully aligned anymore at $B = 0$. That is evident from the appearance of a feature in the lineshapes with a width that is typical for hyperfine fields. For $d = 84$ nm (not shown) the magnitude of the fringe fields is around 0.02 T. At those fields, the magnetoconductance in a device without a magnetic layer is not saturated, see the point labeled b in Figure 7.1(c). The effective magnetic fields are thus not fully aligned by the fringe fields that are present at $d = 84$ nm. Therefore, applying an external magnetic field will reduce the amount of spin mixing. This can be seen in Figure 7.1(d) for $d = 100$ nm—for which the fringe fields are even smaller—where the typical lineshape with a width

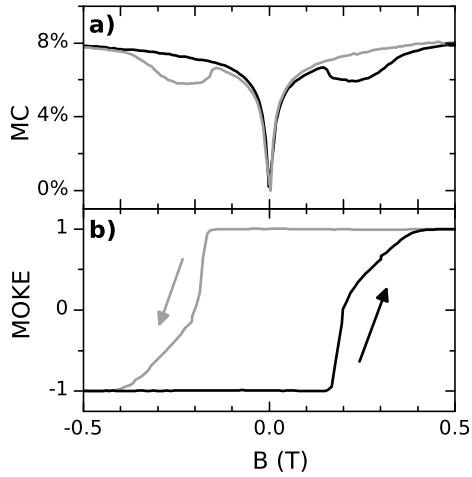

Figure 7.3 (a) Magnetoconductance and (b) magnetization of the magnetic layer as a function of the applied magnetic field B. Figure adapted from Reference 123.

of a few millitesla is recovered. The amount of 5% of magnetoconductance found for $d = 100$ nm is smaller than the 11% found in a device without a magnetic layer, because even at $B = 0$ the non-zero fringe fields lead to some alignment of the effective magnetic fields.

The effects of the alignment of the effective magnetic fields and of the ΔB-mechanism can be seen more clearly in another measurement from Wang and coworkers, shown in Figure 7.3, where a different magnetic layer was used. There, the magnetic layer's magnetization flips at an applied magnetic field that is much larger than the hyperfine-field scale, such that the effects of alignment and of the fringe fields are separated. At small magnetic fields ($B < 0.1$ T) the familiar lineshape due to the alignment of the effective magnetic fields is visible. Around $B = 0.2$ T, where the effective magnetic fields are almost completely aligned, the magnetic layer flips and fringe fields appear. The increase in spin mixing caused by the gradient in the fringe fields leads to a decrease in current.

7.5 Conclusions and outlook

In conclusion, even when all effective magnetic fields in an organic semiconductor are aligned, spin mixing still takes place between the singlet and T_0 triplet. The amount of this spin mixing is proportional to the difference in magnitude of the effective magnetic fields at neighboring sites and inversely proportional to the hopping rate. We conclude that this spin mixing, caused by the gradients in the fringe fields of a magnetic layer, is the likely origin of the recently observed magnetoconductance by Wang and coworkers.[123]

The next step would be to calculate the fringe fields as a function of the applied magnetic field and the distance above the magnetic layer and to use those fringe

fields as input for the theory presented in Section 7.3. In that way, lineshapes could be calculated and compared with the experimentally found lineshapes. From that comparison, also values for the hopping rate and for the relative singlet exciton formation rate γ could be determined.

8

Conclusions and outlook

The goals of this thesis are both to explain experimentally observed magnetic field effects in organic semiconductors and to make predictions of how even larger magnetic field effects can be obtained. In the first section of this chapter, the main conclusions of the previous chapters are summarized. In the second section an outlook on the future of modeling of magnetic field effects in organic semiconductors is given.

8.1 Conclusions

We conclude that, in general, the largest magnetic field effects—in the current and electroluminescence—are found when the hopping rate is much slower than the hyperfine frequency. In that case the maximal amount of spin mixing takes place (Chapter 3). When the hopping rate increases and becomes comparable to the hyperfine frequency the magnetic field effects decrease. The magnetic field effects disappear when the hopping rate is much larger than the hyperfine frequency. However, when the effects of Coulomb attraction between electron and hole and of energetic disorder are included, magnetic field effects are found even for hopping rates that are several orders of magnitude larger than the hyperfine frequency (Chapter 4).

In most cases, the dominant contribution to magnetic field effects results from the alignment of the effective magnetic fields at the sites of two polarons when an external magnetic field is applied. In that way, the external magnetic field suppresses the amount of spin mixing. However, when the hopping rate is comparable to the hyperfine frequency no complete spin mixing takes place, so the amount of spin mixing can also be increased by increasing the precession frequency. We conclude that this effect leads to a small increase in spin mixing when a small magnetic field is applied, explaining the occurrence of an ultra-small-magnetic-field effect. Due to the same incomplete spin mixing, a very large magnetic field effect was found in the singlet fraction when singlet excitons are formed several orders of

magnitude slower than triplet excitons at formation rates that are comparably to the hyperfine frequency (Chapter 3). Even when the effective magnetic fields on different sites are completely aligned, the amount of spin mixing depends on the hopping rate and the difference in magnitude of the effective magnetic fields. We conclude that this so-called ΔB-mechanism causes the magnetoconductance in a device where the magnetic-field-dependent magnetization of a magnetic layer causes fringe fields in the organic semiconductor that vary from site to site (Chapter 7).

A question that is much debated in the literature is whether the statistical ratio of 1:3 singlet–versus–triplet excitons formed can be violated. We find a magnetic field dependence of the singlet fraction—a measure for the electroluminescence—only if the singlet fraction deviates from the statistical fraction of 0.25. Since magnetoluminescence is experimentally observed, we conclude that the statistical ratio must be violated (Chapter 3). Furthermore, we conclude that it can be violated even when hopping is too fast for spin mixing by the hyperfine fields to take place, because electron-hole pairs can split up after which both the electron and hole can recombine with a different hole and electron (Chapter 4).

An effective way of obtaining a very large magnetoconductance is by restricting the charge transport to one dimension. In that case, the magnetic-field-dependent blocking of electrons by dopant sites (Chapter 5) or by trapped electrons (Chapter 6) is very effective. In both cases a larger magnetoconductance is found when the charge concentration is increased. We suggest that this is the mechanism behind the huge magnetoconductance that is measured in wires of DXP molecules in a zeolite crystal.

Trapping caused by only the energetic disorder results in neither the right magnitude nor in the right electric field dependence of the magnetoconductance in the molecular wires as compared to the measurements. When traps are introduced in the wires both the magnitude and the electric field dependence found from our simulations are comparable to those found experimentally. We suggest that the potassium ions that are present in the zeolite lead to the necessary trapping (Chapter 6).

8.2 Outlook

It seems to have been established by now that spin mixing by hyperfine fields underlies the magnetic field effects that are observed in organic semiconductors at a magnetic field scale of milliteslas. Deuteration experiments have proven the importance of hyperfine interactions and experimental results have been qualitatively explained by modeling and simulations, giving the right trends and order of magnitude. What remains challenging, though, is to quantitatively model the experimental results. A more quantitative comparison between experiments and theory is needed, especially because there are so many different mechanisms (see Section 1.2.4 on page 12) that could be acting at the same time.

This problem should be solved by an approach from two sides. Firstly, modelling should become more extensive and more detailed. We have seen that in a multi-site model effects appear that are not present in a two-site model, like the occurrence of magnetic field effects at hopping rates much larger than the hyperfine frequency. Furthermore, the input parameters of the models should be calculated or measured more accurately. The magnitude of the hyperfine field is often assumed to be about $\sim$1 mT. However, if the hyperfine field strength were accurately known for different materials, it would be possible to more accurately compare measured lineshapes with theoretical ones. In a device that consists of a blend of two materials or that contains traps, the lineshape depends on the material in which the spin-dependent reactions underlying the magnetic field effect take place. It would therefore be possible to derive from the lineshape in which material those reactions take place. Another issue is the magnitude of the hopping rate. The size and linewidth of the magnetic field effect depend on the relative hopping rate. When the hopping rate is comparable to the hyperfine frequency new features appear, like the ultra-small-magnetic-field effect. Finally, the effect of spin-orbit coupling is often assumed to be negligible. However, for some materials it could play an important role and its influence on the spin mixing by hyperfine fields should therefore be investigated.

Secondly, our understanding of magnetic field effects could be increased by new kinds of experiments. Experiments could be designed to exclude some spin-dependent processes, so attention can be focussed on others. For example, OFETs already offer a promising way to study truly unipolar charge transport,[94] thereby reducing the number of mechanisms that could give rise to a magnetic field effect. Furthermore, the gate voltage can be used to control the charge density, which can have a large influence on the magnetic field effects, as we have seen in Chapter 5. Also experiments where electrons or holes (or both) are injected with spin polarization into the organic semiconductor—like in a spin-OLED[80]—can help determine whether the measured magnetic field effect arises from a unipolar or bipolar mechanism. For example, changing between spin-polarized and spin-unpolarized injection of one carrier type could give an indication of the origin of the measured magnetic field effect—whether it results from a unipolar mechanism involving one carrier type or from a bipolar mechanism between electrons and holes. A unipolar mechanism would be influenced by the polarized injection of only one carrier type, whereas a bipolar mechanism would much less so. Lastly, the ΔB-mechanism could be employed to tune the amount of spin mixing. By engineering the gradients in the magnetic field in the organic semiconductor—by making them position dependent—information could be obtained about the position at which the spin-dependent processes that give rise to magnetic field effects take place.

A

Equivalence of exciton formation and bipolaron formation

The mathematical description of bipolaron formation in a one-dimensional system and exciton formation are equivalent, as will be shown here. The stochastic Liouville equation for both processes is given by:

$$\frac{\partial \rho_{\mathrm{PP}}}{\partial t} = -\frac{i}{\hbar}[H, \rho_{\mathrm{PP}}] - \frac{1}{2}\{\Lambda, \rho_{\mathrm{PP}}\} + \Gamma, \tag{A.1}$$

where H is the spin Hamiltonian Equation 2.4 on page 25. For exciton formation we have: $\Lambda = \sum_\lambda k_\lambda |\lambda\rangle\langle\lambda|$ for $\lambda = \mathrm{S}, \mathrm{T}_-, \mathrm{T}_0, \mathrm{T}_+$. And the dimensionless parameter $\gamma = k_{\mathrm{T}}/k_{\mathrm{S}}$. On the other hand, for bipolaron formation we have $\Lambda = |\mathrm{S}\rangle\langle\mathrm{S}|k_{\alpha\to\beta} + \mathrm{I}\,k_{\alpha\to\mathrm{e}}$, where I is the identity operator. Now, we have as a dimensionless parameter the branching ratio $b = k_{\alpha\to\beta}/k_{\alpha\to\mathrm{e}}$.[16] For both cases, we have $\Gamma = k(1 - \mathrm{Tr}[\rho])\mathrm{I}$.

It is easy to see that those two equations are equivalent when $k_{\alpha\to\beta} = k_{\mathrm{S}} - k_{\mathrm{T}}$ and $k_{\alpha\to\mathrm{e}} = k_{\mathrm{T}}$. That yields the following relation between the dimensionless parameters: $\gamma = 1 + b$.

In a wire, where the current is proportional to the rate of bipolaron formation relative to hopping back:

$$r_{\mathrm{Bip}} = \frac{\mathrm{Tr}\left[k_{\alpha\to\beta}|\mathrm{S}\rangle\langle\mathrm{S}|\rho\right]}{\mathrm{Tr}\left[k_{\alpha\to\beta}|\mathrm{S}\rangle\langle\mathrm{S}|\rho\right] + \mathrm{Tr}[k_{\alpha\to\mathrm{e}}\rho]}, \tag{A.2}$$

is equivalent to the fraction of singlet excitons formed:

$$\chi_{\mathrm{S}} = \frac{\mathrm{Tr}[k_{\mathrm{S}}|\mathrm{S}\rangle\langle\mathrm{S}|\rho]}{\mathrm{Tr}[k_{\mathrm{S}}|\mathrm{S}\rangle\langle\mathrm{S}|] + \mathrm{Tr}\left[\sum_{\lambda=\mathrm{T}_0,\mathrm{T}_-,\mathrm{T}_+} k_T|\lambda\rangle\langle\lambda|\rho\right]} \tag{A.3}$$

Summary

Magnetic Field Effects in Organic Semiconductors: Theory and Simulations

Organic semiconductors are a promising class of materials, offering several advantages over inorganic semiconductors. They are light, flexible, easy and cheap to produce, and easily chemically tunable. Organic semiconductors are currently used for lighting applications and in the displays of some smartphones and televisions. Exciting magnetic field effects have been observed in the current through and light production of organic semiconductors. A magnetoconductance and magneto-electroluminescence of up to 30% have been measured in organic semiconductor films. Recently, an even larger magnetoconductance with a magnitude of 93% was found in molecular wires.

The magnetic field effects are remarkably independent of the specific material used, always having either a Lorentzian or a so-called non-Lorentzian lineshape with a width of a few millitesla. The hyperfine interaction between nuclear magnetic moments and the spins of the particles—electrons, hole, excitons, bipolarons, etc.—in an organic semiconductor can be approximated by an effective magnetic field that acts on the spins. The difference in those so-called hyperfine fields experienced by two particles leads to spin mixing that can be suppressed by applying an external magnetic field. Magnetic field effects arise because quantities like the current and light output depend on processes that are spin-dependent and are thus affected by the amount of spin mixing.

The goals of this thesis are to explain experimentally observed magnetic field effects and to make predictions for obtaining even larger effects. This is done analytically using stochastic Liouville equations as well as using Monte Carlo simulations.

A much-discussed question that is related to magneto-electroluminescence is whether the statistical ratio of one singlet to three triplets can be violated in exciton formation. We have studied this question using a two-site model in Chapter 3. We found that, if the singlet and triplet exciton formation rates differ, the statistical singlet–to–triplet exciton ratio of 1:3 is violated when hopping is slower than or comparable to the hyperfine frequency—the precession frequency of an electron spin due to the hyperfine field. Furthermore, for those hopping rates, we found a magnetic field dependence of the singlet fraction—a measure of the electroluminescence—if and only if singlet and triplet exciton formation rates differ. We also found that an ultra-small-magnetic-field effect that is sometimes observed can result from the increase in spin mixing when a magnetic field is applied that is comparable in magnitude to the hyperfine fields.

In Chapter 4 we found that the violation of the statistical ratio and its magnetic field effect occur at hopping rates that are several orders of magnitude higher than the hyperfine frequency when Coulomb interaction and energetic disorder are present. In addition, a violation of the statistical ratio can be found even in the fast hopping limit, because electron-hole pairs can split up after which both can recombine with another electron and hole. This violation of the singlet fraction does not depend on the magnetic field.

The main conclusion of Chapter 5 is that very large magnetic field effects in both the current and diffusion constant can be obtained in doped polymers. The one-dimensionality of the charge transport through the polymer leads to effective spin blocking at dopant sites. This blocking occurs even in absence of an electric field and is amplified when the charge concentration is increased.

A huge magnetoconductance has been measured in molecular wires embedded in a zeolite L crystal. We have modeled the conduction through those wires using a chain of sites in Chapter 6. We conclude that a similar mechanism as in the doped polymers leads to spin blocking in the wires, where trapped electrons instead of dopant sites lead to spin blocking. We suggest that the potassium ions that are present in the zeolite lead to the necessary trapping, because trapping by just the energetic disorder results in neither the right magnitude nor in the right electric field dependence of the magnetoconductance as compared to the experiment.

When all effective magnetic fields are aligned, the amount of spin mixing depends on the hopping rate and the difference in magnitude of the effective magnetic fields felt by two particles on different sites. The effective magnetic fields vary from site to site due to the random nature of the hyperfine fields. However, in Chapter 7 we show that additional spin mixing happens when an external magnetic field is present that varies more strongly as a function of position than the hyperfine fields do. We conclude that the magnetoconductance that was measured in a device with a single magnetic electrode is the result of this kind of spin mixing. The magnetization of the magnetic layer changes as a function of the applied magnetic field. The resulting change in the fringe fields throughout the organic semiconductor leads to a change in spin mixing and thus in a change in the current.

Finally, the main conclusions of this thesis are summarized and an outlook on the future of modeling of magnetic field effects in organic semiconductors is given in Chapter 8.

Curriculum Vitæ

Sander Kersten was born on November 20, 1984, in Schelluinen, The Netherlands. In the nearby town Gorinchem, he went to high school at Oude Hoven. He graduated in 2003 and started his studies in Applied Physics at the Eindhoven University of Technology. After doing an internship studying the optical properties of self-assembling wires under supervision of dr. P.A. Bobbert and prof. dr. ir. P.P.A.M van der Schoot, he got his bachelor's degree cum laude. After that, Sander pursued a master's degree at the same university, which he was awarded in 2009 after successfully finishing a graduation projected in the group of prof. dr. A. Fiore studying photonic crystals using a scanning near-field optical microscope. During that period, he did an internship at the University of Kaiserslautern where he performed computer simulations to investigate the use of clusters of nickel atoms as logic gates. His supervisors were dr. G. Lefkidis and prof. dr. B. Koopmans. In 2009, Sander decided to stay in Eindhoven as a PhD candidate in the group Theory of Polymers and Soft Matter, with prof. dr. M.A.J. Michels and prof. dr. B. Koopmans as promotors and dr. P.A. Bobbert as copromotor.

In 2003, Sander placed second in the Nationale Natuurkunde Olympiade (National Physics Olympiad) and subsequently earned an Honourable Mention at the Internal Physics Olympiad which was held in Taiwan that year. He was awarded the Jong Talent Aanmoedigingsprijs by de Koninklijke Nederlandse Akademie van Wetenschappen in 2004.

List of Publications

S. P. Kersten, S. C. J. Meskers, and P. A. Bobbert. *Route towards huge magnetoresistance in doped polymers.* Phys. Rev. B **86**, 045210 (2012).

S. P. Kersten, A. J. Schellekens, B. Koopmans, and P. A. Bobbert. *Magnetic-Field Dependence of the Electroluminescence of Organic Light-Emitting Diodes: A Competition between Exciton Formation and Spin Mixing.* Phys. Rev. Lett. **106**, 197402 (2011).

S. P. Kersten, A. J. Schellekens, B. Koopmans, and P. A. Bobbert. *Effect of hyperfine interactions on exciton formation in organic semiconductors.* Synth. Met. **161**, 613 (2011).

R. N. Mahato, H. Lülf, M. H. Siekman, S. P. Kersten, P. A. Bobbert, M. P. de Jong, L. de Cola, and W. G. van der Wiel. *Giant Organic Magnetoresistance in One-Dimensional Molecular Wires.* Manuscript submitted for publication,

A. J. Schellekens, W. Wagemans, S. P. Kersten, P. A. Bobbert, and B. Koopmans. *Microscopic modeling of magnetic-field effects on charge transport in organic semiconductors.* Phys. Rev. B **84**, 075204 (2011).

Acknowledgements

Writing this thesis would have been less pleasurable or not even possible without the help and support of several people.

Als eerste wil ik Peter Bobbert, mijn directe begeleider en copromotor, bedanken. Zonder jouw hulp en ondersteuning de afgelopen vier jaar was het me niet gelukt dit project goed af te ronden. In het bijzonder wil ik je bedanken voor alle correcties en suggesties die je gemaakt hebt voor dit proefschrift. Ik wil Thijs Michels en Bert Koopmans bedanken dat ze mijn eerste en tweede promotor wilden zijn en voor het commentaar dat ze gegeven hebben op mijn proefschrift.

Next, I would like to thank the other members of my reading committee, Markus Wohlgenannt, Wilfred van der Wiel, and Stefan Meskers. Thank you for reading my thesis and giving me suggestions on how to improve it. Also our earlier discussions have been valuable for doing my research.

Markus, Michael Flatté, Nick Harmon and other group members, thank you for you hospitality during my visits to Iowa. Besides scientific discussions, you have shown me more restaurants in the few weeks I was in Iowa than I have been to in Eindhoven the past few years.

Een groot deel van mijn onderzoek bestond uit het doen van berekeningen en simulaties die niet mogelijk waren geweest zonder Polyxena, ons computercluster. Ik wil Arieh Tal en Erik Smeets ervoor bedanken het cluster werkend te hebben gehouden.

Helmi, bedankt voor je hulp met administratieve zaken.

Ik ben Paul Janssen en Matthijs Cox dankbaar voor de gesprekken die we gehad hebben over met name experimentele complicaties die een rol spelen bij het begrijpen van hoe magnetische veldeffecten ontstaan. Sjors Schellekens, bedankt dat je stochastische Liouville vergelijkingen onder mijn aandacht hebt gebracht; die bleken een elegantere formulering te zijn van de berekeningen die aan het doen was en dat heeft me veel tijd gescheeld. Frank van Oost, ik heb jouw Monte Carlo code dankbaar als basis gebruikt voor veel van de simulaties die ik gedaan heb.

I am also grateful to all current members, and those who have left the last four year, of the group theory of polymers and soft matter for the great time I have had. The prospect of seeing you have always motivated me to go to work in the morning. I will not forget the interesting lunch and coffee breaks and the occasional Borrel and movie nights. In particular I would like to thank the people with whom I have shared an office over the past years, Jeroen van der Holst, Jeroen Cottaar, Murat, Andrea, and Augusto, for the nice working environment and useful discussions about work and the frustrations that are sometimes part of being a PhD student.

Abhinav, I have really enjoyed the discussions we have had about questions that seem much more important than our daily work, like what is consciousness and how does a mind work? Of course we were never really able to answer those questions, but it was fun to discuss them anyway.

Tot slot wil ik mijn ouders Paul en Margriet, mijn broer Martijn en Anda bedanken voor het vertrouwen dat ze altijd in mij gehad hebben en de steun die ze gegeven hebben.

Bibliography

1 V. Ambegaokar, B. I. Halperin, and J. S. Langer. *Hopping Conductivity in Disordered Systems.* Phys. Rev. B **4**, 2612 (1971). (pages 32, 61)

2 P. W. Anderson. *A Mathematical Model for the Narrowing of Spectral Lines by Exchange or Motion.* J. Phys. Soc. Jpn. **9**, 316 (1954). (page 25)

3 S. A. Bagnich, U. Niedermeier, C. Meizer, W. Sarfert, and H. von Seggern. *Origin of magnetic field effect enhancement by electrical stress in organic light emitting diodes.* J. Appl. Phys. **105**, 123706 (2009). (page 17)

4 W. J. Baker, T. L. Keevers, J. M. Lupton, D. R. McCamey, and C. Boehme. *Slow Hopping and Spin Dephasing of Coulombically Bound Polaron Pairs in an Organic Semiconductor at Room Temperature.* Phys. Rev. Lett. **108**, 267601 (2012). (page 48)

5 W. J. Baker, D. R. McCamey, K. J. van Schooten, J. M. Lupton, and C. Boehme. *Differentiation between polaron-pair and triplet-exciton polaron spin-dependent mechanisms in organic light-emitting diodes by coherent spin beating.* Phys. Rev. B **84**, 165205 (2011). (page 14)

6 H. Bässler. *Charge Transport in Disordered Organic Photoconductors: A Monte Carlo Simulation Study.* phys. stat. sol. (b) **175**, 15 (1993). (page 3)

7 H. Bässler. *Charge transport in disordered organic photoconductors: A Monte-Carlo study.* Phys. Stat. Sol. (b) **175**, 15 (1993). (page 30)

8 H. Bentmann, A. A. Demkov, R. Gregory, and S. Zollner. *Eletronic, optical, and surface properties of PtSi thin films.* Phys. Rev. B **78**, 205302 (2008). (page 75)

9 J. D. Bergeson, V. N. Prigodin, D. M. Lincoln, and A. J. Epstein. *Inversion of Magnetoresistance in Organic Semiconductors.* Phys. Rev. Lett. **100**, 067201 (2008). (pages 5, 15)

10 A. Bernanose, M. Comte, and P. Vouaux. *Sur un noveau mode d'émission lumineuse chez certains composés organiques.* J. Chim. Phys. **50**, 64 (1953). (page 1)

11 P. W. M. Blom, M. J. M. de Jong, and J. J. M. Vleggaar. *Electron and hole transport in poly(p-phenylene vinylene) devices.* Appl. Phys. Lett. **68**, 3308 (1996). (page 49)

12 F. L. Bloom, M. Kemerink, W. Wagemans, and B. Koopmans. *Sign inversion of magnetoresistance in injection limited organic devices.* Phys. Rev. Lett. **103**, 066601 (2009). (page 14)

13 F. L. Bloom, W. Wagemans, M. Kemerink, and B. Koopmans. *Separating positive and negative magnetoresistance in organic semiconductor devices.* Phys. Rev. Lett. **99**, 257201 (2007). (pages 57, 60)

14 K. Blum. *Density Matrix Theory and Applications* (Springer-Verlag, 1996). (page 23)

15 P. A. Bobbert. *Organic semiconductors: what makes the spin relax?* Nature Materials **9**, 288 (2010). (page 58)

16 P. A. Bobbert, T. D. Nguyen, F. W. A. van Oost, B. Koopmans, and M. Wohlgenannt. *Bipolaron Mechanism for Organic Magnetoresistance.* Phys. Rev. Lett. **99**, 216801 (2007). (pages 12, 14, 35, 45, 58, 99)

17 P. A. Bobbert, W. Wagemans, F. W. A. van Oost, B. Koopmans, and M. Wohlgenannt. *Theory for Spin Diffusion in Disordered Organic Semiconductors.* Phys. Rev. Lett. **102**, 156604 (2009). (pages 8, 12, 36, 48)

18 A. B. Bortz, M. H. Kalos, and J. L. Lebowitz. *A new Algorithm for Monte Carlo Simulation of Ising Spin Systems.* J. Comp. Phys. **17**, 10 (1975). (page 30)

19 C. Brabec, V. Dyakonov, J. Parisi, and N. Sariciftci. *Organic Photovoltaics: Concepts and Realization* (Springer-Verlag, 2003). (page 1)

20 J. H. Burroughes, D. D. C. Bradley, A. R. Brown, R. N. Marks, K. Mackay, R. H. Friend, P. L. Burns, and A. B. Holmes. *Light-emitting diodes based on conjugated polymers.* Nature **347**, 539 (1990). (page 1)

21 M. N. Bussac and L. Zuppiroli. *Bipolaron singlet and triplet states in disordered conducting polymers.* Phys. Rev. B **47**, 5493 (1993). (page 13)

22 Y. Cao, I. D. Parker, G. Yu, C. Zhang, and A. J. Heeger. *Improved quantum effciency for electroluminescence in semiconducting polymers.* Nature **397**, 414 (1999). (pages 7, 36)

23 M. Carvelli, R. A. J. Janssen, and R. Coehoorn. *Determination of the exciton singlet-to-triplet ratio in single-layer organic light-emitting diodes.* Phys. Rev. B **83**, 075203 (2011). (pages 7, 36)

24 O. Chauvet, A. Sienkiewicz, L. Forro, and L. Zuppiroli. *High-pressure electron-spin dynamics in disordered conducting polymers.* Phys. Rev. B **52**, R13118 (1995). (page 13)

25 C. K. Chiang, C. R. Fincher, Jr., Y. W. Park, A. J. Heeger, H. Shirakawa, E. J. Louis, S. C. Gau, and A. G. MacDiarmid. *Electrical Conductivity in Doped Polyacetylene.* Phys. Rev. Lett. **39**, 1098 (1977). (page 1)

26 M. Cinchetti, K. Heimer, J.-P. Wüstenberg, O. Andreyev, M. Bauer, S. Lach, C. Ziegler, Y. Gao, and M. Aeschlimann. *Determination of spin injection and transport in a ferromagnet/organic semiconductor heterojunction by two-photon photoemission.* Nature Mat. **8**, 115 (2008). (page 20)

27 A. E. Cohen. *Nanomagnetic Control of Intersystem Crossing.* J. Phys. Chem. A **113**, 11084 (2009). (pages 19, 85)

28 J. Cottaar and P. A. Bobbert. *Calculating charge-carrier mobilities in disordered semiconducting polymers: Mean field and beyond.* Phys. Rev. B **74**, 115204 (2006). (page 33)

29 J. Cottaar, L. J. A. Koster, R. Coehoorn, and P. A. Bobbert. *Scaling Theory for Percolative Charge Transport in Disordered Molecular Semiconductors.* Phys. Rev. Lett. **107**, 136601 (2011). (pages 32, 33)

30 Z. Dance, Q. Mi, D. McCamant, M. Ahrens, M. Ratner, and M. Wasielewski. *Time-resolved EPR studies of photogenerated radical ion pairs separated by p-phenylene oligomers and of triplet states resulting from charge recombination.* Phys. Chem. B **110**, 25163 (2006). (page 71)

31 V. A. Dediu, L. E. Hueso, I. Bergenti, and C. Taliani. *Spin routes in organic semiconductors.* Nature Mat. **8**, 707 (2009). (pages 7, 19)

32 P. Desai, P. Shakya, T. Kreouzis, and W. P. Gillin. *Magnetoresistance in organic light-emitting diode structures under illumination.* Phys. Rev. B **76**, 235202 (2007). (pages 8, 35, 36, 57, 58, 60)

33 A. S. Dhoot, D. S. Ginger, D. Beljonne, Z. Shuai, and N. C. Greenham. *Triplet formation and decay in conjugated polymer devices.* Chem. Phys. Lett. **360**, 195 (2002). (pages 7, 36)

34 A. J. Drew, J. Hoppler, L. Schulz, F. L. Pratt, P. Desai, P. Shakya, T. Kreouzis, W. P. Gillin, A. Suter, N. A. Morley, V. K. Malik, A. Dubroka, K. Kim, H. Bouyanfif, F. Bourqui, C. Bernhard, R. Scheuermann, G. J. Nieuwenhuys, T. Prokscha, and E. Morenzoni. *Direct measurement of the electronic spin diffusion length in a fully functional organic spin valve by low-energy muon spin rotation.* Nature Mat. **23**, 11 (2008). (page 20)

35 U. Fano. *Description of States in Quantum Mechanics by Density Matrix and Operator Techniques.* Rev. Mod. Phys. **29**, 74 (1957). (page 23)

36 T. L. Francis, Ö. Mermer, G. Veeraraghavan, and M. Wohlgenannt. *Large magnetoresistance at room temperature in semiconducting polymer sandwich devices.* New J. Phys. **6**, 185 (2004). (pages 8, 35, 57, 60)

37 E. Frankevich, A. Lymarev, I. Sokolik, F. Karasz, S. Blumstengel, R. Baughman, and H. Hoerhold. *Polaron pair generation in poly(phenylene vinylenes).* Phys. Rev. B **46**, 9320 (1992). (pages 8, 10)

38 C. Gärditz, G. Mückl, and M. Cölle. *Influence of an external magnetic field on the singlet and triplet emissions of tris-(8-hydroxyquinoline)aluminum(III) (Alq_3).* J. Appl. Phys. **98**, 104507 (2005). (pages 16, 82)

39 D. T. Gillespie. *A General Method for Numerically Simulating the Stochastic Time Evolution of Coupled Chemical Reactions.* J. Comp. Phys. **22**, 403 (1976). (page 30)

40 S. Goffri, C. Müller, N. Stingelin-Stutzmann, D. W. Breiby, C. P. Radano, J. Andreasen, R. Thompson, R. A. J. Janssen, M. M. Nielsen, P. Smith, and H. Sirringhaus. *Multicomponent semiconducting polymer systems with low crystallization-induced percolation threshold.* Nature Mater. **5**, 950 (2006). (page 71)

41 C. Gould, C. Rüster, T. Jungwirth, E. Girgis, G. M. Schott, R. Giraud, K. Brunner, G. Schmidt, and L. W. Molenkamp. *Tunneling Anisotropic Magnetoresistance: A Spin-Valve-Like Tunnel Magnetoresistance Using a Single Magnetic Layer.* Phys. Rev. Lett. **93**, 117203 (2004). (page 19)

42 D. J. Griffiths. *Introduction to Quantum Mechanics, 2nd Edition* (Pearson Prentice Hall, 2005). (page 12)

43 R. P. Groff, R. E. Merrifield, A. Suna, and P. Avakian. *Magnetic Hyperfine Modulation of Dye-Sensitized Delayed Fluorescence in an Organic Crystal.* Phys. Rev. Lett. **29**, 429 (1972). (page 25)

44 E. Havinga, W. ten Hoeve, and H. Wynberg. *Alternate Donor-Acceptor Small-Band-Gap Semiconducting Polymers; Polysquaraines and Polycroconaines.* Synth. Met. **55-57**, 299 (1993). (page 71)

45 M. Helbig and H.-H. Hörhold. *Investigation of Poly(Arylenevinylene)s, 40. Electrochemical studies on Poly(p-Phenylenevinylene)s.* Makromol. Chem. **194**, 1607 (1993). (page 14)

46 J. J. M. van der Holst, M. A. Uijttewaal, R. Balasubramanian, R. Coehoorn, P. A. Bobbert, G. A. de Wijs, and R. A. de Groot. *Modeling and analysis of the three-dimensional current density in sandwich-type single-carrier devices of disordered organic semiconductors.* Phys. Rev. B **79**, 085203 (2009). (page 4)

47 H. Houili, E. Tutiš, I. Batistić, and L. Zuppiroli. *Investigation of the charge transport through disordered organic molecular heterojunctions.* J. Appl. Phys. **100**, 033702 (2006). (page 30)

48 B. Hu and Y. Wu. *Tuning magnetoresistance between positive and negative values in organic semiconductors.* Nature Mat. **6**, 985 (2007). (pages 15, 35, 57, 58, 60)

49 I. N. Hulea, H. B. Brom, A. J. Houtepen, D. Vanmaekelbergh, J. J. Kelly, and E. A. Meulenkamp. *Wide Energy-Window View on the Density of States and Hole Mobility in Poly(p-Phenylene Vinylene).* Phys. Rev. Lett. **93**, 166601 (2004). (page 3)

50 F. J. Jedema, H. B. Heersche, A. T. Filip, J. J. A. Baselmans, and B. J. van Wees. *Electrical detection of spin precession in a metallic mesoscopic spin valve.* Nature **416**, 713 (2002). (page 19)

51 R. C. Johnson and R. E. Merrifield. *Effects of Magnetic Fields on the Mutual Annihilation of Triplet Excitons in Anthracene Crystals.* Phys. Rev. B **1**, 896 (1979). (page 25)

52 R. C. Johnson, R. E. Merrifield, P. Avakian, and R. B. Flippen. *Effects of Magnetic Fields on the Mutual Annihilation of Triplet Excitons in Molecular Crystals.* Phys. Rev. Lett. **19**, 285 (1967). (page 16)

53 J. Kalinowski, M. Cocchi, D. Virgili, P. Di Marco, and V. Fattori. *Magnetic field effects on emission and current in Alq_3-based electroluminescent diodes.* Chem. Phys. Lett. **380**, 710 (2003). (pages 8, 35, 36, 57, 60)

54 K. Kanemoto, H. Matsuoka, Y. Ueda, K. Takemoto, K. Kimura1, and H. Hashimoto. *Displacement current induced by spin resonance in air-treated conjugated polymer diodes.* Phys. Rev. B **86**, 125201 (2012). (page 17)

55 Y. Kawamura, K. Goushi, J. Brooks, J. J. Brown, H. Sasabe, and C. Adachi. *100% phosphorescence quantum efficiency of Ir(III) complexes in organic semiconductor films.* Appl. Phys. Lett. **86**, 071104 (2005). (page 7)

56 S. P. Kersten, S. C. J. Meskers, and P. A. Bobbert. *Route towards huge magnetoresistance in doped polymers.* Phys. Rev. B **86**, 045210 (2012). (pages 57, 105)

57 S. P. Kersten, A. J. Schellekens, B. Koopmans, and P. A. Bobbert. *Effect of hyperfine interactions on exciton formation in organic semiconductors.* Synth. Met. **161**, 613 (2011). (pages 47, 105)

58 S. P. Kersten, A. J. Schellekens, B. Koopmans, and P. A. Bobbert. *Magnetic-Field Dependence of the Electroluminescence of Organic Light-Emitting Diodes: A Competition between Exciton Formation and Spin Mixing.* Phys. Rev. Lett. **106**, 197402 (2011). (pages 35, 47, 58, 105)

59 D. Y. Kondakov, T. D. Pawlik, T. K. Hatwar, and J. P. Spindler. *Triplet annihilation exceeding spin statistical limit in highly efficient fluorescent organic light-emitting diodes.* J. Appl. Phys. **106**, 124510 (2009). (pages 7, 16)

60 R. Kubo. *Note on the Stochastic Theory of Resonance Absorption.* J. Phys. Soc. Jpn. **9**, 935 (1954). (page 25)

61 S. K. Lee, Y. Zu, A. Herrmann, Y. Geerts, K. Müllen, and A. J. Bard. *Electrochemistry, Spectroscopy and Electrogenerated Chemiluminescnece of Perylene, Terrylene, and Quaterrylene Diimides in Aprotic Solution.* J. Am Chem. Soc. **121**, 3513 (1999). (pages 75, 77)

62 S.-Y. Lee, S.-Y. Paik, D. R. McCamey, J. Yu, P. L. Burn, J. M. Lupton, and C. Boehme. *Tuning Hyperfine Fields in Conjugated Polymers for Coherent Organic Spintronics.* JACS **133**, 2019 (2011). (page 10)

63 X. Lou, C. Adelmann, S. A. Crooker, E. S. Garlid, J. Zhang, K. S. N. Reddy, S. D. Flexner, C. J. Palmstrøm, and P. A. Crowell. *Electrical detection of spin transport in lateral ferromagnet-semiconductor devices.* Nature Phys. **3**, 197 (2007). (page 19)

64 F. Macià, F. Wang, N. J. Harmon, M. Wohlgenannt, A. D. Kent, and M. E. Flatté. *Hysteretic control of organic conductance due to remanent magnetic fringe fields.* Appl. Phys. Lett. **102**, 042408 (2013). (pages 86, 91)

65 R. N. Mahato, H. Lülf, M. H. Siekman, S. P. Kersten, P. A. Bobbert, M. P. de Jong, L. de Cola, and W. G. van der Wiel. *Giant Organic Magnetoresistance in One-Dimensional Molecular Wires.* Manuscript submitted for publication, (pages 73–76, 105)

66 R. A. Marcus. *Electron transfer reactions in chemistry. Theory and experiment.* Rev. Mod. Phys. **65**, 599 (1993). (pages 3, 68)

67 J. Y. Mayorova, P. A. Troshin, A. S. Peregudov, S. M. Peregudova, M. G. Kaplunova, and R. N. Lyubovskayaa. *Highly soluble perylene dye: tetrabenzyl 3,4,9,10-perylenetetracarboxylate.* Mendeleev Commun. **17**, 156 (2007). (page 14)

68 D. R. McCamey, K. J. van Schooten, W. J. Baker, S.-Y. Lee, S.-Y. Paik, J. M. Lupton, and C. Boehme. *Hyperfine-Field-Mediated Spin Beating in Electrostatically Bound Charge Carrier Pairs.* Phys. Rev. Lett. **104**, 017601 (2010). (pages 18, 42)

69 D. R. McCamey, H. A. Seipel, S.-Y. Paik, M. J. Walter, N. J. Borys, J. M. Lupton, and C. Boehme. *Spin Rabi flopping in the photocurrent of a polymer light-emitting diode.* Nature Mat. **7**, 723 (2008). (page 18)

70 H. M. McConnel. *Indirect Hyperfine Interactions in the Paramagnetic Resonance Spectra of Aromatic Free Radicals.* J. Chem. Phys. **24**, 764 (1956). (page 11)

71 H. M. McConnell and D. B. Chesnut. *Theory of Isotropic Hyperfine Interactions in π-Electron Radicals.* J. Chem. Phys. **28**, 107 (1958). (page 11)

72 B. Meng and W. H. Weinberg. *Monte Carlo simulations of temperature programmed desorption spectra.* J. Chem. Phys. **100**, 5280 (1994). (page 30)

73 Ö. Mermer, G. Veeraraghavan, T. L. Francis, Y. Sheng, D. T. Nguyen, M. Wohlgenannt, A. Kohler, M. K. Al-Suti, and M. S. Khan. *Large magnetoresistance in nonmagnetic π-conjugated semiconductor thin film devices.* Phys. Rev. B **72**, 205202 (2005). (page 58)

74 Ö. Mermer, G. Veeraraghavan, T. L. Francis, and M. Wohlgenannt. *Large magnetoresistance at room-temperature in small-molecular-weight organic semiconductor sandwich devices.* Solid State Commun. **134**, 631 (2005). (pages 8, 9)

75 N. Metropolis. *The beginning of the Monte Carlo method.* Los Alamos Science **Special Issue**, 125 (1987). (page 30)

76 N. Metropolis and S. Ulam. *The Monte Carlo Method.* J. Am. Stat. Ass. **44**, 335 (1949). (page 30)

77 A. Miller and E. Abrahams. *Impurity conduction at low concentrations.* Phys. Rev. **120**, 745 (1960). (pages 3, 68)

78 W. J. M. Naber, S. Faez, and W. van der Wiel. *Organic spintronics.* J. Phys. D: Appl. Phys. **40**, R205 (2007). (page 19)

79 A. M. Nardes, M. Kemerink, M. M. de Kok, E. Vinken, K. Maturova, and R. A. J. Janssen. *Conductivity, work function, and environmental stability of PEDOT:PSS thin films treated with sorbitol.* Org. Electr. **9**, 727 (2008). (page 75)

80 T. D. Nguyen, E. Ehrenfreund, and Z. V. Vardeny. *Spin-Polarized Light-Emitting Diode Based on an Organic Bipolar Spin Valve.* Science **337**, 204 (2012). (pages 8, 97)

81 T. D. Nguyen, E. Ehrenfreund, and Z. V. Vardeny. *The spin-polarized organic light emitting diode.* Synth. Met. **doi: 10.1016/j.synthmet.2012.11.015**, (2013). (page 8)

82 T. D. Nguyen, B. R. Gautam, E. Ehrenfreund, and Z. V. Vardeny. *Magnetoconductance Response in Unipolar and Bipolar Organic Diodes at Ultrasmall Fields.* Phys. Rev. Lett. **105**, 166804 (2010). (pages 9, 10, 14, 45, 46, 57, 58, 60)

83 T. D. Nguyen, G. Hukic-Markosian, F. Wang, L. Wojcik, X.-G. Li, E. Ehrenfreund, and Z. V. Vardeny. *Isotope effect in spin response of π-conjugated polymer films and devices.* Nature Materials **9**, 345 (2010). (pages 10, 36, 42–44, 48, 57, 58, 60)

84 T. D. Nguyen, Y. Sheng, J. Rybicki, G. Veeraraghavan, and M. Wohlgenannt. *Magnetoresistance in π-conjugated organic sandwich devices with varying hyperfine and spin-orbit coupling strengths, and varying dopant concentrations.* J. Mat. Chem. **17**, 1995 (2007). (page 72)

85 T. D. Nguyen, Y. Sheng, J. Rybicki, and M. Wohlgenannt. *Magnetic field-effects in bipolar, almost hole-only and almost electron-only tris-(8-hydroxyquinoline) aluminum devices.* Phys. Rev. B **77**, 235209 (2008). (page 8)

86 U. Niedermeier, M. Vieth, R. Pätzold, W. Sarfert, and H. von Seggern. *Enhancement of organic magnetoresistance by electrical conditioning.* Appl. Phys. Lett. **92**, 193309 (2008). (pages 17, 57, 60)

87 R. Österbacka, M. Wohlgenannt, D. Chinn, and Z. V. Vardeny. *Optical studies of triplet excitations in poly(p-phenylene vinylene).* Phys. Rev. B **60**, 16 (1999). (pages 16, 82)

88 R. H. Parmenter and W. Rupel. *Two-carrier Space-Charge-Limited Current in a Trap-Free Insulator.* J. Appl. Phys. **30**, 1548 (1959). (page 5)

89 W. F. Pasveer, J. Cottaar, C. Tanase, R. Coehoorn, P. A. Bobbert, P. W. M. Blom, D. M. de Leeuw, and M. A. J. Michels. *Unified Description of Charge-Carrier Mobilities in Disordered Semiconducting Polymers.* Phys. Rev. Lett. **94**, 206601 (2005). (pages 36, 48)

90 R. Peierls. *Quantum theory of solids* (Clarendon,) (page 3)

91 Philips. *Philips presents world's first OLED-based interactive lighting concepts*. (2009) URL: http://www.newscenter.philips.com/main/standard/about/news/press/20090423_oled.wpd (page 2)

92 V. Prigodin, J. Bergeson, D. Lincoln, and A. Epstein. *Anomalous room temperature magnetoresistance in organic semiconductors.* Synth. Metals **156**, 757 (2006). (pages 15, 35, 36, 57, 58, 60)

93 S. van Reenen, P. Matyba, A. Dzwilewski, R. A. J. Janssen, L. Edman, and M. Kemerink. *A Unifying Model for the Operation of Light-Emitting Electrochemical Cells.* J. Am. Chem. Soc. **132**, 13776 (2010). (page 15)

94 T. Reichert, T. P. I. Saragi, and J. Salbeck. *Magnetoresistive field-effect transistors based on organic donorÐacceptor blends.* RSC Adv. **2**, 7388 (2012). (pages 14, 97)

95 T. Ritz, P. Thalau, J. B. Phillips, R. Wiltschko, and W. Wiltschko. *Resonance effects indicate a radical-pair mechanism for avian magnetic compass.* Nature **429**, 177 (2004). (page 18)

96 N. J. Rolfe, M. Heeney, P. B. Wyatt, A. J. Drew, T. Kreouzis, and W. P. Gillin. *Elucidating the role of hyperfine interactions on organic magnetoresistance using deuterated aluminium tris(8-hydroxyquinoline).* Phys. Rev. B **80**, 241201(R) (2009). (page 42)

97 N. J. Rolfe, M. Heeney, P. B. Wyattc, A. J. Drew, T. Kreouzis, and W. P. Gillin. *The effect of deuteration on organic magnetoresistance.* Synth. Met. , 608 (2011). (page 10)

98 C. Rothe, S. M. King, and A. P. Monkman. *Direct Measurement of the Singlet Generation Yield in Polymer Light-Emitting Diodes.* Phys. Rev. Lett. **97**, 076602 (2006). (pages 7, 36)

99 J. Rybicki, R. Lin, F. Wang, M. Wohlgenannt, C. He, T. Sanders, and Y. Suzuki. *Tuning the Performance of Organic Spintronic Devices Using X-Ray Generated Traps.* Phys. Rev. Lett. **109**, 076603 (2012). (page 17)

100 G. Salis, S. F. Alvarado, M. Tschudy, T. Brunschwiler, and R. Allenspach. *Hysteretic electroluminescence in organic light-emitting diodes for spin injection.* Phys. Rev. B **70**, 085203 (2004). (page 19)

101 S. Sanvito. *Organic Electronics: Spintronics goes plastic.* Nature Mat. **6**, 803 (2007). (page 19)

102 S. Sanvito. *Molecular spintronics.* Chem. Soc. Rev. **40**, 3336 (2011). (page 19)

103 A. J. Schellekens, W. Wagemans, S. P. Kersten, P. A. Bobbert, and B. Koopmans. *Microscopic modeling of magnetic-field effects on charge transport in organic semiconductors.* Phys. Rev. B **84**, 075204 (2011). (pages 16, 17, 82, 105)

104 G. Schönherr, H. Bässler, and M. Silver. *Dispersive hopping transport via sites having a Gaussian distribution of energies.* Phil. Mag. Part B **44**, (1981). (page 30)

105 K. Schulten and P. Wolynes. *Semiclassical description of electron spin motion in radicals including the effect of hopping.* J. Chem. Phys. **68**, 3292 (1978). (pages 11, 37, 58)

106 M. Segal, M. A. Baldo, R. J. Holmes, S. R. Forrest, and Z. G. Soos. *Excitonic singlet-triplet ratios in molecular and polymeric organic materials.* Phys. Rev. B **68**, 075211 (2003). (pages 7, 36, 42)

107 Z. Shuai, D. Beljonne, R. J. Silbey, and J. L. Brédas. *Singlet and triplet exciton formation rates in conjugated polymer light-emitting diodes.* Phys. Rev. Lett. **84**, 131 (2000). (page 50)

108 H. Sirringhaus, P. J. Brown, R. H. Friend, M. M. Nielsen, K. Bechgaard, B. M. W. Langeveld-Voss, A. J. H. Spiering, R. A. J. Janssen, E. W. Meijer, P. Herwig, and D. M. de Leeuw. *Two-dimensional charge transport in self-organized, high-mobility conjugated polymers.* Nature **401**, 685 (1999). (page 1)

109 S. Stafström. *Electron localization and the transition from adiabatic to nonadiabatic charge transport in organic conductors.* Chem. Soc. Rev. **39**, 2484 (2010). (pages 3, 68)

110 T. T. Steckler, X. Zhang, J. Hwang, R. Honeyager, S. Ohira, X.-H. Zhang, A. Grant, S. Ellinger, S. A. Odom, D. Sweat, D. B. Tanner, A. G. Rinzler, S. Barlow, J.-L. Brédas, B. Kippelen, S. R. Marder, and J. R. Reynolds. *A Spray-Processable, Low Bandgap, and Ambipolar Donor-Acceptor Conjugated Polymer.* J. Am. Chem. Soc. **131**, 2824 (2009). (page 71)

111 U. E. Steiner and T. Ulrich. *Magnetic Field Effects in Chemical Kinetics and Related Phenomena.* Chem. Rev. **89**, 51 (1989). (pages 9, 58)

112 A. Suna. *Kinematics of Exciton-Exciton Annihilation in Molecular Crystals.* Phys. Rev. B **1**, 1716 (1970). (page 25)

113 C. W. Tang and S. A. VanSlyke. *Organic electroluminescent diodes.* Appl. Phys. Lett. **51**, 913 (1987). (page 1)

114 Y. Tanimura. *Stochastic Liouville, Langevin, Fokker-Planck, and Master Equation Approaches to Quantum Dissipative Systems.* J. Phys. Soc. Jap. **75**, 082001 (2006). (page 25)

115 Y.-S. Tyan. *Organic light-emitting-diode lighting overview.* J. Photon. Energy **1**, 011009-1 (2011). (page 7)

116 H. Uoyama, K. Goushi, K. Shizu, H. Nomura, and C. Adachi. *Highly efficient organic light-emitting diodes from delayed fluorescence.* Nature **492**, 234 (2012). (page 7)

117 Z. Vardeny, E. Ehrenfreund, O. Brafman, M. Nowak, H. Schaffer, A. J. Heeger, and F. Wudl. *Photogeneration of confined soliton pairs (Bipolarons) in polythiophene.* Phys. Rev. Lett. **56**, 671 (1986). (page 14)

118 J. von Neumann. *Wahrscheinlichkeitstheoretischer Aufbau der Quantenmechanik.* Göttinger Nachrichten **1**, 245 (1927). (page 23)

119 A. F. Voter. *Introduction to the Kinetic Monte Carlo Method*. URL: http://www.ipam.ucla.edu/publications/matut/matut_5898_preprint.pdf (page 30)

120 W. Wagemans. *Plastic Spintronics*. PhD thesis, Eindhoven University of Technology (2012). (page 20)

121 W. Wagemans, F. Bloom, P. Bobbert, M. Wohlgenannt, and B. Koopmans. *A two-site bipolaron model for organic magnetoresistance.* J. Appl. Phys. **103**, 07F303 (2008). (page 87)

122 K. Walzer, B. Maennig, M. Pfeiffer, and K. Leo. *Highly efficient organic devices based on electrically doped transport layers.* Chem. Rev. **107**, 1233 (2007). (pages 5, 6, 71)

123 F. Wang, F. Macià, M. Wohlgenannt, A. D. Kent, and M. E. Flatté. *Magnetic Fringe-Field Control of Electronic Transport in an Organic Film.* Phys. Rev. X **2**, 021013 (2012). (pages 19, 86–88, 91, 92)

124 F. J. Wang, H. Bässler, and Z. V. Vardeny. *Magnetic Field Effects in π-Conjugated Polymer-Fullerene Blends: Evidence for Multiple Components.* Phys. Rev. Lett. **101**, 236805 (2008). (pages 14, 17, 36, 57, 60)

125 S. I. Weissman. *Hyperfine Splittings in Polyatomic Free Radicals.* J. Chem. Phys. **22**, 1378 (1954). (page 11)

126 J. S. Wilson, A. S. Dhoot, A. J. A. B. Seeley, M. S. Kahn, A. Köhler, and R. H. Friend. *Spin-dependent exciton formation in π-conjugated compounds.* Nature **413**, 828 (2001). (pages 7, 36)

127 M. Wohlgenannt, K. Tandon, S. Mazumdar, S. Ramasesha, and Z. V. Vardeny. *Formation cross-sections of singlet and triplet excitons in π-conjugated polymers.* Nature **409**, 494 (2001). (pages 7, 36)

128 Z. H. Xiong, D. Wu, Z. V. Vardeny, and J. Shi. *Giant magnetoresistance in organic spin-valves.* Nature **427**, 821 (2004). (page 8)

129 Y. Yoshida, A. Fujii, M. Ozaki, K. Yoshino, and E. L. Frankevich. *Magnetic Field Effect as a Test for Effectiveness of the Light Emission at the Recombination of Injected Charge Carriers in Polymeric Semiconductors.* Mol. Cryst. Liquid Cryst. **426**, 19 (2005). (pages 7, 36)

130 W. Young and E. Elcock. *Monte Carlo studies of vacancy migration in binary ordered alloys: I.* Proc. Phys. Soc. **89**, 735 (1966). (page 30)

131 Z. G. Yu. *Spin-Orbit Coupling, Spin Relaxation, and Spin Diffusion in Organic Solids.* Phys. Rev. Lett. **106**, 106602 (2011). (pages 8, 12)

132 Z. G. Yu. *Spin-orbit coupling and its effects in organic solids.* Phys. Rev. B **85**, 115201 (2012). (pages 12, 16, 17)

133 A. A. Zezin, V. I. Feldman, J. M. Warman, J. Wildeman, and G. Hadziioannou. *EPR study of positive holes on phenylene vinylene chains: tom dimer to polymer.* Chem. Phys. Lett. **389**, 108 (2004). (page 12)

134 Y. Zhang and S. R. Forrest. *Triplets Contribute to Both an Increase and Loss in Fluorescent Yield in Organic Light Emitting Diodes.* Phys. Rev. Lett. **108**, 267404 (2012). (pages 7, 16)

135 Y. Zhang, R. Liu, Y. L. Lei, and Z. H. Xiong. *Low temperature magnetic field effects in Alq3-based organic light emitting diodes.* Appl. Phys. Lett. **94**, 083307 (2009). (page 16)

136 J. Zhou, Y. C. Zhou, J. M. Zhao, C. Q. Wu, X. M. Ding, and X. Y. Hou. *Carrier density dependence of mobility in organic solids: A Monte Carlo simulation.* Phys. Rev. B **75**, 153201 (2007). (page 30)

Index